AD-A109 627 ANALYSIS AND TECHNOLOGY INC NORTH STONINGTON CT F/G 12/1
TARGET MOTION ANALYSIS WITH A PRIORI INFORMATION.(U)
OCT 81 C B BILLING, H F JARVIS N00014-80-C-0379
UNCLASSIFIED P-515-2-81 NL

1 OF 2
AD
A109627

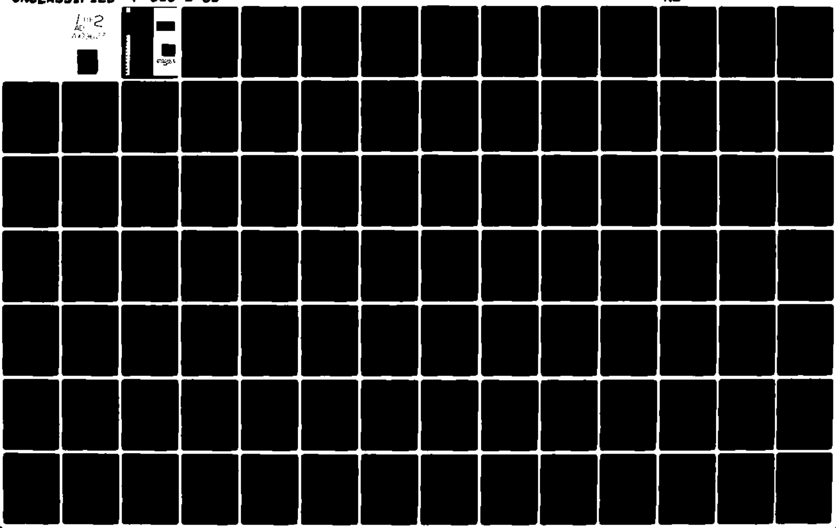

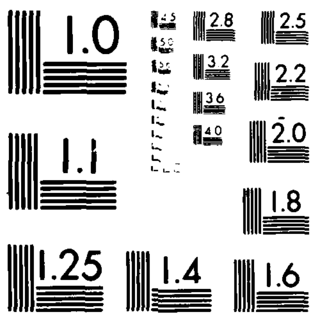

MICROCOPY RESOLUTION TEST CHART

NATIONAL BUREAU OF STANDARDS 1963 A

(12)

AD A109627

OPERATIONS RESEARCH

SYSTEMS ENGINEERING

SYSTEMS ANALYSIS

OCEAN SCIENCES

SIMULATION

ANALYTICAL MODELING

COMPUTER SCIENCES

82 01 13 071

ANALYSIS & TECHNOLOGY INC.

ANALYSIS & TECHNOLOGY

TARGET MOTION ANALYSIS WITH *A PRIORI* INFORMATION

Analysis & Technology, Inc.
Report No. P-515-2-81

Contract N00014-80-C-0379
Task Number (NR 274-302)

19 October 1981

Prepared by:

Clare B. Billing, Jr.
Harold F. Jarvis, Jr.

Approved by: T. M. Downie

T. M. Downie, Manager
Systems Research &
Analysis Dept.

Prepared for:

Office of Naval Research
800 No. Quincy Street
Arlington, VA 22217
(Attn: Mr. James G. Smith, Code 411 S&P)

Analysis & Technology, Inc. — Technology Park, P. O. Box 220, North Stonington, Connecticut 06359 — (203) 599-3910

UNCLASSIFIED

SECURITY CLASSIFICATION OF THIS PAGE (When Data Entered)

REPORT DOCUMENTATION PAGE		READ INSTRUCTIONS BEFORE COMPLETING FORM
1. REPORT NUMBER	2. GOVT ACCESSION NO. AD-A109 627	3. RECIPIENT'S CATALOG NUMBER
4. TITLE (and Subtitle) TARGET MOTION ANALYSIS WITH *A PRIORI* INFORMATION		5. TYPE OF REPORT & PERIOD COVERED Final Report
		6. PERFORMING ORG. REPORT NUMBER P-515-2-81
7. AUTHOR(s) Clare B. Billing, Jr. Harold F. Jarvis, Jr.		8. CONTRACT OR GRANT NUMBER(s) N00014-80-C-0379
9. PERFORMING ORGANIZATION NAME AND ADDRESS Analysis & Technology, Inc. P.O. Box 220 North Stonington, CT 06359		10. PROGRAM ELEMENT, PROJECT, TASK AREA & WORK UNIT NUMBERS 65152N RO-145TW NR 274-302
11. CONTROLLING OFFICE NAME AND ADDRESS Office of Naval Research Arlington, VA 22217		12. REPORT DATE 19 October 1981
		13. NUMBER OF PAGES 122
14. MONITORING AGENCY NAME & ADDRESS(if different from Controlling Office)		15. SECURITY CLASS. (of this report) UNCLASSIFIED
		15a. DECLASSIFICATION/DOWNGRADING SCHEDULE N/A

16. DISTRIBUTION STATEMENT (of this Report)

Approved for Public Release;
Distribution Unlimited

17. DISTRIBUTION STATEMENT (of the abstract entered in Block 20, if different from Report)

18. SUPPLEMENTARY NOTES

19. KEY WORDS (Continue on reverse side if necessary and identify by block number)

20. ABSTRACT (Continue on reverse side if necessary and identify by block number)

The investigation of the value of incorporating *a priori* information into the TMA solution is continued in this study by computer simulations using an asymptotically optimum estimation procedure. Two modifications to the Maximum Likelihood and Maximum *A Posteriori* estimation methods for bearings-only TMA are examined with a view toward their capability to improve numerical

DD FORM 1473 1 JAN 73 EDITION OF 1 NOV 65 IS OBSOLETE
S/N 0102-014-6601

UNCLASSIFIED

SECURITY CLASSIFICATION OF THIS PAGE (When Data Entered)

4 176

convergence of the solution during early parts of the problem. The modifications are made to develop procedures which optimally use all available measurements and information and to determine the true value of *a priori* information incorporated into an optimum procedure. The Gauss-Newton algorithm employed is modified such that at each solution iteration an optimum step is taken along the calculated direction. This is accomplished by a line-search minimization of the cost function (logarithm of the *a posteriori* density function). The previous procedure iterated towards a null in the linearized gradient of the density function using only step-size bounds. The other modification examined is the estimation of an observable (three-state) relative-motion solution during the first leg which is then combined with *a priori* information to obtain the full solution after a maneuver. In addition to the study of the above modifications, multisensor MLE and MAP procedures are developed which solve the TMA problem using bearing and frequency measurements without own-ship maneuvers. Simulations are run to ascertain the impact of range, speed, and center frequency *a priori* information on the numerical convergence and solution accuracy of the multisensor algorithm.

The modified Gauss-Newton algorithm with optimum step-size calculation improves numerical convergence for both the MLE and MAP solutions. However, the use of *a priori* range estimates does further increase the probability of convergence as well as decrease the number of iterations required, especially during periods of poor observability. In addition, the modified procedure does provide significant improvement in course and speed solution accuracy during periods of poor observability when *a priori* range estimates are included. The three-state relative-motion problem provides an observable solution which consistently converges with little cost during the first TMA leg when the full solution is not observable. However, when coupled with *a priori* range and speed information and post-maneuver measurements during the second leg, it does not significantly improve numerical convergence or solution accuracy over the zero speed initialization. The numerical convergence and solution quality of the multisensor bearing/frequency algorithm is in general improved by the use of range, speed, and center frequency *a priori* information. This is particularly so for the cases and periods with low observability and for the use of accurate center frequency estimates.

TABLE OF CONTENTS

TABLE OF CONTENTS (Cont'd)

LIST OF ILLUSTRATIONS

LIST OF ILLUSTRATIONS (Cont'd)

LIST OF ILLUSTRATIONS (Cont'd)

LIST OF ILLUSTRATIONS (Cont'd)

LIST OF TABLES

ABSTRACT

The investigation of the value of incorporating *a priori* information into the TMA solution is continued in this study by computer simulations using an asymptotically optimum estimation procedure. Two modifications to the Maximum Likelihood and Maximum *A Posteriori* estimation methods for bearings-only TMA are examined with a view toward their capability to improve numerical convergence of the solution during early parts of the problem. The modifications are made to develop procedures which optimally use all available measurements and information and to determine the true value of *a priori* information incorporated into an optimum procedure. The Gauss-Newton algorithm employed is modified such that at each solution iteration an optimum step is taken along the calculated direction. This is accomplished by a line-search minimization of the cost function (logarithm of the *a posteriori* density function). The previous procedure iterated towards a null in the linearized gradient of the density function using only step-size bounds. The other modification examined is the estimation of an observable (three-state) relative-motion solution during the first leg which is then combined with *a priori* information to obtain the full solution after a maneuver. In addition to the study of the above modifications, multisensor MLE and MAP procedures are developed which solve the TMA problem using bearing and frequency measurements without own-ship maneuvers. Simulations are run to ascertain the impact of range, speed, and center frequency *a priori* information on the numerical convergence and solution accuracy of the multisensor algorithm.

The modified Gauss-Newton algorithm with optimum step-size calculation improves numerical convergence for both the MLE and MAP solutions. However, the use of *a priori* range estimates does further increase the probability of convergence as well as decrease the number of iterations required, especially during periods of poor observability. In addition, the modified procedure does provide significant improvement in course and speed solution accuracy during periods of poor observability when *a priori* range estimates are included. The three-state relative-motion problem provides an observable solution which consistently converges with little cost during the first TMA

leg when the full solution is not observable. However, when coupled with *a priori* range and speed information and post-maneuver measurements during the second leg, it does not significantly improve numerical convergence or solution accuracy over the zero speed initialization. The numerical convergence and solution quality of the multisensor bearing/frequency algorithm is in general improved by the use of range, speed, and center frequency *a priori* information. This is particularly so for the cases and periods with low observability and for the use of accurate center frequency estimates.

CHAPTER I
INTRODUCTION AND OBJECTIVES

Classical Target Motion Analysis (TMA) from a time series of sensor measurements involves estimating a target track which best fits the measurement sequence according to some criteria of optimality. When the measurements are accurate and sufficiently robust to ensure existence of a unique solution, the problem can usually be solved in a timely manner using a variety of automatic and/or manual techniques. In many cases of interest, measurements are not sufficiently accurate and/or not uniquely definitive to arrive at a complete solution. In those cases, solutions based solely on sensor measurements may not converge or may require observation intervals that are tactically unacceptable. The addition of *a priori* information or physical constraints may provide tactically useful estimates when the solution is not directly observable from only the measurements. This *a priori* information may take the form of discrete multiple range and/or speed estimates along with some assessment of the uncertainty in the estimates. These estimates may be obtained from acoustic performance prediction, auxillary measurements (e.g., turn count) or from physical constraints.

This study continues an investigation (reported in Reference 4) of the value of incorporating *a priori* information into a TMA solution. Several statistical and empirical techniques exist for solving the TMA problem which can incorporate *a priori* information in some manner. Among the statistical techniques, the Extended Kalman Filter (EKF) and Maximum Likelihood Estimate (MLE) are most attractive from a computation viewpoint. Of the two methods, the EKF has a much smaller computational burden but suffers from errors caused by "boot strap" linearization. For this reason, the MLE was selected as the baseline TMA algorithm. This is generalized to a Maximum *A Posteriori* (MAP) estimate by incorporating the probability density function (p.d.f.) of the *a priori* estimates. When the *a priori* p.d.f.s are multi-modal (as in the case of discrete range bands obtained from acoustic performance prediction), the problem is segmented into parallel solutions for each mode. The parallel solutions are continued until incorrect alternatives can be dismissed.

The previous study (Reference 4) investigated the potential value of incorporating external information such as range, target speed and vertical arrival angle (D/E) into the bearings-only TMA problem. The formulation of the TMA algorithm was based on an MLE method modified to incorporate the external information as *a priori* estimates of the TMA solution with statistical uncertainty. This Maximum *A Posteriori* Probability (MAP) estimate and the original MLE, although not optimum in a minimum estimation error sense, are asymptotically optimum as the data base increases without bound. The evaluation approach taken was the direct simulation of both the MAP and MLE algorithms using common initialization to determine the specific impact of the *a priori* information on an "optimal" bearings-only TMA algorithm. The *a priori* range information was treated as multiple bands of possible target range representing the likely propagation paths. The speed information was unimodal with various assumed uncertainty. The results of Monte Carlo simulations indicated that:

1. *A priori* range information did not provide the expected improvement in solution performance over a solution procedure that used the range information as initial estimates, but it did improve the numerical convergence of the iteration technique.

2. *A priori* speed information did improve both solution performance and numerical convergence.

3. *A priori* range information with D/E estimates based on assumed propagation path substantially improved the solution performance for conical-angle measurement (i.e., from a line or towed array), although more refined estimates would be beneficial.

Since the principal benefits derived from the use of *a priori* information were found to be associated with the numerical convergence properties of the algorithm, work was continued to explore this aspect in more detail. It was conjectured that the algorithms previously studied may not optimally use the *a priori* information during the first several TMA legs where there is poor observability. In addition, although at each numerical iteration a step size

limit was used to aid solution stability, optimum (in terms of maximum *a posteriori* probability) steps were not used. Because of the large computation expense incurred when numerical convergence is poor early in the TMA problem time, it is desirable to explore ways of optimally utilizing all available information. The objectives of this study are therefore:

1. Determine whether convergence probability and/or execution time of the MLE and MAP algorithms are improved by the use of an optimum step size calculation at each solution iteration.

2. Determine the value, with respect to solution convergence and accuracy, of utilizing procedures early in the solution to extract only observable information.

3. Determine the value of *a priori* range and target speed information optimally incorporated into the improved algorithms.

4. Address the value of *a priori* information in a multisensor configuration (e.g., bearing and frequency measurements).

The first two areas address improving solution performance during times when measurements do not support complete, bearings-only TMA solutions. These "improvements" were incorporated into both the MLE and MAP algorithms. The first approach involves addition of a line search along the calculated step direction. The optimum step size is determined at each iteration. In the second approach, a three-state solution is implemented (in the bearings-only TMA algorithms) during the first leg where the full solution is not observable. After a maneuver, the observable solution components are optimally combined with any *a priori* information and subsequent bearing measurements to solve the full four-state problem. A multisensor bearing/frequency TMA algorithm is developed and evaluated using the measurements without ownship maneuvers. The influence of *a priori* information on numerical convergence time reduction and solution accuracy improvement is investigated.

These study areas should provide benchmark results covering many of the problem areas associated with current TMA systems. The emphasis throughout is placed on determining the value of external information on automatic TMA solution algorithms. As in the previous study, the computer simulations are based on 30 Monte Carlo repetitions. The geometries simulated are typical submarine maneuvering sequences. The magnitude of bearing errors used are representative of many passive sonar systems.

CHAPTER II

MATHEMATICAL ALGORITHMS AND NUMERICAL APPROACHES EMPLOYED

2.0 PROBLEM FORMULATION AND THE MAXIMUM LIKELIHOOD ESTIMATION ALGORITHM

The basic target localization/motion analysis problem is formulated, as in the previous study, in horizontal Cartesian coordinates on a North-East reference frame. The TMA solution, assuming a target with constant course and speed, is completely defined by the four-dimensional state vector, $\underline{x}(t_k)$, at some time, t_k, along with its state or position keeping (PK) equations.

$$\underline{x}(t_k) \equiv \begin{bmatrix} x_1(t_k) \\ x_2(t_k) \\ x_3 \\ x_4 \end{bmatrix} = \begin{bmatrix} \text{target position East of origin at } t_k \\ \text{target position North of origin at } t_k \\ \text{East component of target velocity} \\ \text{North component of target velocity} \end{bmatrix} \tag{1}$$

$$\underline{x}(t_k) = \phi_k x(t_0); \; \phi_k = \begin{bmatrix} 1 & 0 & t_k - t_0 & 0 \\ 0 & 1 & 0 & t_k - t_0 \\ 0 & 0 & 1 & 0 \\ 0 & 0 & 0 & 1 \end{bmatrix} \tag{2}$$

The solution is equivalently represented (at a given time) relative to own ship by the target range (R), course (C_T), speed (V_T) and bearing (β), which, in turn, are functions of $\underline{x}(t_k)$.

$$R(t_k) = \left[(x_1(t_k) - x_{os_1}(t_k))^2 + (x_2(t_k) - x_{os_2}(t_k))^2\right]^{\frac{1}{2}} \tag{3}$$

$$C_T = \tan^{-1}\left(\frac{x_3}{x_4}\right) \tag{4}$$

$$V_T = (x_3^2 + x_4^2)^{\frac{1}{2}} \tag{5}$$

$$\beta(t_k) = \tan^{-1}\left[\frac{x_1(t_k) - x_{os_1}(t_k)}{x_2(t_k) - x_{os_2}(t_k)}\right] \tag{6}$$

$\underline{x}_{os}(t_k)$ is the own-ship Cartesian state vector at time t_k.

The TMA solution algorithms studied are the Maximum Likelihood Estimator (MLE) and Maximum *A Posteriori* (MAP) statistical estimation procedures. For the bearings-only case with *a priori* information, this amounts to determining the state estimate $\hat{x}$ which minimizes the cost function defined as the negative logarithm of the joint *a posteriori* probability density function for the measurement sequence $\beta_m(t_k)$, k=1, N. That is

$$\nabla_{\underline{x}} J^N \Big|_{\underline{x}=\hat{\underline{x}}} = \underline{0} \tag{7}$$

where

$$J^N = \sum_{k=1}^{N} \frac{(\beta_m(t_k) - \hat{\beta}(t_k))^2}{2\sigma_{\beta_k}^2(t_k)} + \frac{(\hat{R}(t_0) - \overline{R}_0)^2}{2\sigma_R^2} + \frac{(\hat{V}_T - \overline{V}_0)}{2\sigma_V^2} \tag{8}$$

and where $\overline{R}_0$, $\overline{V}_0$ are the *a priori* values of range and target speed with assumed Gaussian uncertainties σ_R, σ_V. The details of this formulation, as well as the Gauss-Newton numerical procedure for its solution, are described in Appendix A of the previous study report (Reference 4).

The essence of the Gauss-Newton method used previously and modified in the present study involves a numerical iteration sequence to solve Equation (7) and thereby achieve a local minimum of the function J^N. The standard iteration algorithm obtained by expanding the gradient in a multidimensional Taylor series about a previous or initial solution $\hat{\underline{x}}^{\ell}(t_k)$ is:

$$\hat{\underline{x}}^{\ell+1}(t_k) = \hat{\underline{x}}^{\ell}(t_k) + a[\psi^{\ell}]^{-1}\underline{Y}^{\ell};\ 0 < a \leq 1 \tag{9}$$

where "a" is the scalar step size of the iteration, $\underline{\gamma}^{\ell}$ is the gradient vector of J^N at $\hat{\underline{x}}^{\ell}(t_k)$ and ψ^{ℓ} is the expected value of the second partial (or Hessian) matrix of J^N at $\hat{\underline{x}}^{\ell}(t_k)$.

$$\underline{\gamma}^{\ell} = \nabla_{\underline{x}^{\ell}} J^N \tag{10}$$

$$\psi^{\ell} = E\left[\nabla_{\underline{x}^{\ell}} \nabla^T_{\underline{x}^{\ell}} J^N\right] \tag{11}$$

ψ^{ℓ} is also Fisher's Information Matrix for the estimation problem, and its inverse represents a lower bound on the covariance matrix of the solution when evaluated at the true solution. Equation (9) is solved by Gaussian elimination at each iteration step until a stopping criterion, based on the normalized magnitude of the vector $\hat{\underline{x}}^{\ell+1}(t_k) - \hat{\underline{x}}^{\ell}(t_k)$, is satisfied. The derivations for the calculation of $\underline{\gamma}^{\ell}$ and ψ^{ℓ} and of the solution $\hat{\underline{x}}(t_k)$ at each time step are given, as well, in Appendix A of Reference 4.

The present study investigates two modifications to the previously used Gauss-Newton algorithm for the MLE/MAP solution for bearings only TMA. An optimum step size, a, is calculated at each iteration of Equation (9) along the calculated Gauss-Newton step $([\psi^{\ell}]^{-1}\underline{\gamma}^{\ell})$. The previous procedure merely limited the magnitude of the solution step of each Gauss-Newton iteration. In the second approach, a three-state relative motion solution is implemented during the first leg, where the full solution is theoretically unobservable, of the bearings-only TMA problem. In addition, a method for bearing/frequency multisensor TMA is developed and evaluated without own-ship maneuvers using the same numerical approaches.

2.1 OPTIMUM STEP SIZE CALCULATION

During the previous study, the step size for each solution iteration (Equation 9) was limited to a physically appropriate maximum size. This was done to facilitate convergence by not allowing the solutions to make wild

oscillations by continually overshooting the optimization surface minimum due to poor observability (shallow minima) or linearization errors in the solution calculation. The solution step was normally selected as the Gauss-Newton correction vector (with a=1), unless its normalized vector magnitude was greater than some predetermined limit, in which case the correction was reduced to meet the limit, i.e.,

$$a = \begin{cases} 1 \text{ if } \varepsilon^2 \leq W^2 \\ \sqrt{\dfrac{W^2}{\varepsilon^2}} \text{ otherwise} \end{cases} \tag{12}$$

where

$$\varepsilon^2 \equiv (\underline{\hat{x}}^{\ell+1}(t_k) - \underline{\hat{x}}^{\ell}(t_k))^T \Sigma^{-1} (\underline{\hat{x}}^{\ell+1}(t_k) - \underline{\hat{x}}^{\ell}(t_k))$$

$$W^2 = \frac{\sigma_R^2}{\sigma_1^2} + \frac{\sigma_V^2}{\sigma_2^2}$$

and where

$$\Sigma = \begin{bmatrix} \sigma_1^2 & 0 & 0 & 0 \\ 0 & \sigma_1^2 & 0 & 0 \\ 0 & 0 & \sigma_2^2 & 0 \\ 0 & 0 & 0 & \sigma_2^2 \end{bmatrix}, \text{ and } \sigma_1, \sigma_2 \text{ are defined constant weights.}$$

The locus of points which generate a constant ε define a spheroid whose radius is σ_1 in the x_1, x_2 plane and σ_2 in the x_3, x_4 plane, and whose center is at the previous solution. The surface ε=1 therefore defines a small region about the previous iteration. When $\varepsilon^2 \leq 1$, the iteration process is assumed to be converged and $\underline{x}^{\ell+1}(t_k)$ is the final solution.

Although this step size limiting scheme did improve convergence, it also was found to reduce the advantage attributable to *a priori* information. To determine the extent to which the numerical procedure impacts the comparison,

it was decided to use an optimum step size calculation to determine the convergence properties for solutions obtained both with and without *a priori* information. The difference then should define more accurately the value of *a priori* information.

The optimization of the step size parameter "a" of Equation (9) is accomplished by a one-dimensional optimization (line search) along the Gauss-Newton direction, based on minimizing the cost function. Therefore, the optimum step size, a*, is that value of "a" between a_{min} and a_{max} which minimizes $J^N(a)$ along the direction on the optimization surface defined by the solution $[\psi^{\ell}]^{-1}\Upsilon^{\ell}$. The minimum is determined by the combination of a Fibinacci search and a quadratic fit to $J^N(a)$. The limits of search are

$$a_{min} = 1/\varepsilon$$

$$a_{max} = \begin{cases} 2, \text{ if } \frac{W}{\varepsilon} \geq 2 \\ W/\varepsilon, \text{ otherwise.} \end{cases} \tag{13}$$

The Fibinacci search reduces the interval containing the minimum to $1/4(a_{max} - a_{min})$ by comparing the value of J^N for selected intervals. The two end points and center value of this interval are then fitted to a quadratic function for which the minimum is calculated by

$$a^* = \frac{1}{2}\,\frac{J^N(a_1)(a_3^2 - a_2^2) + J^N(a_2)(a_1^2 - a_3^2) + J^N(a_3)(a_2^2 - a_1^2)}{J^N(a_1)(a_3 - a_2) + J^N(a_2)(a_1 - a_3) + J^N(a_3)(a_2 - a_1)} \tag{14}$$

which is the minimum of a quadratic function fitted by Lagrangian interpolation. The step size "a" to be used in the solution iteration is then

$$a = \begin{cases} a_{max}, \text{ if } a^* < a_{min} \text{ or } a^* > a_{max} \\ 1 \quad, \text{ if } a^* > 2 \text{ and } a_{max} > 1 \\ a^* \quad, \text{ otherwise.} \end{cases} \tag{15}$$

When convergence is achieved ($\varepsilon^2 < 1$), "a" is then calculated as the value minimizing J^N between $a_{min}=0$ and $a_{max}=2$ along the solution direction.

2.2 THREE-STATE SOLUTION

During the initial leg of bearings-only TMA, the full solution is not theoretically observable. Even during the first few legs, after one or two maneuvers, observability is poor, especially for convergence-zone ranges. To obtain useful information during the early stages of the solution when observability is poor, a three-parameter solution was calculated and used together with the *a priori* information to solve the full four-parameter problem. Three possible approaches that were considered are relative motion, constrained range and constrained speed. The relative motion solution was selected because it is directly applicable to both MLE and MAP methods. There is no subset of the four Cartesian coordinates which is directly observable without own-ship maneuvers. One can observe bearing and all derivatives of bearing at some reference time (t_0). A three-state solution which defines all observable information consists of bearing and a pair of orthogonal velocity components normalized by range. The velocity components which most naturally relate the derivatives of bearing are the cross range and down range velocities (i.e., $R\dot{\beta}$ and $\dot{R}$, respectively). In this formulation, the solution vector at time t_0 is

$$\underline{\eta}(t_0) \equiv \begin{bmatrix} \beta_0 \\ \dot{\beta}_0 \\ \dot{\rho}_0 \end{bmatrix}$$

where

$$\dot{\rho}_0 \equiv \dot{R}_0/R_0 \qquad (16)$$

The bearing acceleration at "t_0" is given by

$$\ddot{\beta}_0 = -2\dot{\beta}_0\dot{\rho}_0 \qquad (17)$$

Note that $\ddot{\beta}_0$ is not a suitable coordinate because the actual bearing time function is not representable by a quadratic polynomial. The three coordinates presented above allow exact extrapolation to any time (t) as long as neither ship maneuvers. The expression for bearing at any time (t_k) can be developed by simple geometry as

$$\beta(t_k) = \beta_0 + \tan^{-1}\left(\frac{\dot{\beta}_0 \Delta t_k}{1 + \dot{\rho}_0 \Delta t_k}\right)$$

$$\Delta t_k = t_k - t_0 \tag{18}$$

The normalized range at t_k is

$$\rho(t_k) = \frac{R(t_k)}{R_0} = \sqrt{(\dot{\beta}_0\ t_k)^2 + (1 + \hat{\rho}_0 \Delta t_k)^2} \tag{19}$$

Expressions for $\dot{\beta}(t_k)$ and $\dot{\rho}(t_k)$ can be obtained by differentiating Equations (18)and (19).

$$\dot{\beta}(t_k) = \dot{\beta}_0/\rho^2(t_k) \tag{20}$$

$$\dot{\rho}(t_k) = (\dot{\rho}_0 + (\dot{\beta}_0^2 + \dot{\rho}_0^2)\Delta t_k)/\rho^2(t_k) \tag{21}$$

Note that Equations (19) through (21) are not required to solve for $\hat{\underline{\eta}}(t_0)$ but allow one to extrapolate an estimate at "t_0" to any other time. The solution procedure for estimating the three-state solution ($\hat{\underline{\eta}}(t_0)$) is a three-state MLE algorithm using the modified Gauss-Newton iteration procedure. The gradient of $\hat{\beta}(t_k)$ with respect to $\eta(t_0)$ is readily shown to be

$$\nabla_{\underline{\eta}}\hat{\beta}(t_k) = \begin{bmatrix} 1 \\ \dfrac{\Delta t_k \cos \hat{\beta}(t_k)}{\hat{\rho}(t_k)} \\ -\dfrac{\Delta t_k \sin \hat{\beta}(t_k)}{\hat{\rho}(t_k)} \end{bmatrix} \tag{22}$$

With $\hat{\beta}(t_k)$, $\hat{\rho}(t_k)$ defined in Equations (18) and (19). Thus, the iteration equation for the relative motion solution is

$$\underline{\eta}^{\ell+1}(t_0) = \underline{\eta}^{\ell}(t_0) + a\underline{\Delta}\eta^{\ell} \tag{23}$$

where $\underline{\Delta}\eta^{\ell}$ is the solution of

$$\underline{\Upsilon}^{\ell} + \psi^{\ell}\underline{\Delta}\eta^{\ell} = 0 \tag{24}$$

with

$$\underline{\Upsilon}^{\ell} = -\frac{1}{\sigma_{\beta}^{2}} \sum_{k=0}^{N} (\beta_m(t_k) - \hat{\beta}(t_k))\nabla_{\underline{\eta}}\hat{\beta}(t_k) \tag{25}$$

and

$$\psi = \frac{1}{\sigma_{\beta}^{2}} \sum_{k=0}^{N} \nabla_{\underline{\eta}}\hat{\beta}(t_k)\nabla_{\underline{\eta}}^{T}\hat{\beta}(t_k). \tag{26}$$

"a" is the optimum step size weight calculated using the procedure developed for the full solution. The iterations continue until $\epsilon^2 < 1$ or the maximum number of iterations is reached.

$$\epsilon^2 = \frac{(\Delta\hat{\beta})^2}{3\sigma_1^2} + \frac{(\Delta\hat{\dot{\beta}})^2 + (\Delta\hat{\dot{\rho}})^2}{3\sigma_2^2} \tag{27}$$

with

$$\sigma_1 = .01°$$

$$\sigma_2 = \sigma_1/T$$

The relative motion solution continues until own ship maneuvers. At that time, the relative motion solution is combined with *a priori* information to generate a four-state initialization solution. The relationships between the relative motion solution, target speed and target range at time t_k is a function of initial range (R_0).

$$R(t_k) = R_0\sqrt{(1 + \dot{\rho}_0\Delta t_k)^2 + (\dot{\beta}_0\Delta t_k)^2} \tag{28}$$

$$V^2 = (R_0\dot{\beta}_0 - V_{os}\sin(\beta_0 - C_0))^2 + (R_0\dot{\rho}_0 - V_{os}\cos(\beta_0 - C_0))^2 \tag{29}$$

The MAP solution can be optimized directly, since $\hat{\underline{\eta}}$ minimizes the sum squared bearing residuals for any value of R_0. Then one can find the value of $\hat{R}_0$ which minimizes the *a priori* terms in the cost function subject to the constraint of Equation (29). Let

$$J_{a\ priori} = \frac{(\hat{R}_0 - \overline{R}_0)^2}{2\sigma_{R_0}^2} + \frac{(\hat{V} - \overline{V})^2}{2\sigma_{V_0}^2} \tag{30}$$

where $\overline{R}_0$ and $\overline{V}$ are *a priori* estimates of range and speed and σ_{R0}^2 and σ_{V0}^2 are the respective variances of the estimates. Using Equation (29), $\hat{V}$ can be explicitly defined as a function of $\hat{R}_0$ so the minimization is a one-dimensional problem. When *a priori* speed measurements are available, the minimization must be performed numerically. When only range information is available, then $\overline{V}$=0 and σ_V represent a physical constraint on practical target speeds. In that case, the optimum range estimate is

$$\hat{R}_0 = \bar{R}_0 \left[\frac{1 - \left(\frac{\sigma_{R_0}}{\bar{R}_0}\right)^2 \left(\frac{V_{os}}{\sigma_{V_0}}\right) \left(\frac{\bar{R}_0 \hat{\dot{\rho}}_0 \cos(\hat{\beta}_0 - C_0) - \bar{R}_0 \hat{\dot{\beta}}_0 \sin(\hat{\beta}_0 - C_0)}{\sigma_{V_0}}\right)}{1 + \left(\frac{\sigma_{R_0}}{\bar{R}_0}\right)^2 \left(\frac{(\bar{R}_0 \hat{\dot{\beta}}_0)^2 + (\bar{R}_0 \hat{\dot{\rho}}_0)^2}{\sigma_{V_0}^2}\right)} \right] \tag{31}$$

This procedure generates an initial solution for the second leg of the TMA problem, which is based on solving for the information observable from the bearing data using a modified Gauss-Newton MLE algorithm, which is then optimally combined with *a priori* information to generate a complete solution. This procedure should provide the optimum solution available from the first leg if the *a priori* model is correct. Since the relative motion solution is independent of range, it is common to all propagation path assumptions. If the combination of relative solutions with *a priori* range is performed for all path assumptions, it may be possible to determine the correct path by examining the speed estimates given by Equation (29). This would depend on geometry and bearing accuracy. For example, a high bearing rate, direct-path geometry would be distinguishable from a convergence zone but a closing geometry may not resolve the correct path.

2.3 BEARING AND FREQUENCY MULTISENSOR TMA

For bearings-only problems, own ship must maneuver to obtain a full TMA solution. When additional measurements are available, such as range rate (from Doppler analysis of frequency measurements) or bearings from another array, it may not be necessary to maneuver. Convergence without maneuvers, however, may be too slow for tactical considerations, and thus the use of *a priori* information can potentially be of value in reducing solution convergence time. This aspect of the problem can be investigated by TMA simulations using the MLE and MAP algorithms modified to accept multisensor data. Note that maneuvers were not precluded for this case but were not considered because the problem would be similar to the bearings-only problem. Also, they did not provide additional insight to the value of *a priori* information.

An algorithm for the solution of a bearing/frequency multisensor TMA is developed using the MLE/MAP approach. The problem formulation is the same as that for the bearings-only case, i.e., a four-state horizontal solution in Cartesian coordinates, except that frequency measurements are used along with bearings, and the test runs are made without own-ship maneuvers. There are five solution parameters since the base frequency (f_0) (without Doppler shift) must be estimated. A procedure is developed in the Appendix to optimize $\hat{f}_0$ as an explicit function of the estimated range rate (a function of the state solution), the frequency measurements and the *a priori* estimate of f_0. The value of incorporating *a priori* knowledge of f_0 is therefore evaluated along with that of range and speed.

The development of the computations for the bearing/frequency MLE (or more specifically MAP) approach with *a priori* knowledge of the base frequency is given in the Appendix. The MAP algorithm using additional *a priori* information (range and speed) is formed by incorporating into the *a priori* probability density function (p.d.f.), developed in the Appendix, the appropriate *a priori* p.d.f.s. This results, as in the bearings-only case, in additive terms in the log likelihood ratio for the state vector:

$$J'_{LR} = J_{LR} + \frac{1}{2\sigma^2_{\hat{R}}}(\hat{R}(t_0) - R_0)^2 + \frac{1}{2\sigma^2_{\hat{V}}}(\hat{V}(t_0) - V_0)^2 \tag{32}$$

where J_{LR} is the log likelihood ratio (cost function) from Equation (20) of the Appendix.

The first and second gradients of J'_{LR} with respect to the reference state vector $\underline{x}(t_0)$ are required for the Gauss-Newton solution procedure. The calculations for the gradients of J_{LR} are derived in the Appendix. The gradient calculations for the range and velocity *a priori* terms are the same as in the bearings-only algorithm except for the second gradient of the *a priori* velocity term. When speed is unknown *a priori* but is bounded by physical constraints, the speed estimate is zero and the sigma represents an average speed (or one-half of the maximum speed). The *a priori* velocity term in Equation (32) would be

$$J_{\underline{V}_0} = \frac{\hat{V}^2(t_0)}{2\sigma^2_{V_0}} = \frac{\hat{x}_3^2(t_0) + \hat{x}_4^2(t_0)}{2\sigma^2_{V_0}} \tag{33}$$

The second gradient of $J_{\underline{V}_0}$ is then

$$\nabla_{\underline{x}(t_0)} \nabla^T_{\underline{x}(t_0)} \left[\frac{\hat{V}^2(t_0)}{2\sigma^2_{\hat{V}}} \right] = \begin{bmatrix} 0 & 0 \\ 0 & \frac{I}{\sigma^2_{\hat{V}}} \end{bmatrix} \tag{34}$$

where I is the 2x2 identity matrix. This expression for the second gradient is unfortunately not consistent with that used in the bearings-only cases. The expression presented in the previous study was developed for use with *a priori* speed estimates and does not collapse to the correct expression when *a priori* speed is not available. Fortunately, the speed term does not affect the solution in that case, when only bearing inputs are observed. For bearing and frequency observations, the frequency measurements are related to velocity and it was found that the velocity components of the ψ matrix formed a singular matrix when the incorrect second gradient was used. This did not occur with the bearings-only inputs. During investigation of this problem, it became apparent that MLE should be formulated (when no *a priori* information is available) by incorporating range and speed bounds in the cost function as

$$J'_{MLE} = J_{MLE} + \frac{\hat{R}^2(t_0)}{2R^2_{max}} + \frac{\hat{V}^2(t_0)}{2V^2_{max}} \tag{35}$$

Where R_{max} and V_{max} are chosen to bound the expected range and speed. This form would lead to a ψ matrix of the form

$$\psi = \psi_{MLE} + \begin{bmatrix} \frac{1}{R^2_{max}} I & 0 \\ 0 & \frac{1}{V^2_{max}} I \end{bmatrix} \tag{36}$$

This would have the properties of the Marquardt Gauss-Newton algorithm using a physical constraint. This procedure was not evaluated but it will guarantee a positive definite ψ matrix and will not bias the solution if R_{max} and V_{max} are chosen correctly.

CHAPTER III
SIMULATED TMA SCENARIOS

3.0 OPERATIONAL SCENARIOS

The operational scenarios simulated for the present study are basically the same as those described in the previous report (Reference 4). Own ship to target ranges from 10 to 109 kiloyards were modeled covering direct, first and second convergence zone (CZ) acoustic propagation paths. The acoustic propagation properties assumed are realistic, yet general enough to represent many different oceanographic conditions. The target-ship courses used, which remained constant over a given run, were 146 degrees and 256 degrees. These present an initial broadside (crossing) and closing aspect, respectively. Table 3-1 summarizes the propagation paths and initial true target ranges as well as the initial range estimates and standard deviations used in the TMA computer simulations.

Table 3-1. True and Assumed Acoustic Propagation Paths and Range Values

TARGET COURSE (deg)	PROPAGATION PATH	TRUE PATH RANGE (kyd)	TRUE TARGET RANGE (kyd)	ASSUMED RANGE (kyd)	σ_{R_0} (kyd)
256 (closing)	Direct	0-30	10, 20	15	7.5
	1st CZ	45-55	54	45	4.5
	2nd CZ	90-110	109	90	9
146 (crossing)	Direct	0-30	10, 20	15	7.5
	1st CZ	45-55	46	55	5.5
	2nd CZ	90-110	91	110	11

Initial true bearing was 56 degrees for all runs. Own ship had an initial bearing of 0 degrees and maneuvers consisting of standard 60-degree lead/60-degree lag with leg times of 5 minutes duration and turn rate of 2 degrees per second. Both own ship and target maintained a constant speed of 10 knots.

3.1 SIMULATIONS

Simulations were run in three phases. These were the bearings-only case with optimum step size calculation, the bearings-only case with a three-state relative motion solution during the initial TMA leg, and the bearing/frequency multisensor case with no own-ship maneuvers. Each simulation of all three phases was run with 30 Monte Carlo repetitions, and with run times of 15 minutes for direct-path true range and 30 minutes for the CZ true range cases. Measurements of bearing or bearing and frequency were input to the TMA problem every 20 seconds, and solutions calculated by the MLE or MAP algorithm every minute. Bearing measurement error for the 20-second averages was unbiased with $\sigma_\beta = 0.2$ degrees for all but a few of the bearings-only runs which had $\sigma_\beta = 0.5$ degrees. Frequency measurements were expressed as normalized Doppler shifted values of the true center frequency ($f_0 \equiv 1$) using the true simulated range rate values. The frequency measurement error standard deviations (σ_{f_m}) were 10^{-3} and 10^{-4}, again normalized by the center frequency. The noise component of each measurement time series was simulated from a Gaussian pseudo-random number generator, with an independent sequence used for each Monte Carlo repetition.

3.2 *A PRIORI* ESTIMATES

Initial values for range, speed and center frequency with uncertainties were defined for use as solution initialization and *a priori* estimates. The *a priori* range values and uncertainties assumed in the various runs are listed in Table 3-1. Initialization for the position coordinates of the solution are calculated from these assumed range values and the first bearing measurement. The velocity terms are initialized as zero since no *a priori* course information is assumed. The assumed mean center frequency ($\overline{f}_0$) is taken as the true value for the *a priori* runs and as the first frequency measurement when no *a priori* knowledge is assumed. *A priori* values for velocity and center frequency with their uncertainties that were used in the simulations were:

Velocity: case 1) $\overline{V}_0 = 0;\ \sigma_{V_0} = 15$

2) $\overline{V}_0 = 10;\ \sigma_{V_0} = 4$

3) $\overline{V}_0 = 10;\ \sigma_{V_0} = 2$

Center Frequency: case 1) $\overline{f}_0 = 1;\ \sigma_{f_0} = 10^{-2}$

2) $\overline{f}_0 = 1;\ \sigma_{f_0} = 10^{-4}$

CHAPTER IV
DISCUSSION OF SIMULATION RESULTS

4.0 OVERVIEW OF RESULTS PRESENTED

The TMA scenarios described in the previous chapter were simulated with the overall objective of evaluating the importance of external information in achieving accurate and timely target motion solutions. The MLE and MAP procedures using the numerical algorithms derived in Chapter II were chosen as the methods to best demonstrate the potential utility of such information. The improvement attained by incorporating *a priori* statistical estimates of range, speed and center frequency is shown by comparing the solution results of Monte Carlo simulations using the MAP estimation procedure to those using the MLE. The MLE procedure uses the external information merely for initialization of the iterative numerical solution and not as part of the estimation.

The contribution of the *a priori* information to the bearings-only and bearing/frequency solutions is measured by the improved accuracy and reduced convergence time achieved. The measures of solution accuracy are obtained by calculating the mean and standard deviation of errors over the Monte Carlo repetitions. Measure of potential solution quality from the information available is obtained from the error bounds as calculated from the eigenvalues of the inverse Fisher's information matrix for the estimation problem. These error-bound estimates are the Cramer-Rao lower bounds on solution accuracy when evaluated at the exact solution. Solution convergence is defined as the reduction of the error bounds below some defined level. Improvement in numerical convergence is measured by the reduction of computational burden of the algorithm as represented by the number of Gauss-Newton iterations required for each solution. Numerical convergence probability is determined from the number of Monte Carlo repetitions at each solution time which do converge, defined by satisfying the stopping criteria within 21 iterations.

The results presented in this chapter are separated into three sections, based on the numerical procedure being evaluated. The first two sections present the results for evaluation of modifications to the bearings-only MLE/MAP algorithm which was developed in the previous study. Since the value of *a priori* information may be highly dependent on the particular numerical methods employed, improvements to the algorithms to most efficiently use all available information were studied. The effect of the numerical modifications on solution accuracy and convergence is, therefore, evaluated along with and within the context of the incorporation of *a priori* information. The numerical modifications studied are, respectively, calculation of an optimum step size at each Gauss-Newton iteration by a cost function line search and solution of a three-state, relative-motion problem during the first TMA leg. The third section presents results of simulations which were run to evaluate the incorporation of *a priori* information into a multisensor (bearing and frequency) MLE algorithm without own-ship maneuvers.

4.1 BEARINGS-ONLY MLE USING OPTIMUM STEP-SIZE CALCULATION

The results of the previous study's simulations indicated that the principal advantage of *a priori* range information is related to the numerical convergence of the solution procedure rather than its ultimate accuracy. Modification of the Gauss-Newton algorithm to improve numerical convergence without *a priori* information may therefore affect the observed value of incorporating such information into the algorithm. The Gauss-Newton algorithm used previously was modified, as described in Section 2.1, to optimize the step size taken at each iteration in the calculated direction with respect to the actual cost function. Previously, the step taken was the full solution step of the linearized optimization, subject only to a magnitude limit, without regard to the change in the actual cost function. It was conjectured that optimizing the step size would reduce the numerical convergence time of the algorithms, as well as improve the solution quality early in the problem. This, however, may in turn either negate any improvement previously provided by incorporation of *a priori* information or may enhance such improvement by more optimally using the available information.

The results of Monte Carlo simulation runs are presented using the modified Gauss-Newton procedure. The TMA scenarios simulated are as described in Chapter III and are the same as in the previous study. Both closing and crossing target aspects are analyzed with own ship executing maneuvers. For the direct-path case (range = 20 kiloyards) runs were made with assumed *a priori* ranges in the direct, first CZ and second CZ propagation paths. CZ runs have the same true and assumed paths. In addition, direct-path runs were made with true range of 10 kiloyards and assumed range in the direct path. One direct-path run was also made with bearing error standard deviation of 0.5 degree (all others were with σ_β = 0.2 degree). Additional first CZ runs were made including speed *a priori* information with estimate equal to the true target speed (10 knots) and standard deviations of 4 and 2 knots.

4.1.1 Preliminary Study of the Step-Size Optimization

Before considering the results of the Monte Carlo simulation runs, a preliminary analysis of cost function behavior versus step size and of its minimization is carried out. In addition, the computational cost for the inclusion of the step-size optimization procedure in the MLE algorithms is estimated. This estimate may be used to weigh any benefits from the procedure against its added cost.

The modified Gauss-Newton method solves the non-linear optimization problem with an iterative series of linearized solutions, calculated until satisfying a convergence criterion. The change in the solution at each iteration may be expressed as the vector difference between the previous solution and the present one. This solution update is given at each iteration by:

$$\underline{\Delta\hat{x}} = \alpha\underline{\Delta\hat{x}_0} = -\alpha\psi^{-1}\nabla_{\underline{x}}J \tag{1}$$

where $\underline{\Delta\hat{x}_0}$ is the solution vector calculated by the Gauss-Newton procedure as described in Section 2.1, and α is the magnitude of the step actually taken from the previous solution in the $\underline{\Delta\hat{x}_0}$ direction. Under the assumptions used

to ensure convergence of the modified Gauss-Newton procedure, the change in the cost function, ΔJ, may be modeled approximately as a quadratic function of the solution change vector using terms of the multidimensional Taylor series expansion

$$\Delta J = \nabla_{\underline{x}}^T J \underline{\Delta \hat{x}} + \frac{1}{2} \underline{\Delta \hat{x}}^T \nabla_{\underline{x}} \nabla_{\underline{x}}^T J \underline{\Delta \hat{x}} \tag{2}$$

This may then be expressed as a function of the step size, using Equation (1):

$$\Delta J = -\alpha \nabla_{\underline{x}}^T J \psi^{-1} \nabla_{\underline{x}} J + \frac{\alpha^2}{2} \nabla_{\underline{x}} J \psi^{-1} \nabla_{\underline{x}} \nabla_{\underline{x}}^T J \psi^{-1} \nabla_{\underline{x}} J$$

$$\Delta J = -\alpha \underline{\Delta \hat{x}}_0^T \psi \underline{\Delta \hat{x}}_0 + \frac{\alpha^2}{2} \underline{\Delta x}_0^T \nabla_{\underline{x}} \nabla_{\underline{x}}^T J \underline{\Delta \hat{x}}_0$$

$$\Delta J = \underline{\Delta \hat{x}}_0^T \psi \underline{\Delta \hat{x}}_0 \left(-\alpha + \frac{\alpha^2}{2} r\right) \tag{3}$$

where

$$r = \frac{\underline{\Delta \hat{x}}_0^T \nabla_x \nabla_x^T J \underline{\Delta x}_0}{\underline{\Delta \hat{x}}_0^T \psi \underline{\Delta \hat{x}}_0} \tag{4}$$

for $\alpha \epsilon [0, 1]$.

The step-size limiting procedure used in the previous study set α to a value between the limits of 0 and 1 based on a maximum allowable magnitude for $\underline{\Delta \hat{x}}$ defined by reasonable physical constraints. The modified procedure determines α by a numerical line search minimization of $J(\underline{\hat{x}},\alpha)$ at each iteration. This procedure may be modeled analytically by minimizing Equation (3) with respect to α. This yields

$$\alpha_{min} = \begin{cases} 1/r; & r > 1 \\ 1 & ; \text{otherwise} \end{cases} \tag{5}$$

when subject to the constraint $\alpha\epsilon[0,1]$. The actual procedure used, however, constrains the step size $\alpha\epsilon[\alpha_{min}, \alpha_{max}]$ where $\alpha_{min} > 0$ is the minimum step taken and $\alpha_{max} \leq 2$ is the step-size limit, whose values are determined as described in Section 2.1.

In preliminary runs of the algorithm in both the original and modified form, the behavior of $J(\alpha)$ was observed at several intervals along the calculated solution direction. These observations showed that at numerous iterations the minimum occurred at α's near to or less than zero. This was most prevalent before complete solution observability but also occurred later in the problem. Since the quadratic model above (Equations (2) through (4)) does not predict optimum solutions for $\alpha < 0$, this result reflects a domination by higher order, (unmodeled) terms indicating that $J(\alpha)$ is not approximately quadratic at the trial solution. In fact, if the "optimum" step is taken, the solution collapses to the previous solution. The calculated Gauss-Newton solution is therefore not always consistent with minimization of the cost function. To solve this problem, it was found that taking a limited step in the Gauss-Newton solution direction allowed eventual convergence even though the cost function was not minimized. This observation clearly shows the value of step-size limiting for solution stabilization. However, oscillation between poor solutions may still occur preventing early convergence. Step-size optimization should help convergence further by directing the Gauss-Newton solution towards consistency with the cost function minimum (except under the noted singular conditions). Minimization of the cost function in the vicinity of the converged solution may also improve solution accuracy, especially early in the problem when solution updates are large.

Inclusion of *a priori* information appears to stabilize the Gauss-Newton solution such that wild oscillation would not occur even without step-size limiting. This is clearly seen in the cost function values at and in the direction of the calculated solution. Optimization of step size would therefore not be expected to improve convergence of the MAP algorithm to the same extent that it would for the MLE. However, solution accuracy may be improved during the problem time before solution convergence in the same manner as without *a priori* information.

Estimates for the computation cost of the step-size optimization are made by running simulations for various problem times without the Monte Carlo statistics calculations. Cost estimates are in the form of computer processing (CPU) time. Although such estimates are approximate and the true cost may vary for different data sets and TMA conditions, as well as for different line search algorithms and codings, they may be helpful for rough comparisons between the added calculations' cost and any measured benefit. These test runs produced estimates for the added cost of the step-size calculations to the Gauss-Newton algorithm of 15 to 25 percent. In addition, these direct propagation path simulations indicated that the savings in computation time from better convergence of the modified algorithm did not make up for the added cost of the procedure. However, an enhanced quality of early solutions may be gained.

4.1.2 Numerical Convergence Properties of the Modified Gauss-Newton Algorithm

The numerical convergence properties of the modified bearings-only algorithm are shown in Figures 4-1 through 4-9 for all TMA geometries simulated. The number of Monte Carlo repetitions, out of the 30 run, which meet the numerical convergence criterion are plotted for each calculation time along with the average number of Gauss-Newton iterations required for convergence. These measurements represent, respectively, the probability of obtaining a converged solution at each problem time and the computational requirement for convergence. In each figure, the MLE and MAP solution results are presented for cases assuming the correct propagation path and using a measurement bearing-error standard deviation of 0.2 degree. Results are presented for direct, first CZ and second CZ propagation path cases without use of *a priori* speed estimates. For the first CZ cases, results are also given for the MAP solution with *a priori* speed estimates with standard deviation of 4 and 2 knots (Figures 4-6 and 4-7). Direct-path results are given for cases with initial true ranges of 20 and 10 kiloyards. The results from the use of the step-size limiting algorithm are also included for the direct-path, crossing-course case (Figure 4-2b). Comparison of the two procedures for the other

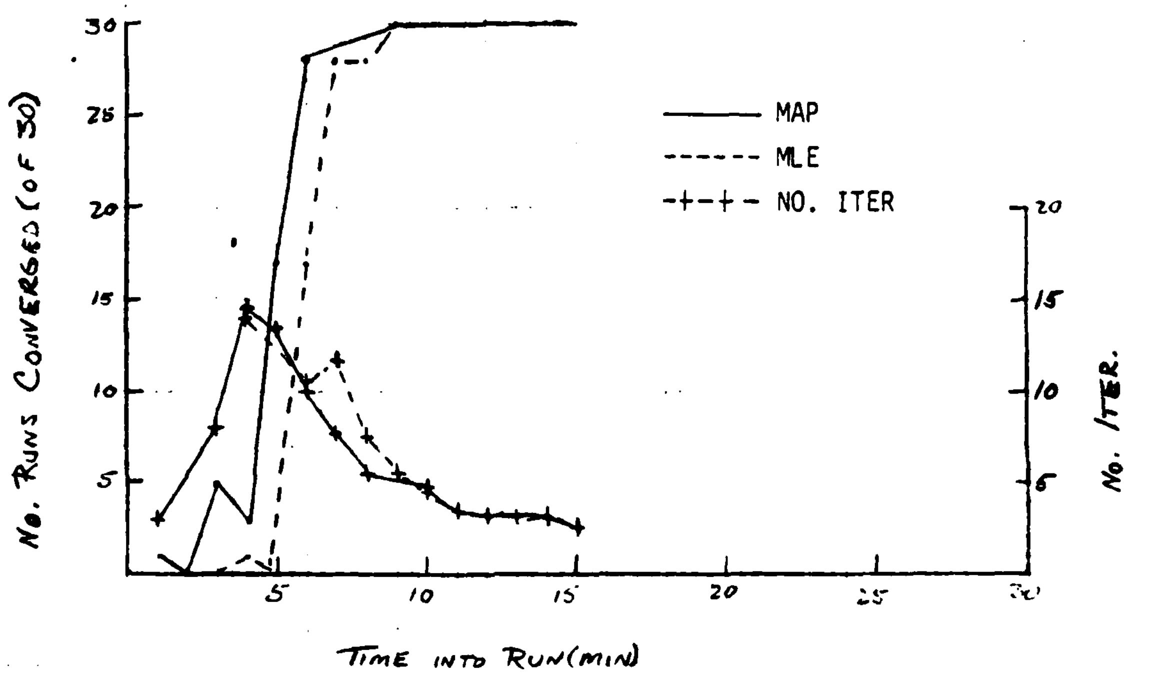

Figure 4-1. Convergence of Bearings-Only Algorithm With Optimum Step, Direct Path (20 kiloyards True Range), Closing Course

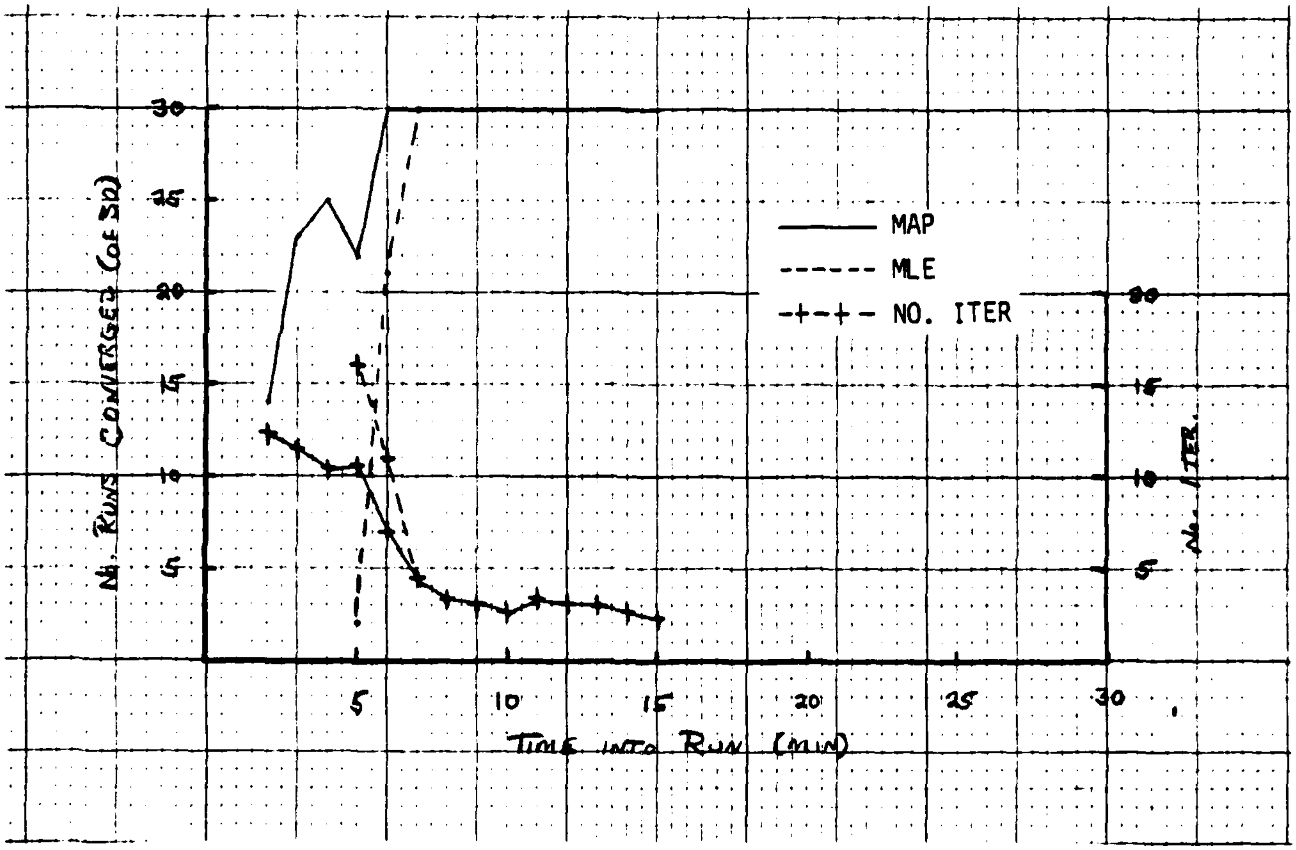

Figure 4-2a. Convergence of Bearings-Only Algorithm With Optimum Step, Direct Path (20 kiloyards True Range), Crossing-Target Course

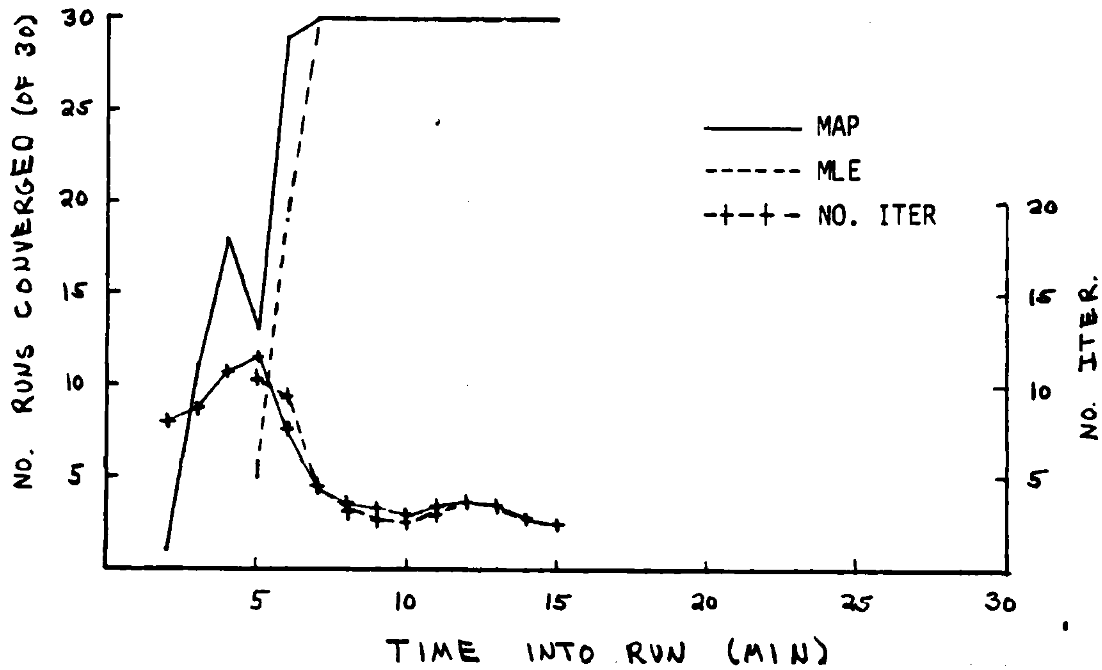

Figure 4-2b. Convergence of Bearings-Only Algorithm With Step-Size Limit, Direct Path (20 kiloyards True Range) Crossing-Target Course

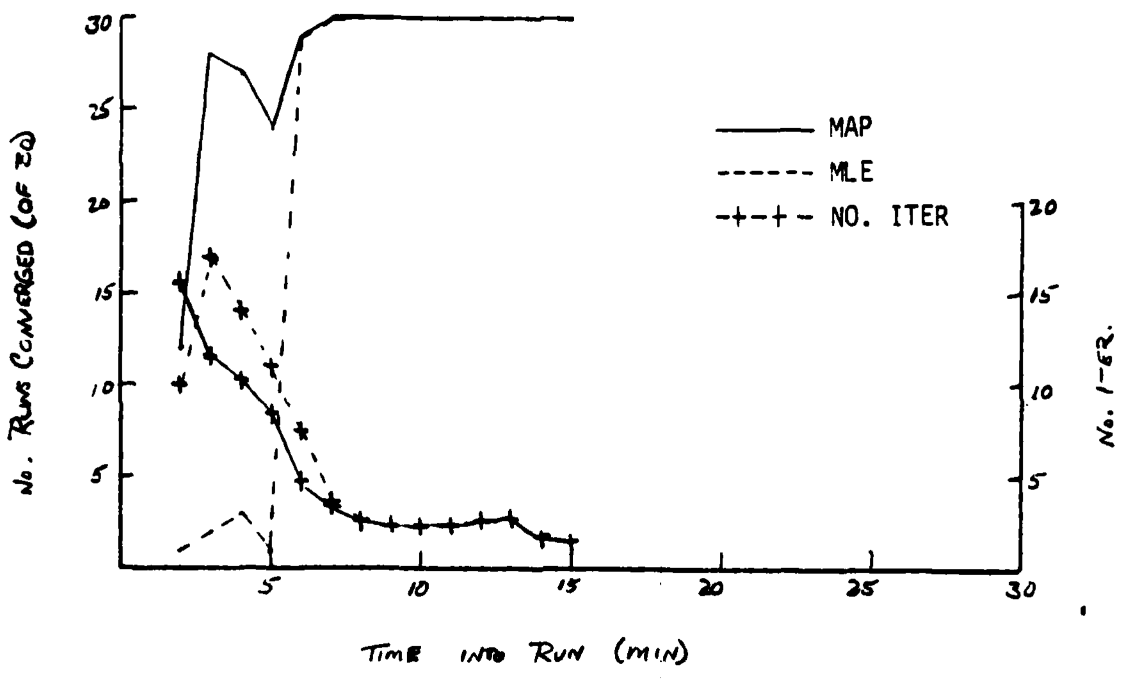

Figure 4-3. Convergence of Bearings-Only Algorithm With Optimum Step, Direct Path (10 kiloyards True Range), Crossing-Target Course

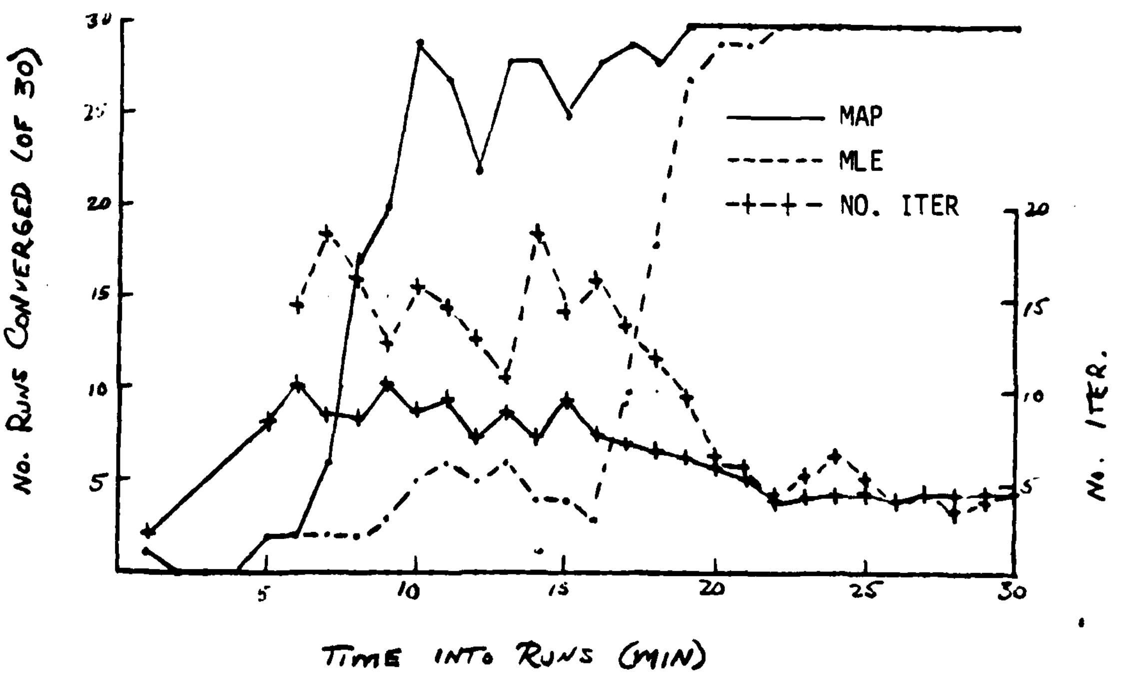

Figure 4-4. Convergence of Bearings-Only Algorithm With Optimum Step, First CZ Path, Closing-Target Course

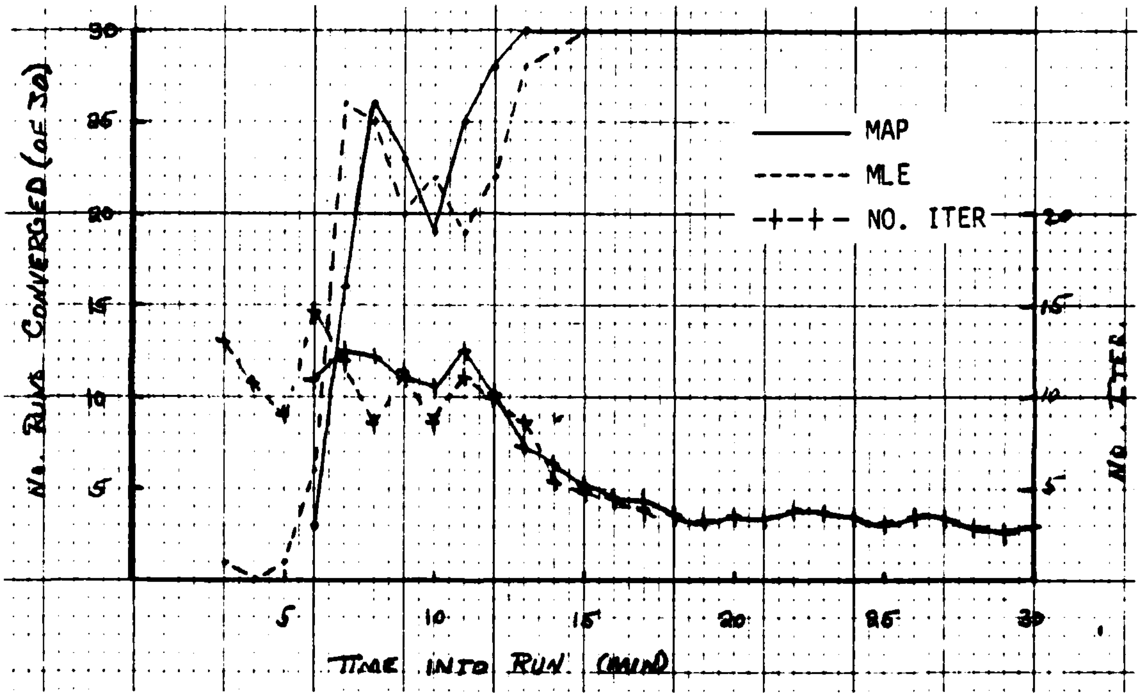

Figure 4-5. Convergence of Bearings-Only Algorithm With Optimum Step, First CZ Path, Crossing-Target Course

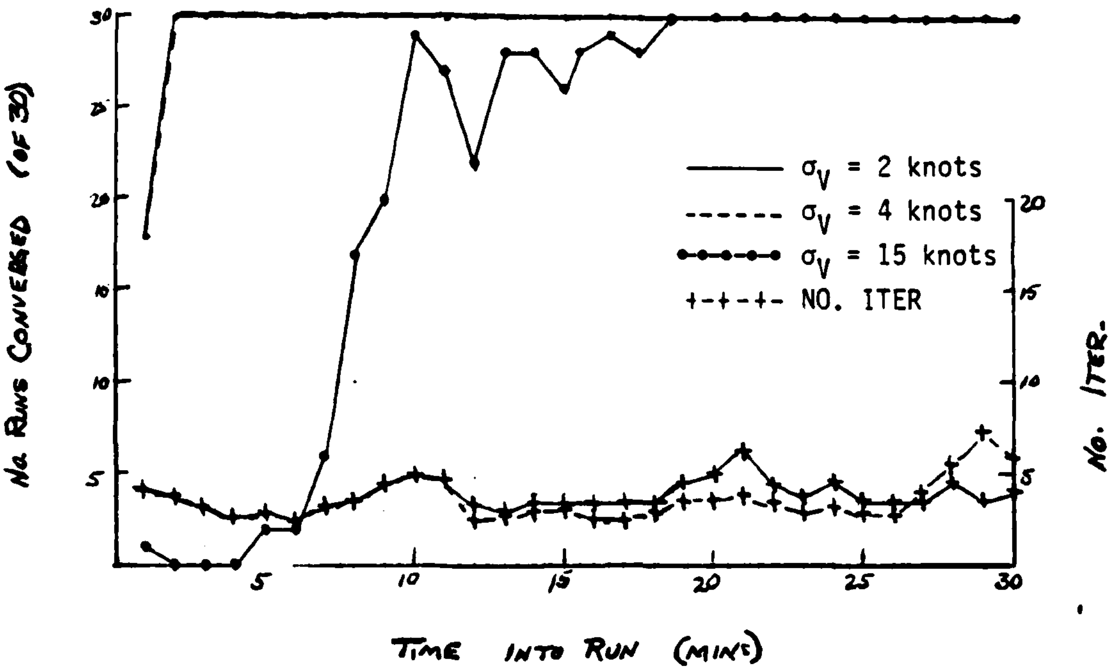

Figure 4-6. Convergence of Bearings-only Algorithm With Optimum Step, First CZ Path, Closing-Target Course ($\overline{V}_0$=10 knots)

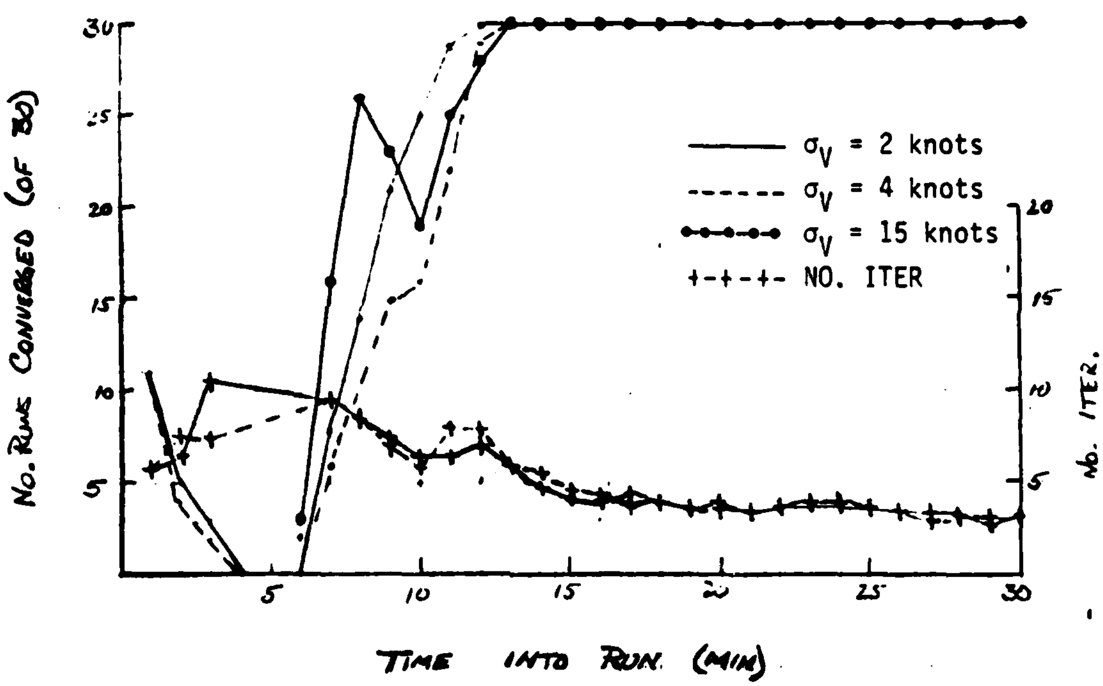

Figure 4-7. Convergence of Bearings-Only Algorithm With Optimum Step, First CZ Path, Crossing-Target Course ($\bar{V}_0$=10 knots)

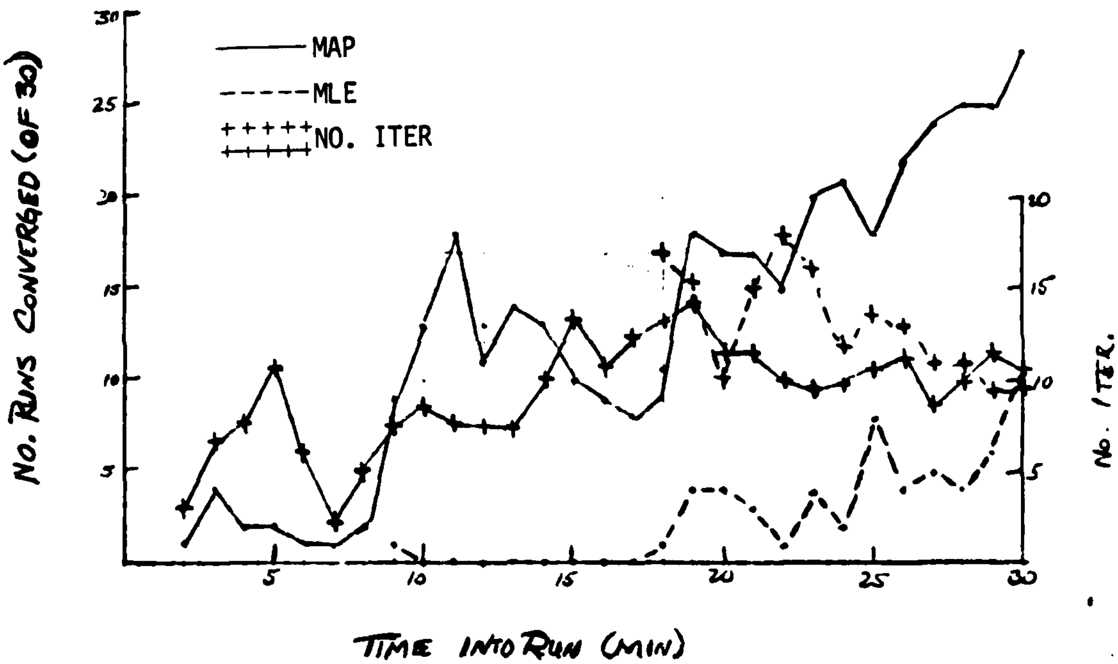

Figure 4-8. Convergence of Bearings-Only Algorithm With Optimum Step, Second CZ Path, Closing-Target Course

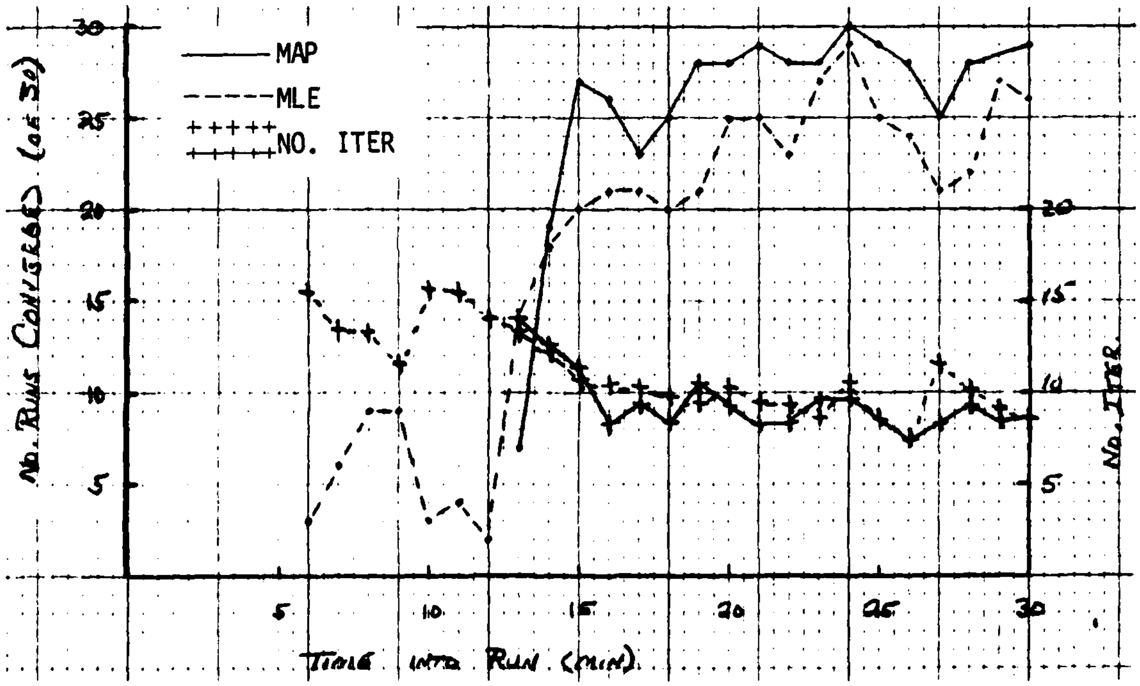

Figure 4-9. Convergence of Bearings-Only Algorithm With Optimum Step, Second CZ Path, Crossing-Target Course

geometries may be made using the results given in Section 3.1.3 of the previous report (Reference 4).

The results of numerical convergence frequency versus problem time for the Monte Carlo repetitions shown here generally agree with those of the previous study. They clearly demonstrate the benefit derived from incorporation of *a priori* range and speed inputs towards increasing the probability of numerical convergence. This is particularly noted for the difficult geometries and during the early parts of the problem. For the direct-path cases, the MAP algorithm frequently converges on the first leg while the MLE almost never does. Since the complete solution is not observable, this behavior is expected and does not represent a significant advantage to the MAP solution. After the first leg, convergence is virtually equivalent for both cases. The MAP solution does converge more frequently during the maneuver. The first and second CZ cases with the closing target course geometry show a marked increase in convergence probability due to the use of the MAP algorithm. This is seen during the second through fourth TMA legs of the first CZ case and throughout the entire run for the second CZ case.

The use of the optimum step-size calculation appears to increase the probability of convergence for both the MAP and MLE algorithms over the step-limiting method. The measured improvement in convergence due to *a priori* information use therefore remains approximately the same.

The previous study concluded that the major computer burden of the algorithms is associated with the unsuccessful search for a (numerically) converged solution, and therefore the MAP solutions require fewer computations than the MLE simply because more solutions converge within the maximum iteration limit. This conclusion is only partially substantiated by the results shown here for the algorithms using optimum step size. The average number of iterations required for convergence versus problem time is plotted for all converged Monte Carlo repetitions. These numbers therefore exclude any computer cost due to a solution failing to converge with the alloted Gauss-Newton repetitions. In general, the results for the crossing-course geometries show

little difference in average iteration number between the MAP and MLE solutions. However, those for the closing course, a more difficult TMA geometry, show the MAP to converge on average with fewer iterations. This is particularly the case during the early legs and with the CZ cases.

4.1.3 Solution Behavior for Correct-Path Hypotheses

The earlier results from MAP and MLE algorithms, not employing step-size optimization, indicated that the major value of *a priori* range information was improved numerical convergence of the solution rather than improvement of the intermediary and ultimate solutions. Therefore, it was observed that although comparison was made to MLE algorithms which benefit from good initialization using the *a priori* range estimates, the value of using correct *a priori* range information in a MAP algorithm was disappointing. Little gain in solution accuracy and solution convergence time was measured.

Figures 4-10 through 4-13 show the solution errors as a function of problem time for simulations employing step-size optimization and using the correct propagation path assumptions for solution initialization and *a priori* estimates. Parts a, b and c of each figure give the range, speed and course errors, respectively, averaged over all numerically converged Monte Carlo repetitions. The solid and dashed lines represent the root mean square errors of the MAP and MLE solutions respectively, and the symbols (• and +) represent the mean errors at each problem time. Results are presented for the direct-path (20-kiloyard range) case with closing course geometry and for all three propagation paths (direct, first CZ and second CZ) with crossing course geometry. The CZ results for the difficult closing geometry are basically very poor and are not presented. The direct-path results show only a very small (if any) decrease in range and course RMS error due to *a priori* information use and no difference in solution convergence time. The speed RMS error for the MAP algorithm is considerably lower during the second TMA leg. A very small negative bias in the MAP speed error is still noted at the later legs after convergence for the closing-course case. The results for the first and second CZ cases with crossing course show a more pronounced decrease due to

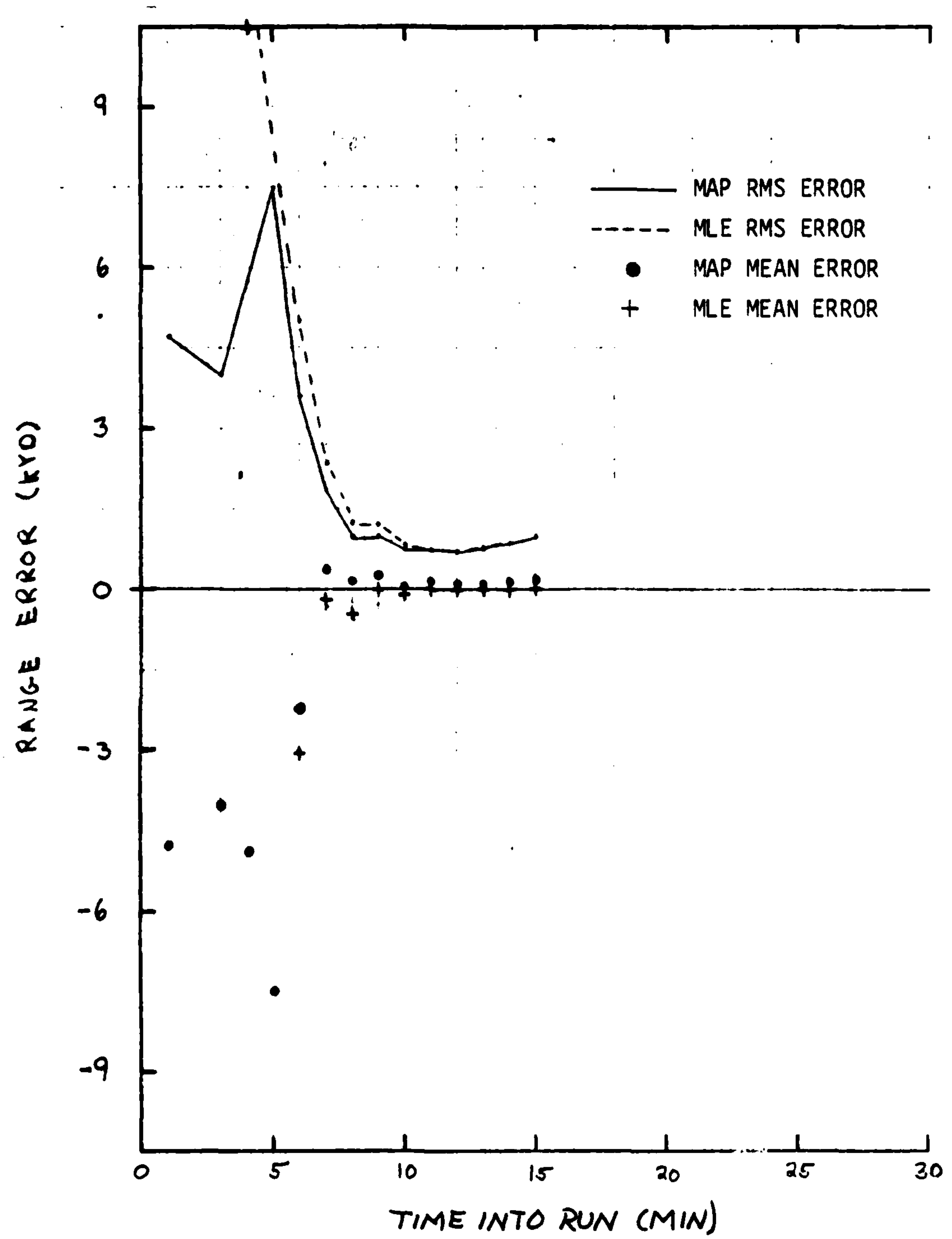

Figure 4-10a. Range Error for Bearings-Only Method With Optimum-Step, Direct-Path, Closing-Target Course

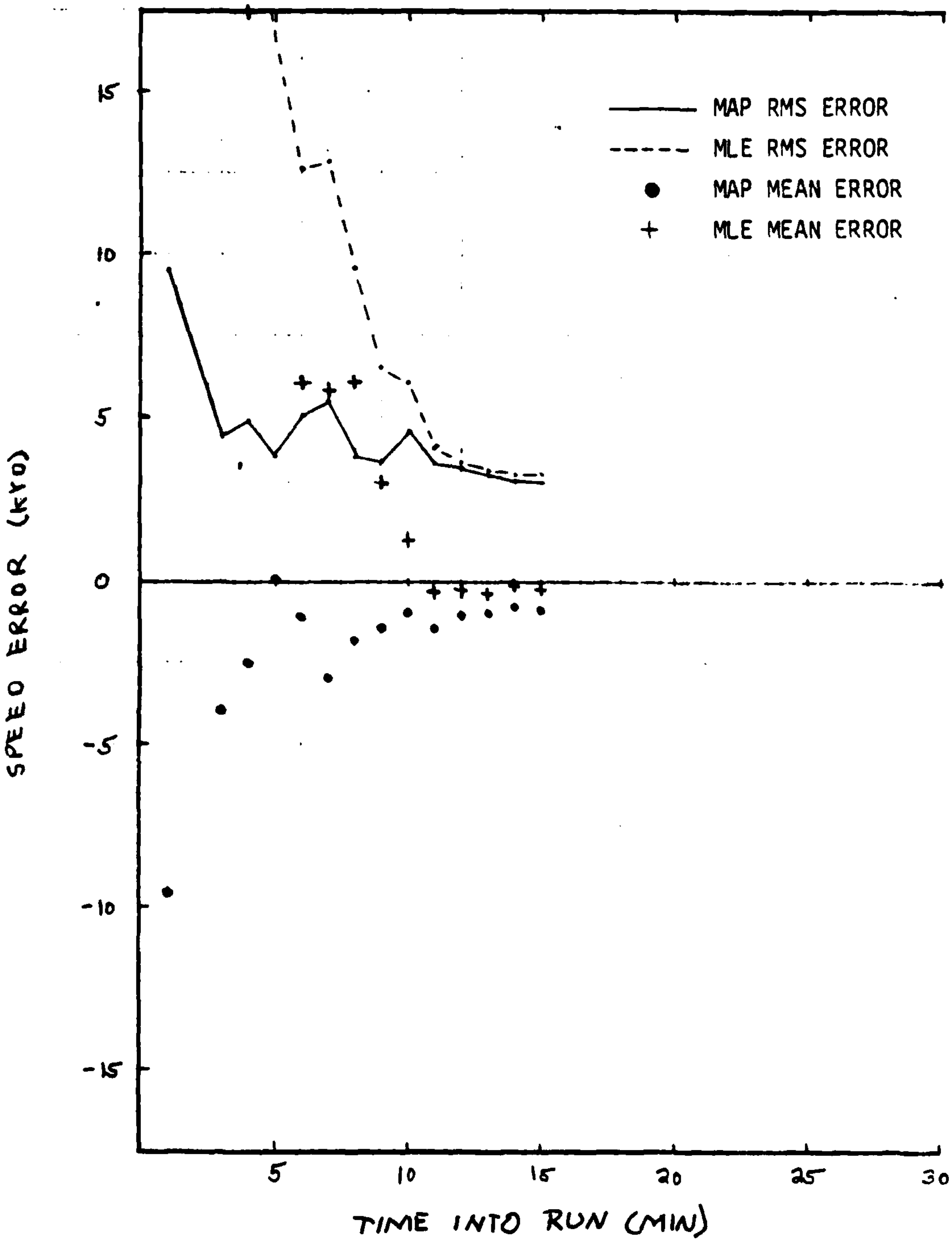

Figure 4-10b. Speed Error for Bearings-Only Method With Optimum-Step, Direct-Path, Closing-Target Course

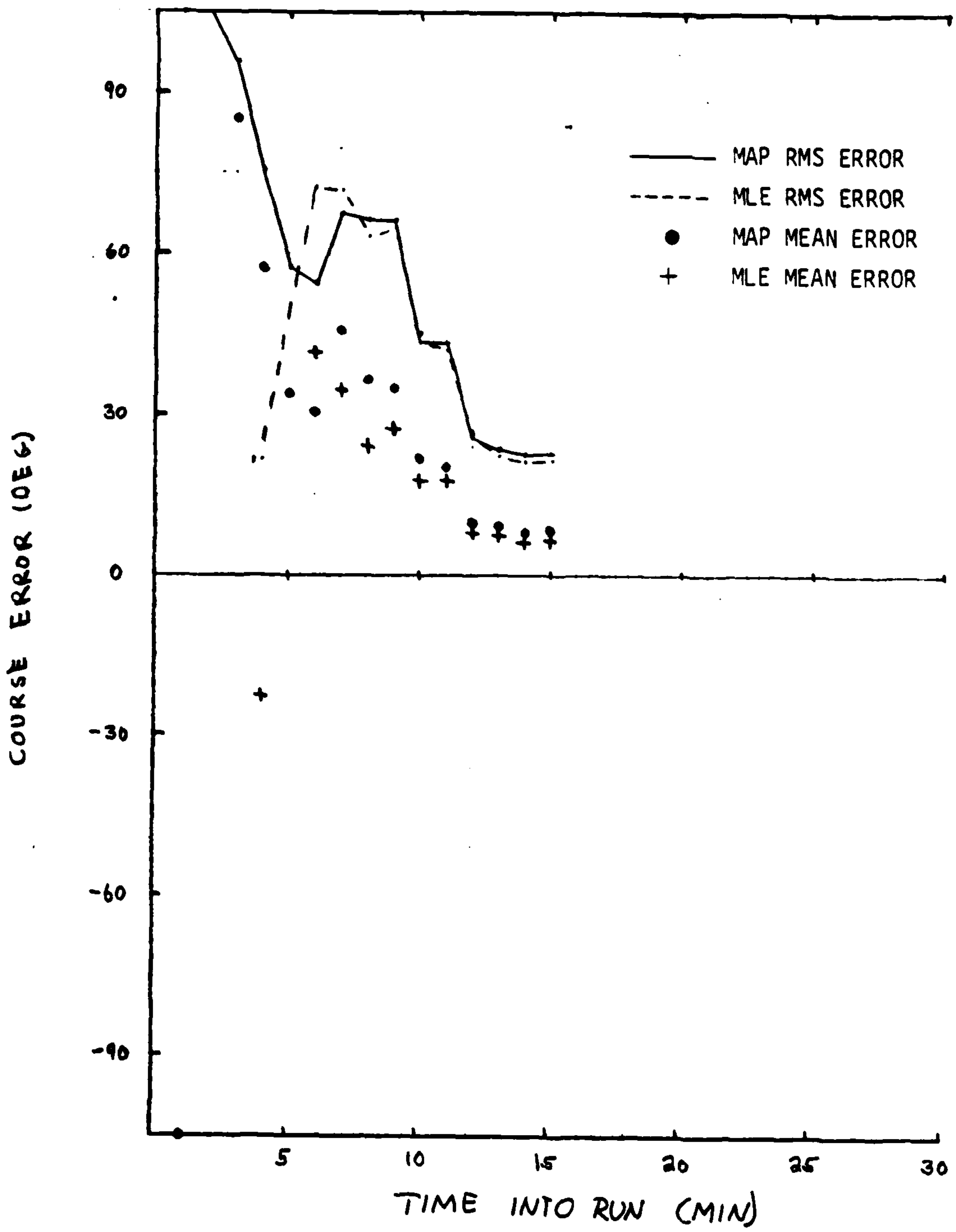

Figure 4-10c. Course Error for Bearings-Only Method With Optimum-Step, Direct-Path, Closing-Target Course

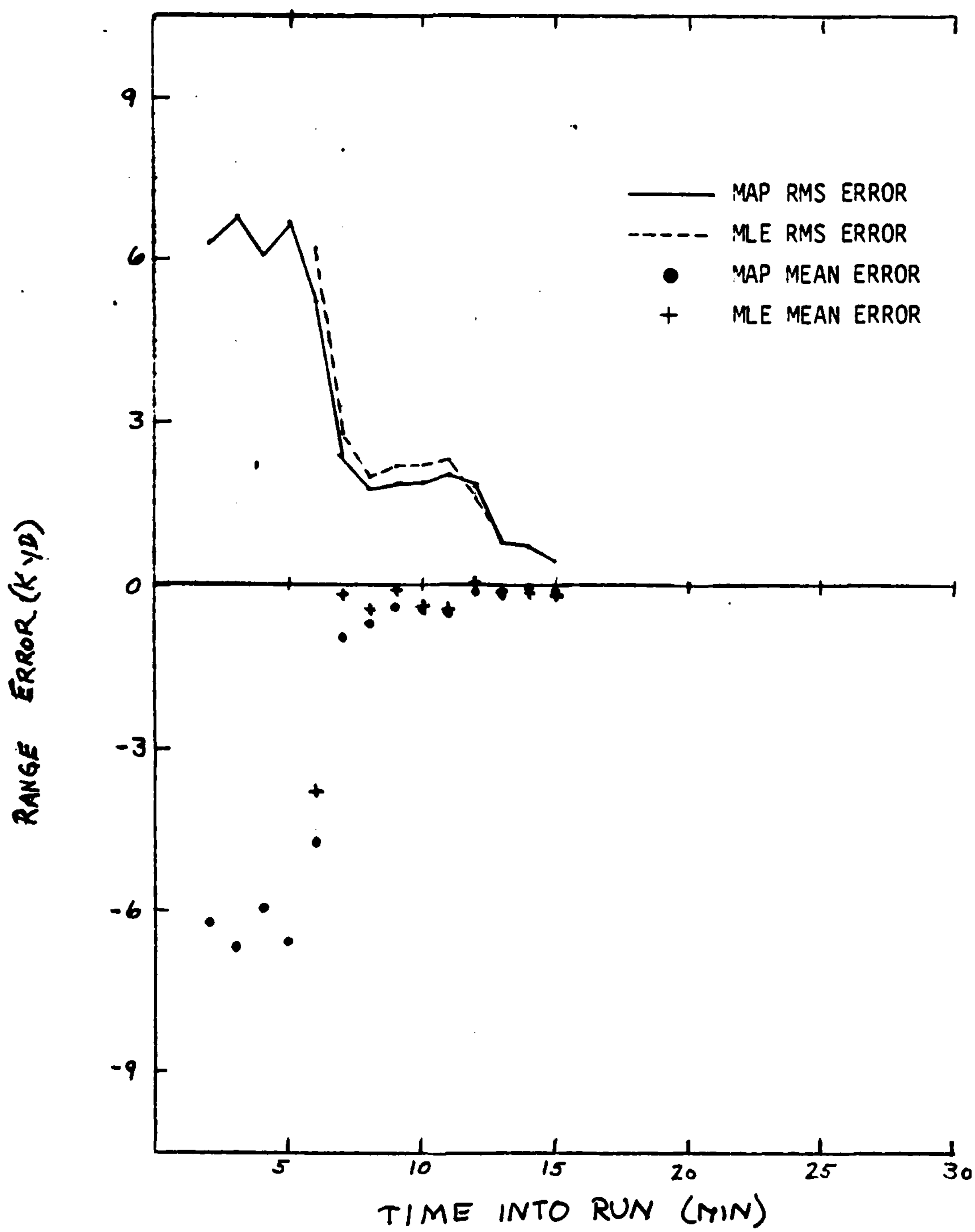

Figure 4-11a. Range Error for Bearings-Only Method With Optimum-Step, Direct-Path, Crossing-Target Course

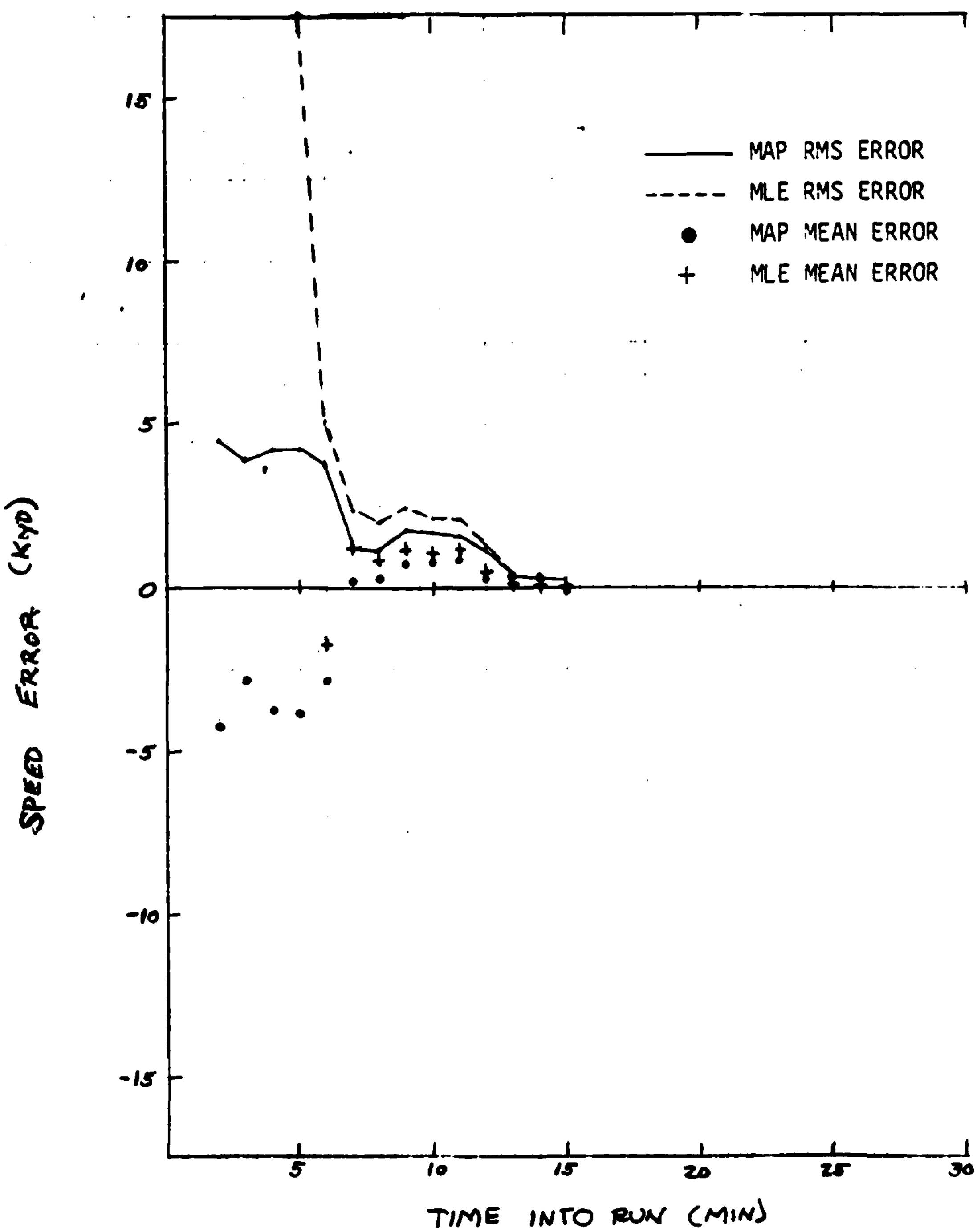

Figure 4-11b. Speed Error for Bearings-Only Method With Optimum-Step, Direct-Path, Crossing-Target Course

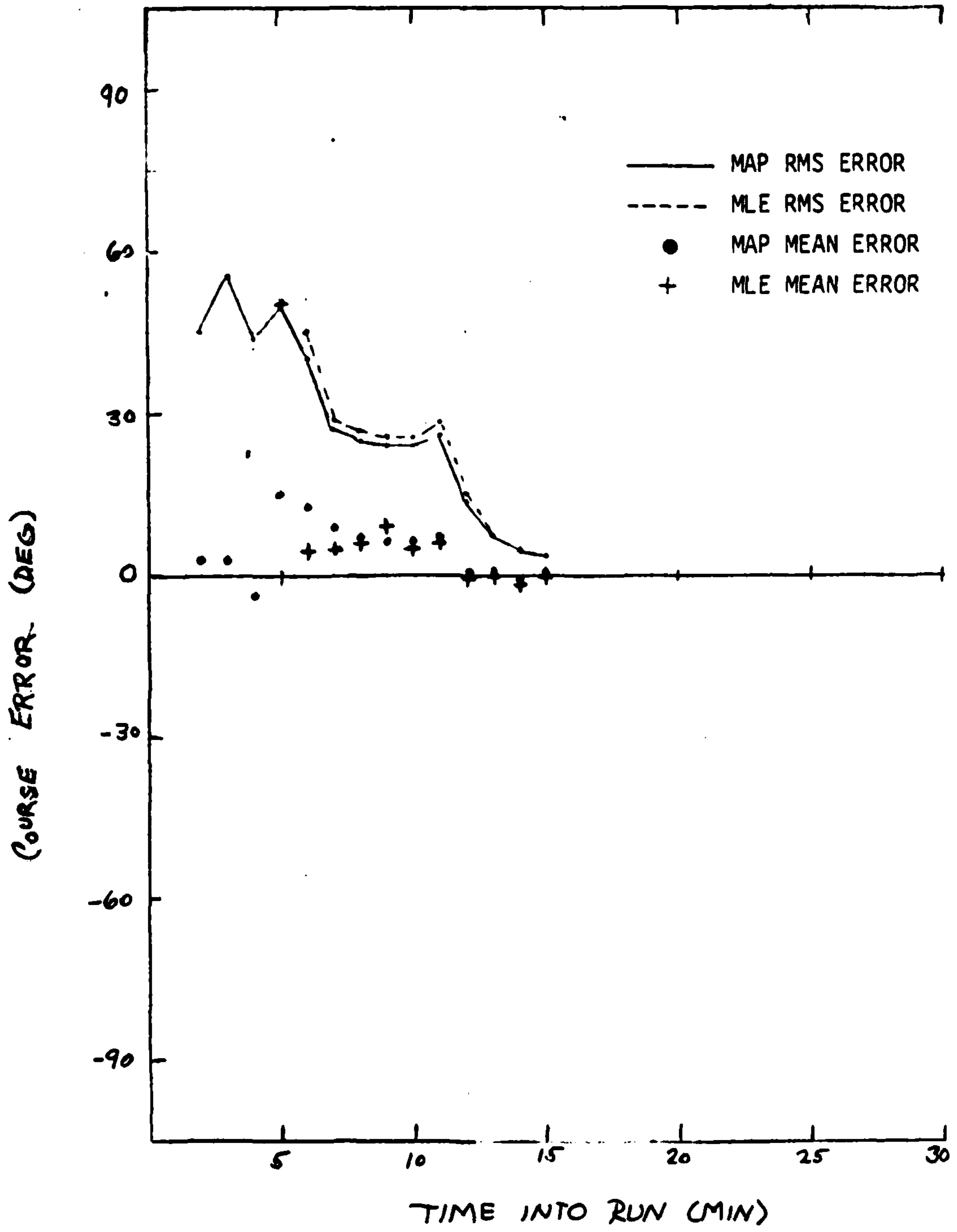

Figure 4-11c. Course Error for Bearings-Only Method With Optimum-Step, Direct-Path, Crossing-Target Course

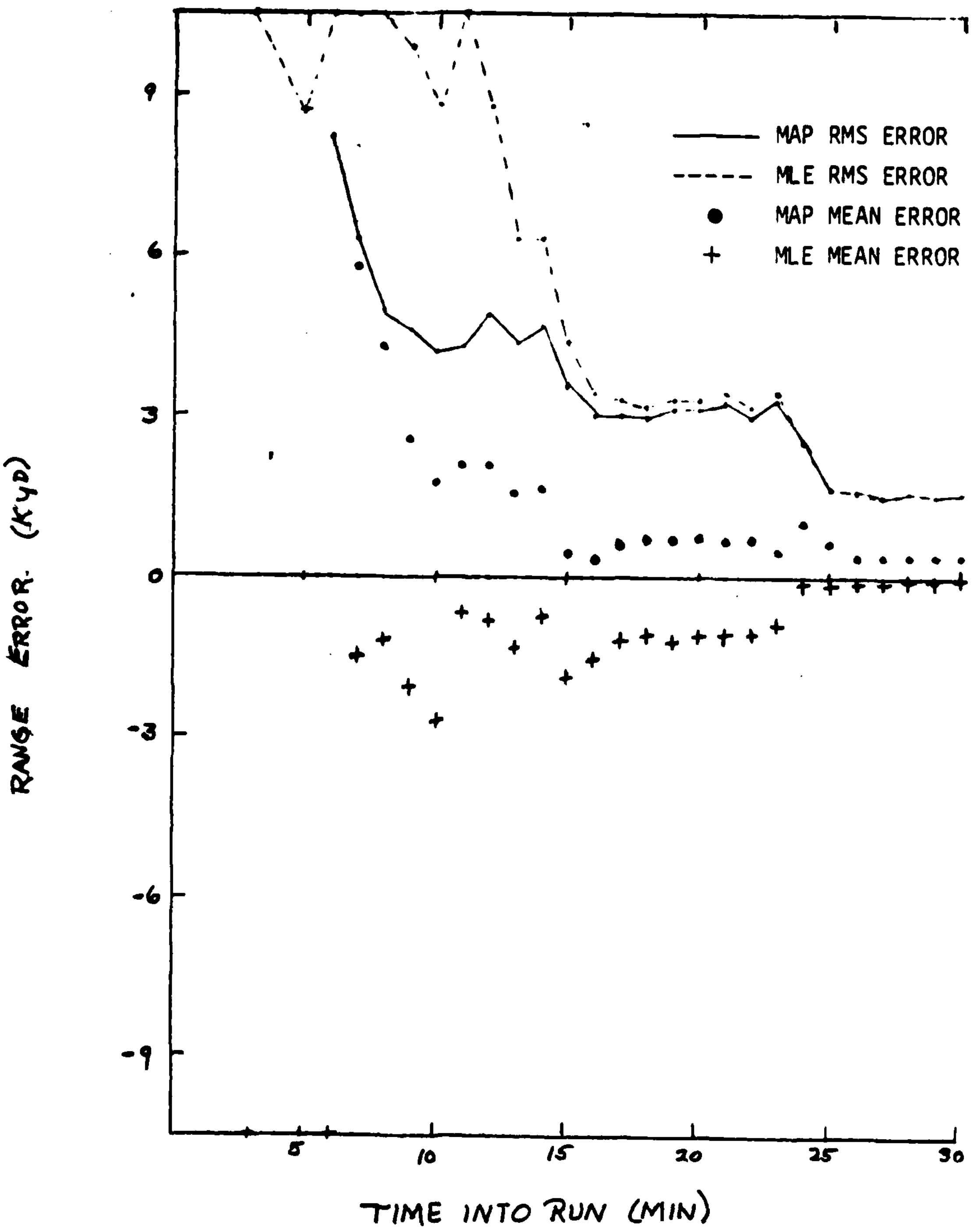

Figure 4-12a. Range Error for Bearings-Only Method With Optimum-Step, First CZ Path, Crossing-Target Course

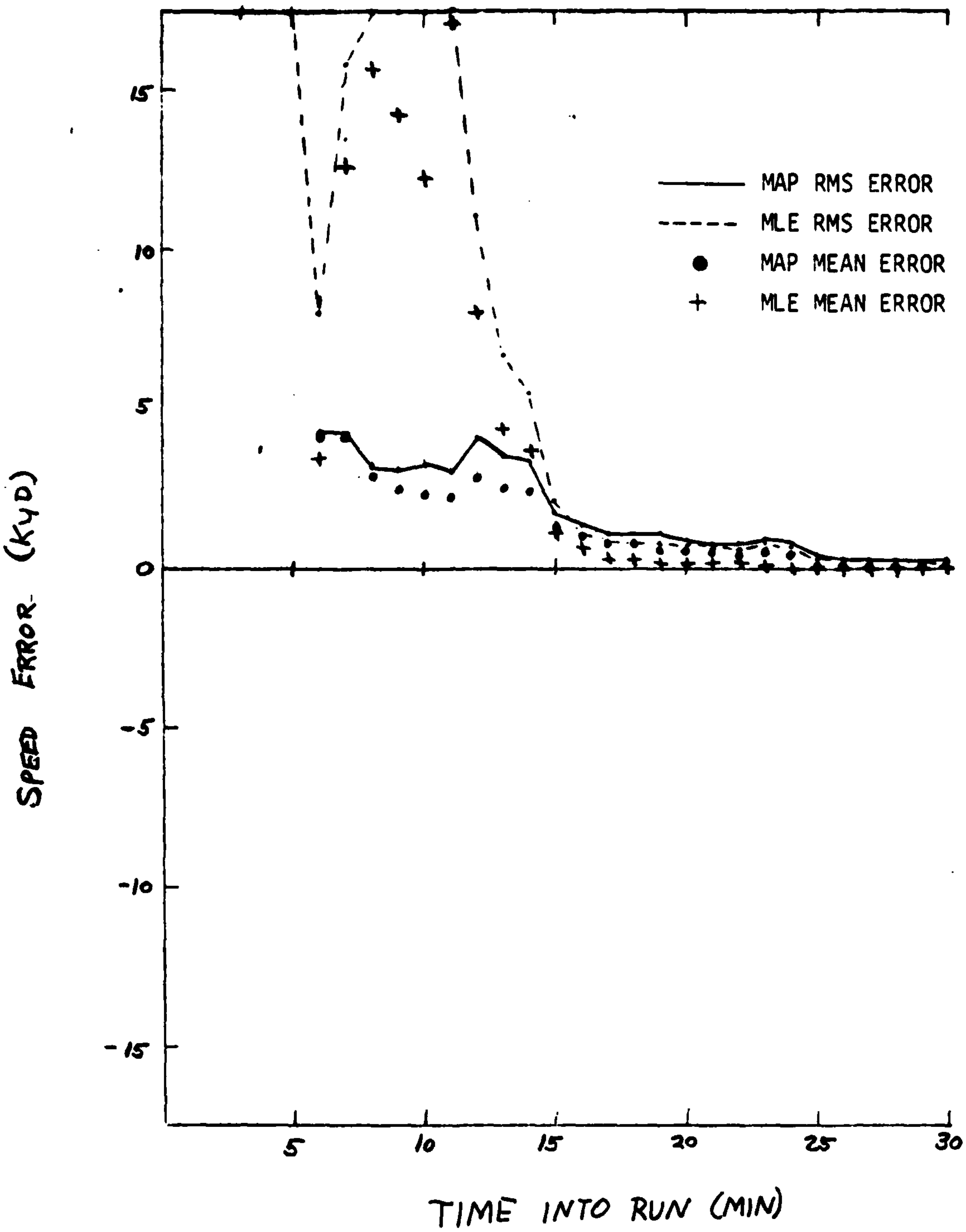

Figure 4-12b. Speed Error for Bearings-Only Method With Optimum-Step, First CZ Path, Crossing-Target Course

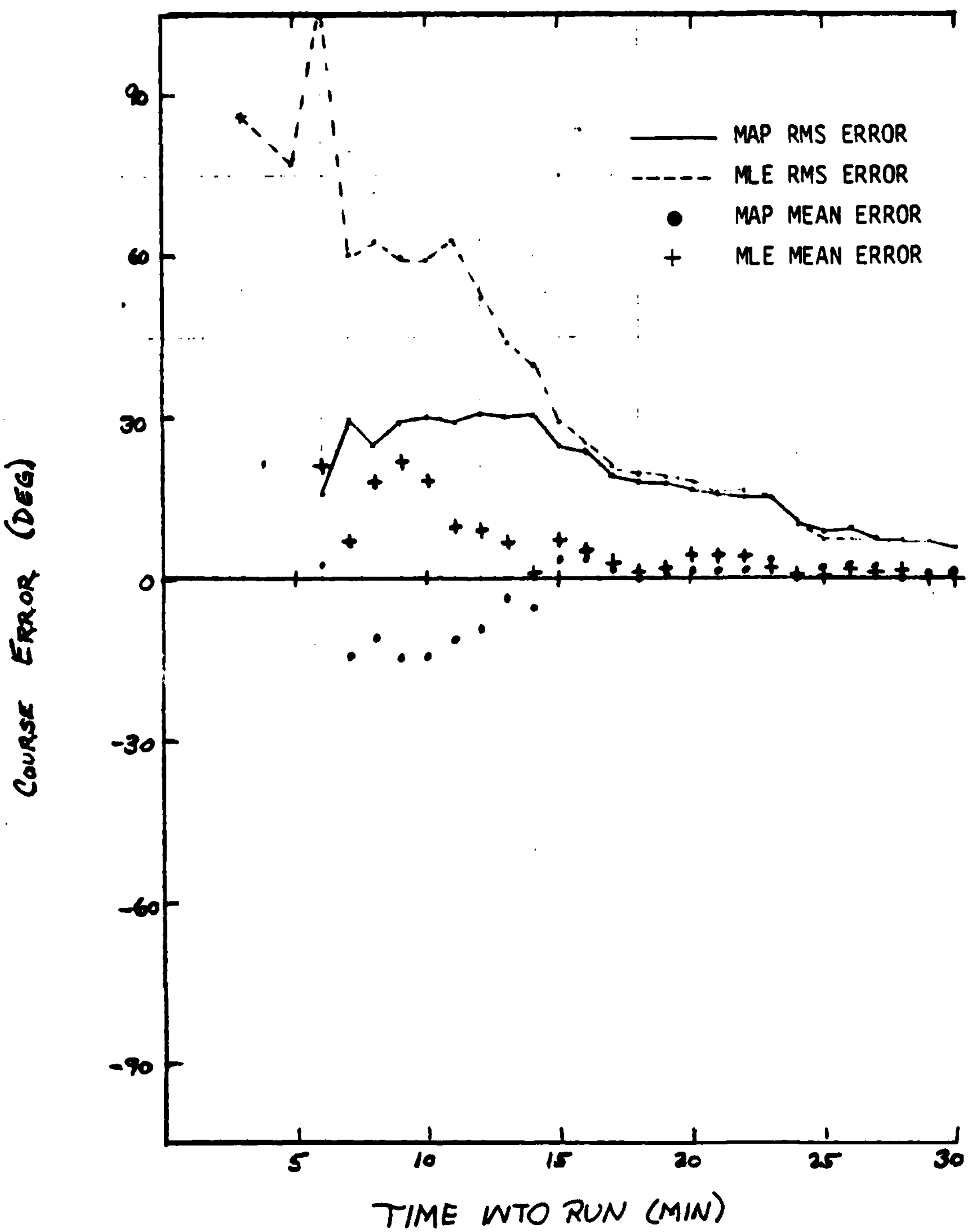

Figure 4-12c. Course Error for Bearings-Only Method With Optimum-Step, First CZ Path, Crossing-Target Course

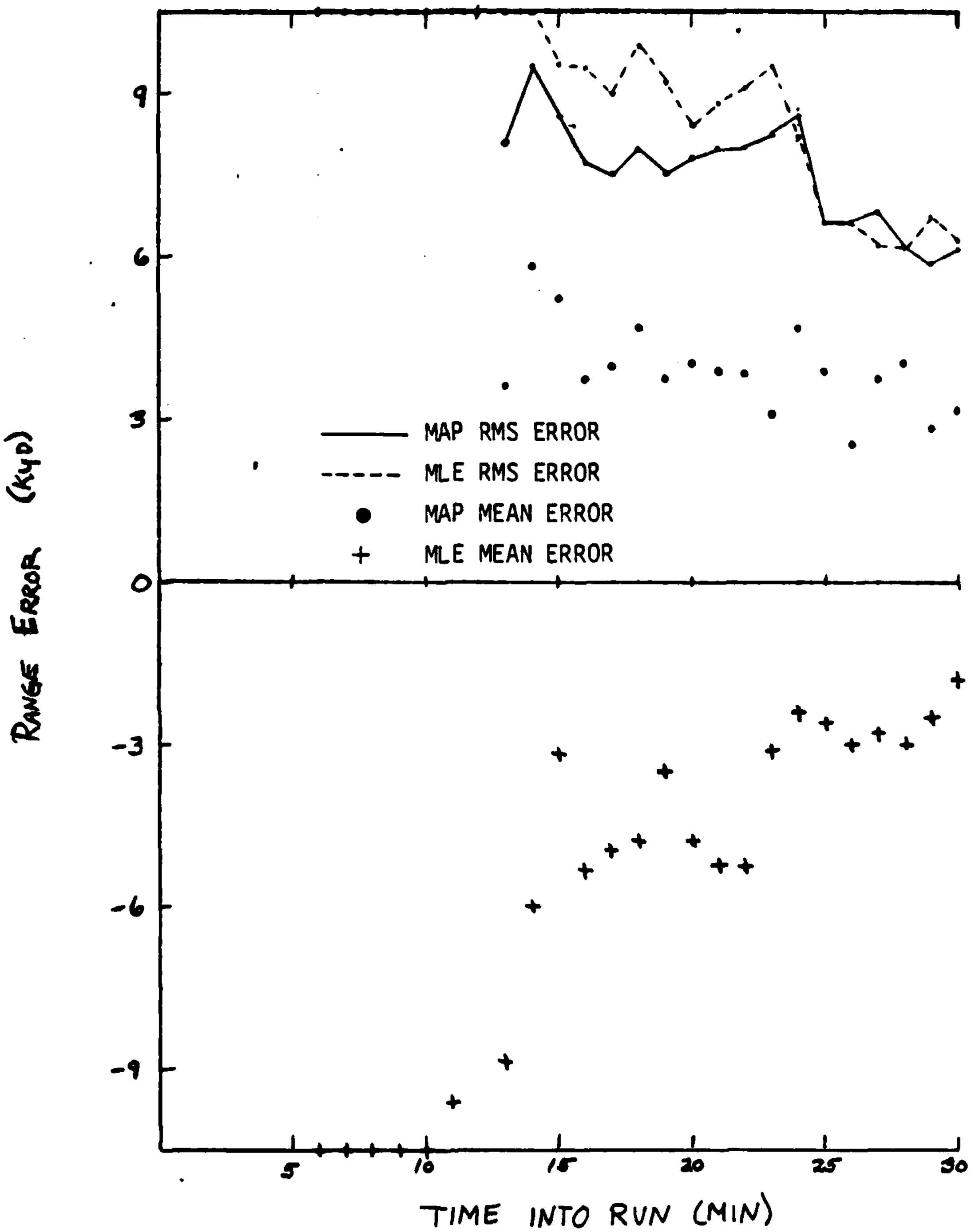

Figure 4-13a. Range Error for Bearings-Only Method With Optimum-Step, Second CZ Path, Crossing-Target Course

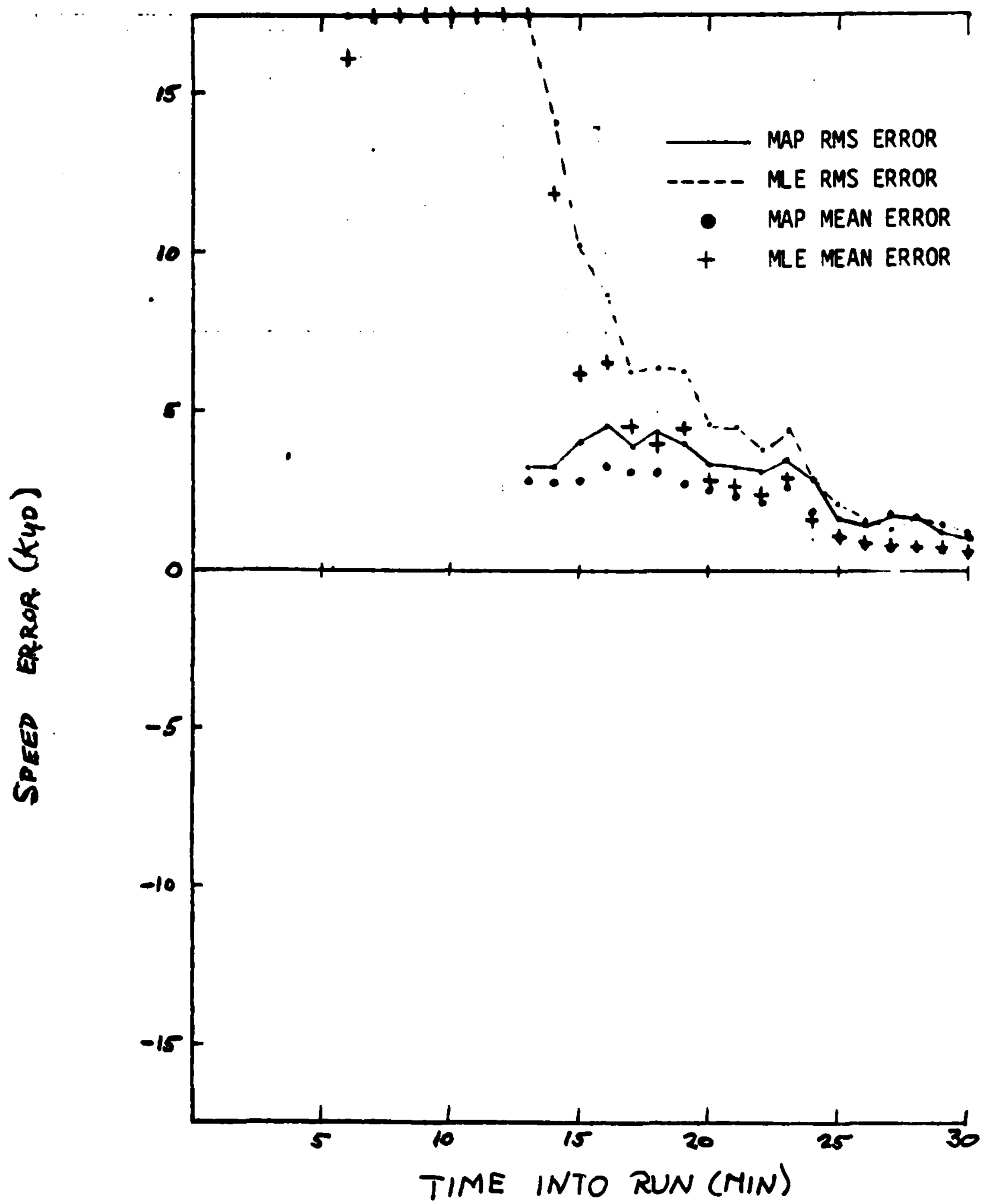

Figure 4-13b. Speed Error for Bearings-Only Method With Optimum-Step, Second CZ Path, Crossing-Target Course

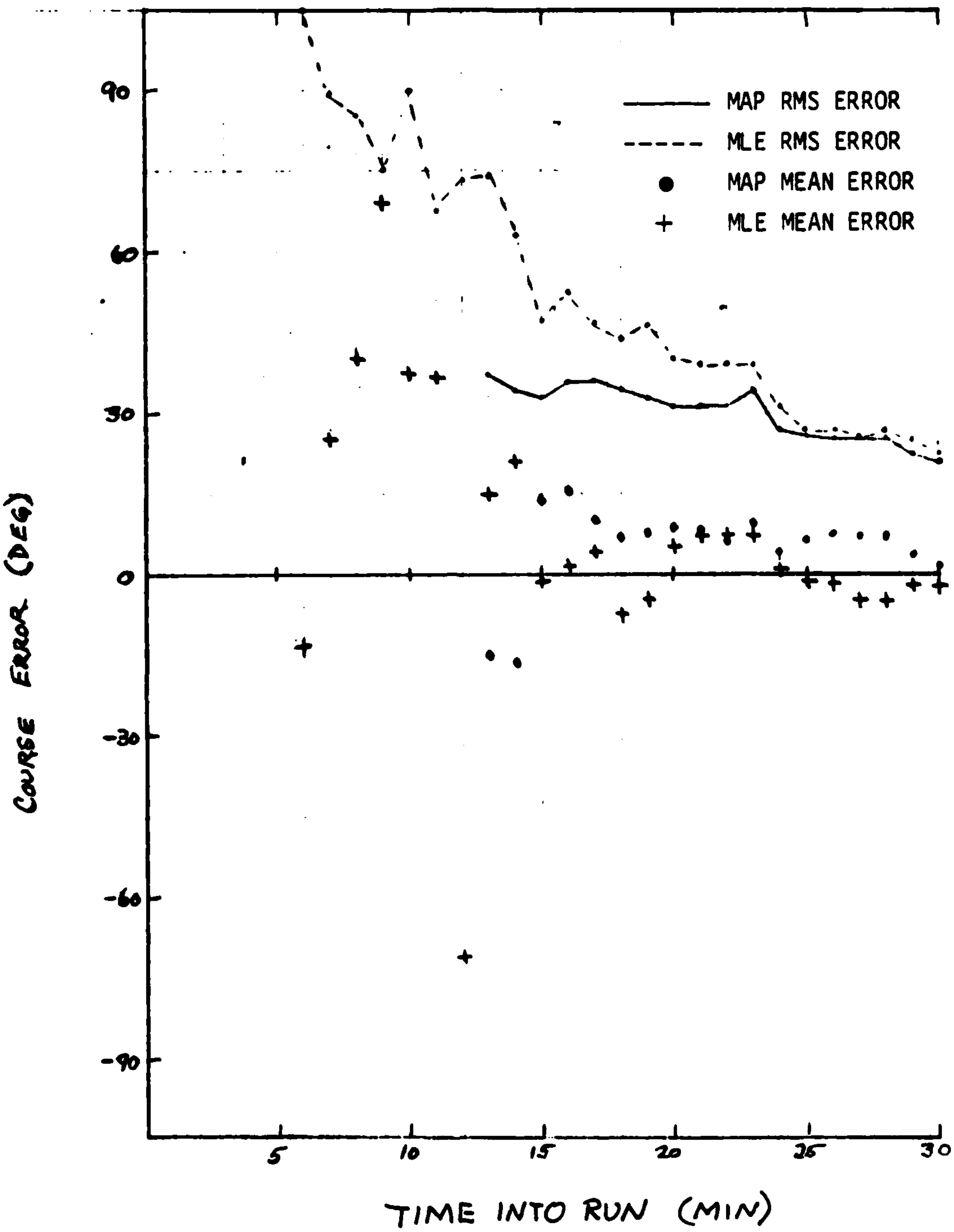

Figure 4-13c. Course Error for Bearings-Only Method With Optimum-Step, Second CZ path, Crossing-Target Course

the MAP algorithm in range, speed and course RMS error in the early legs. This difference disappears at or before solution convergence. The range mean errors for both the MAP and MLE methods are biased even at later problem times, however in opposite directions.

The above results, therefore, do show that for an algorithm using an optimum step-size calculation the incorporation of *a priori* information does yield, for some geometries, significant improvement in early leg solution accuracy. However, ultimate solution convergence and ultimate solution accuracy are not enhanced.

4.1.4 Error Lower Bounds and Solution Convergence

In the operational environment, values for the TMA solution errors are not known. It is important, therefore, to estimate solution performance and convergence status. An estimate for Fisher's information matrix (ψ matrix) is calculated as part of the MLE and MAP solution procedure. The inverse of this matrix, when calculated using the true solution, is the Cramer-Rao lower bound on the solution error covariance. Therefore, this can be used even when calculated at solution estimates, to indicate sensitivity of the solution to additional measurements and to place a relative estimate on the solution quality theoretically obtainable. The covariance lower bound matrix is converted to independent scalar parameters by partitioning the inverse matrix (ψ^{-1}) into 2X2 position and velocity submatrices and computing their eigenvalues. The square root of the larger eigenvalue for each set represents the major axes of the position error ellipse and of the total velocity error ellipse. These are theoretical lower bounds on range error and total velocity vector error, respectively.

The major axes for the range and velocity error bounds are plotted in Figures 4-14 through 4-18 for the direct, first CZ and second CZ path cases. The crossing geometry results are included for all three path cases, whereas the closing course results are for only the direct and first CZ cases. The error bounds for both the MAP and MLE solutions are included (solid and dashed

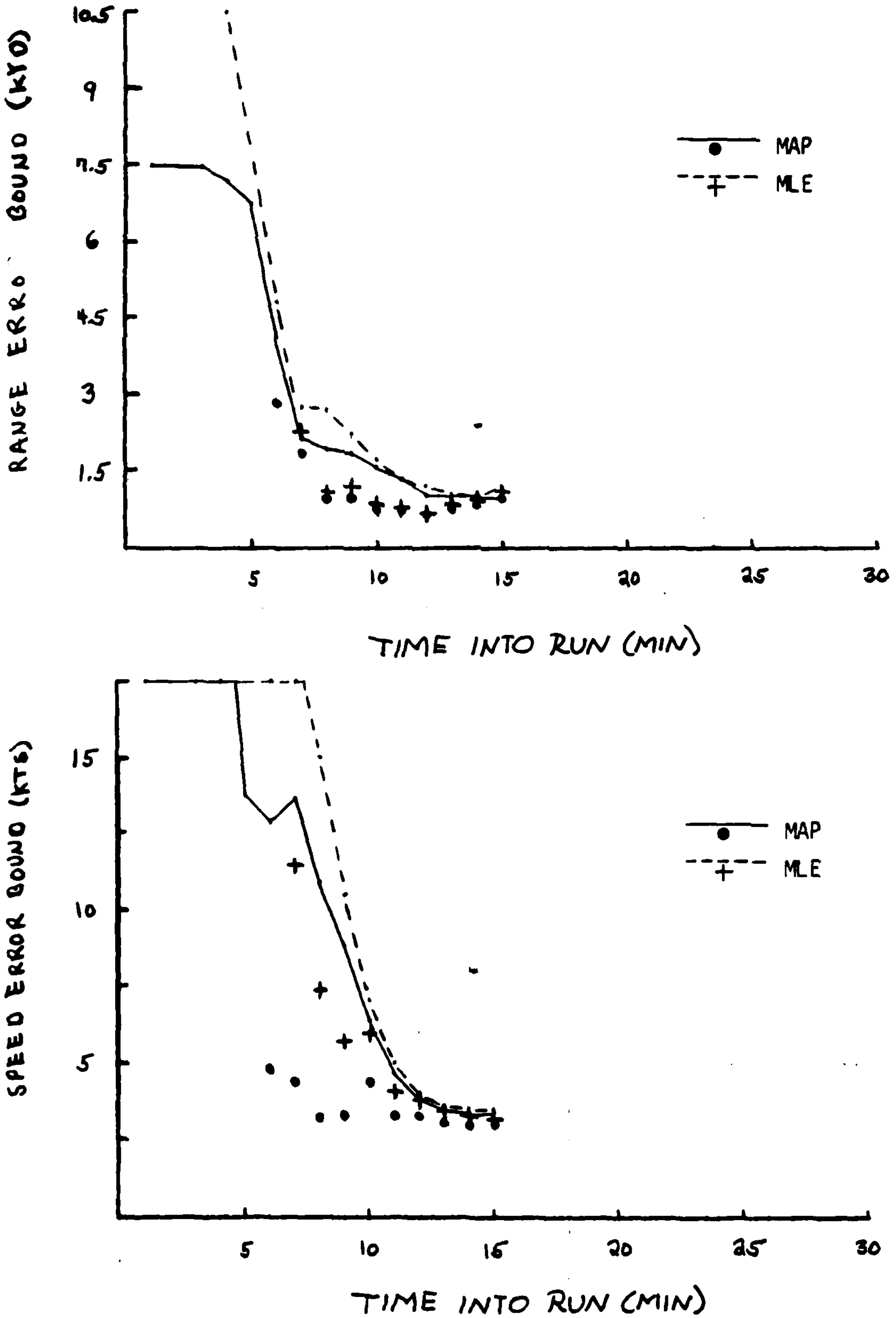

Figure 4-14. Theoretical Lower Bound (Major Ellipse Axis) on Range and Velocity Errors for Optimum-Step Method (Direct-Path, Closing-Target Course)

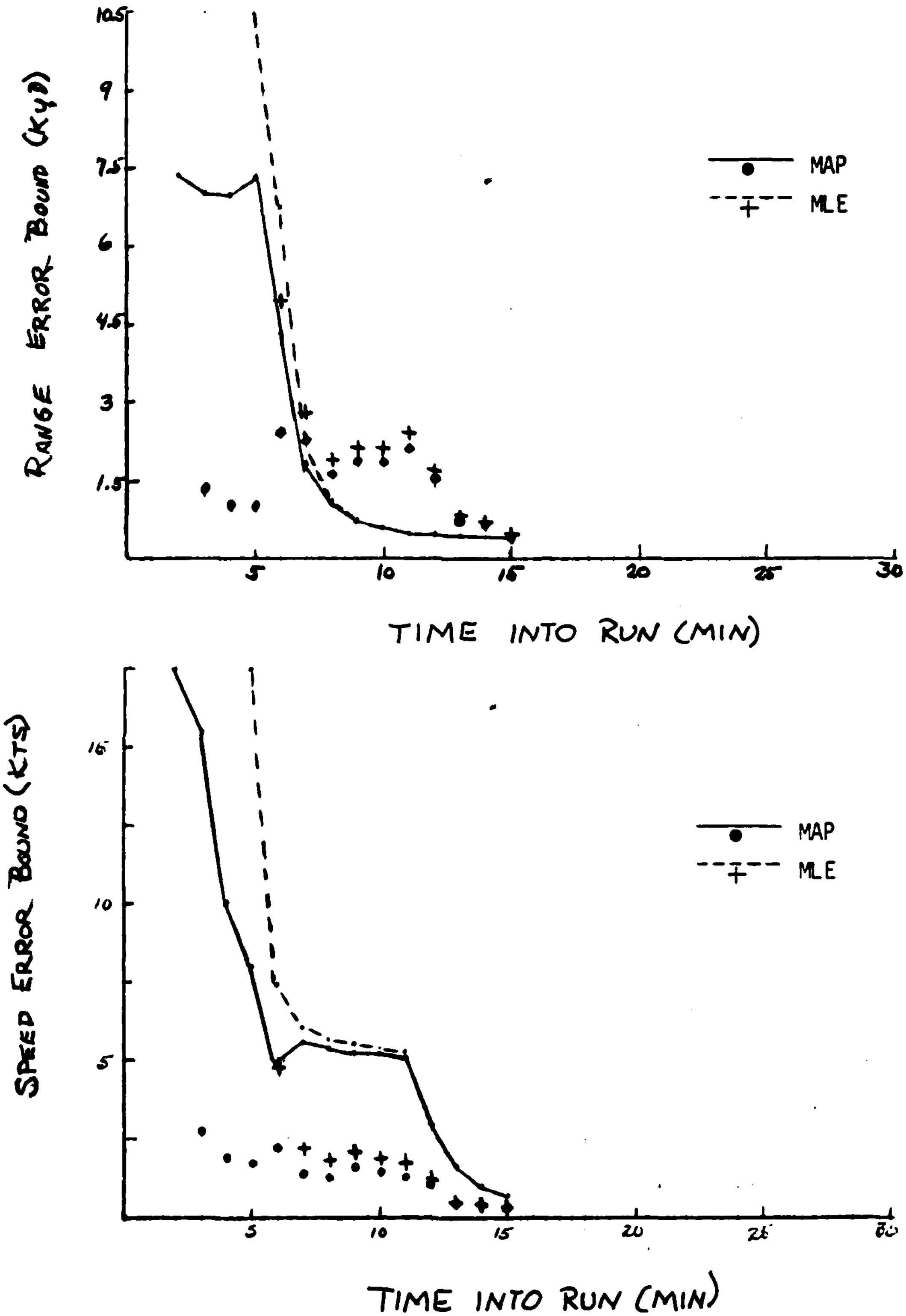

Figure 4-15. Theoretical Lower Bound (Major Ellipse Axis) on Range and Velocity Errors for Optimum-Step Method (Direct-Path, Crossing-Target Course)

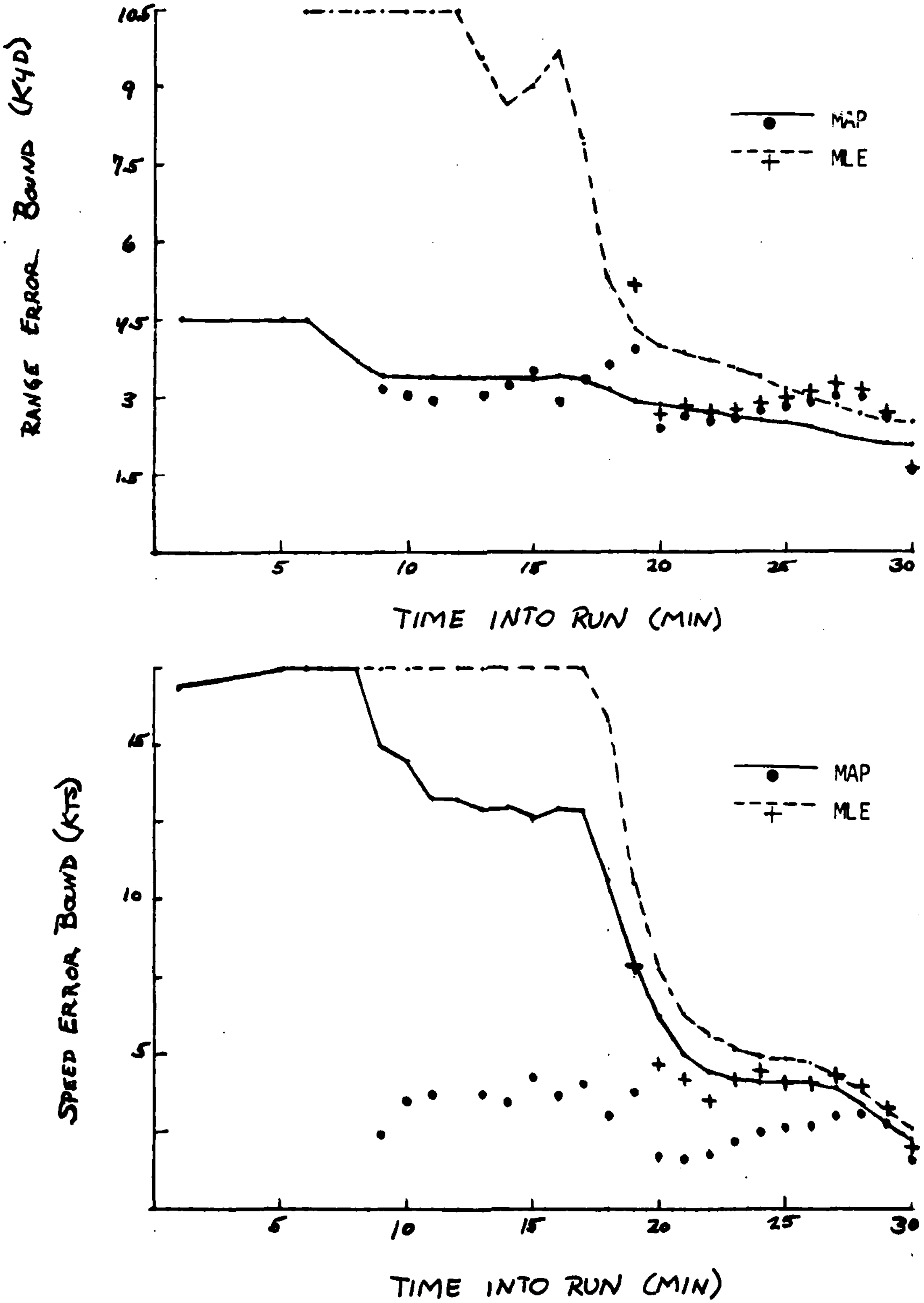

Figure 4-16. Theoretical Lower Bound (Major Ellipse Axis) on Range and Velocity Errors for Optimum-Step Method (First CZ Path, Closing-Target Course)

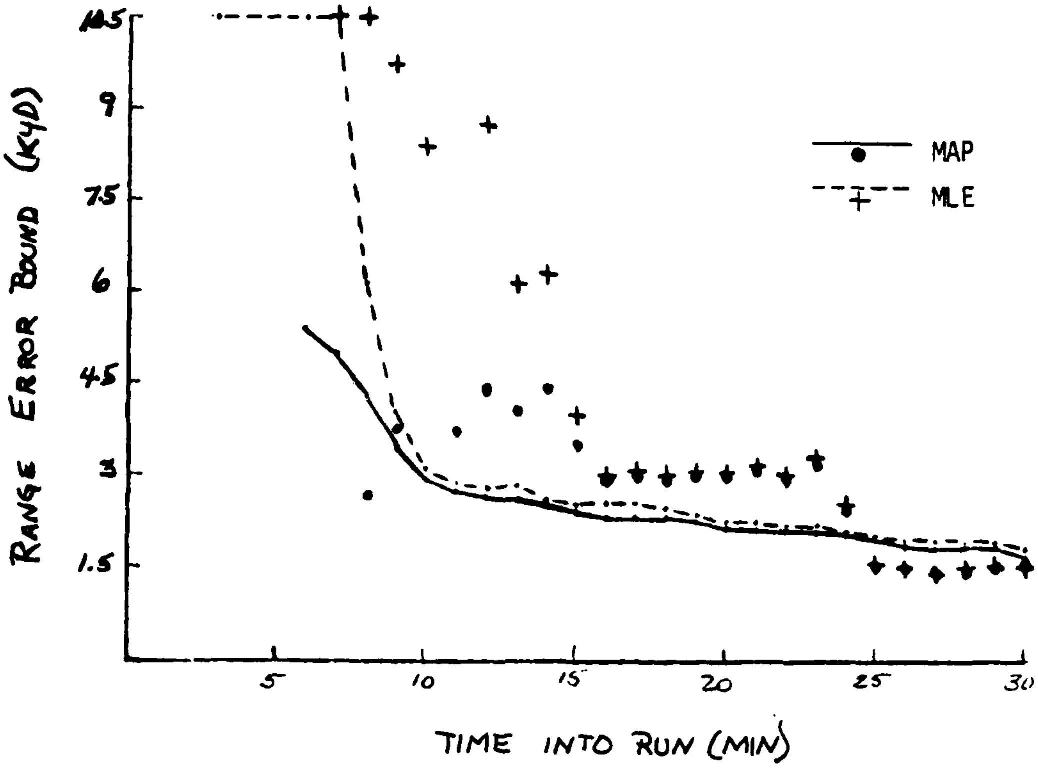

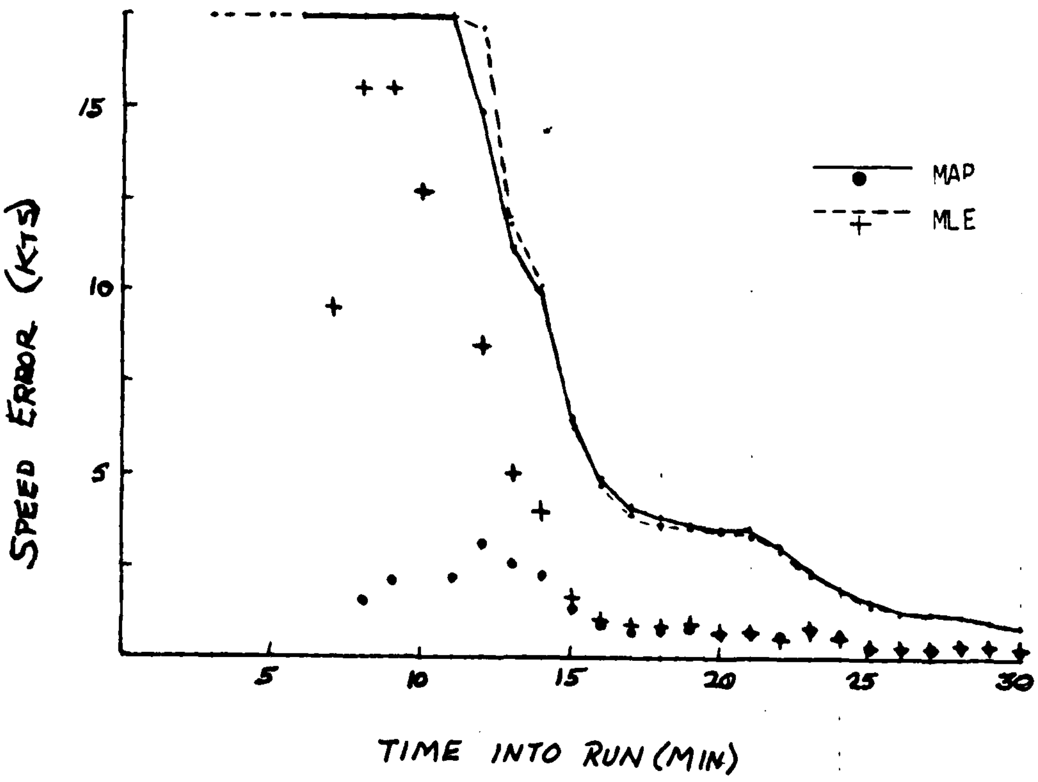

Figure 4-17. Theoretical Lower Bound (Major Ellipse Axis) on Range and Velocity Errors for Optimum-Step Method (First CZ Path, Crossing-Target Course)

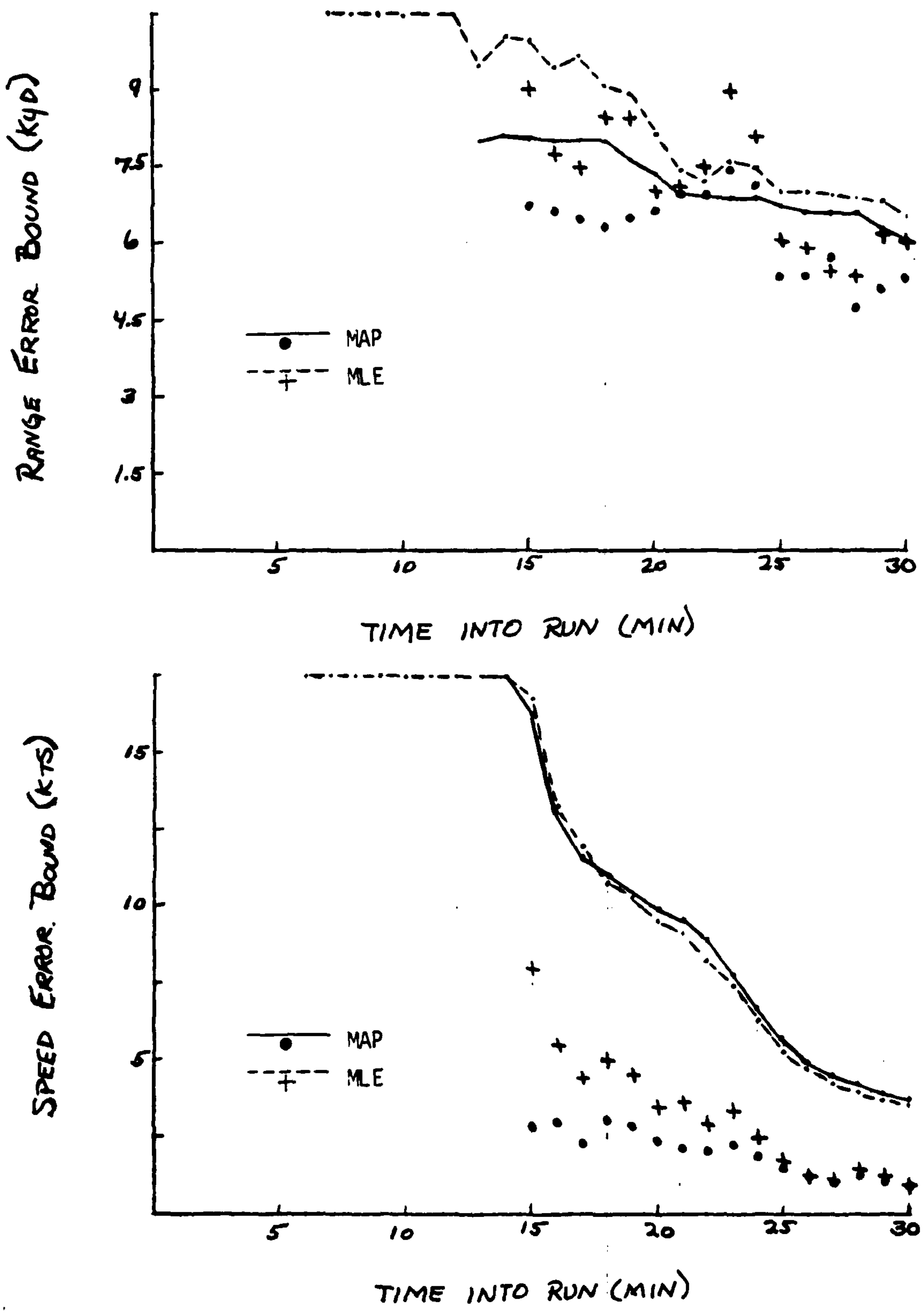

Figure 4-18. Theoretical Lower Bound (Major Ellipse Axis) on Range and Velocity Errors for Optimum-Step Method (Second CZ Path, Crossing-Target Course)

lines) along with the Monte Carlo standard deviations for solution times with a high (>67 percent) probability of convergence (• and +). The observations made from the error-bound plots are essentially the same as those for the algorithm without step optimization presented in the previous report. The error lower bounds are lower for the MAP solutions than those for the MLE, particularly during the early legs. The measured increase in solution accuracy for the MAP algorithm, noted in the previous section but not in the previous report, is therefore due to better utilization of the *a priori* information by the algorithm modified for step optimization rather than due to any enhancement in the best solution theoretically achievable. Consequently, the solution convergence behavior for both the MAP and MLE remains unchanged by the modified algorithm.

Table 4-1 presents a summary of the numerical and solution characteristics for the modified bearings-only MLE and MAP algorithms. Results for simulations of each geometry/path hypothesis are included. Included in the summary for each simulation are averages of the numerical convergence measurements, estimate for solution convergence time and the RMS error characteristics of the solution at the determined convergence time. The criterion for solution convergence was defined as in the previous study as the time at which the velocity major axis error bound reaches 1 knot (10 percent of actual velocity magnitude). This is somewhat arbitrary but is sufficient for comparison purposes. The range error bound and the Monte Carlo solution error statistics may be used to confirm the solution convergence time and the converged solution's validity. The values presented in Table 4-1 may be compared with those in Table 3-1 of the previous study for the algorithms without step optimization.

Using the statistics presented in the table comparison between the MAP and MLE algorithm may be made and thus the value of *a priori* information may be estimated. The number of converged Monte Carlo repetitions and the number of Gauss-Newton iterations per repetition averaged over all solutions of the runs are indicative of the relative computation costs of the runs. The solution convergence time and the RMS errors at that time give a relative indication of the solution's timeliness and quality. In general, the use of *a priori*

Table 4-1. Summary of Bearings-Only TMA Solution Statistics at Solution Convergence Times

TARGET COURSE	PATH*	MAP						MLE					
		SOLUTION CONVERGENCE TIME (min)**	NO. CONVERGED MONTE CARLO RUNS PER SOLUTION TIME***	NO. GAUSS-NEWTON ITER PER SOLUTION TIME	RMS ERROR			SOLUTION CONVERGENCE TIME (min)**	NO. CONVERGED MONTE CARLO RUNS PER SOLUTION TIME***	NO. GAUSS-NEWTON ITER PER SOLUTION TIME	RMS ERROR		
					RANGE (yd)	SPEED (knots)	COURSE (deg)				RANGE (yd)	SPEED (knots)	COURSE (deg)
CLOSING TARGET COURSE	D	>15	21.5	9.8	992	3.15	22.6	>15	18.9	11.1	1014	3.31	22.0
	D (1 assumed)	>15	20.2	11.6	1117	4.48	8.6	>15	18.1	11.7	1018	3.31	21.9
	D (2 assumed)	>15	16.4	13.0	1036	3.92	11.9	>15	17.9	11.9	1025	3.32	22.1
	D (R=10 kyd)	11	26.2	3.7	90	.84	2.0	11	20.1	9.1	100	.36	1.0
	1	>30	21.7	10.3	1730	2.74	10.0	>30	14.2	14.2	1713	2.13	6.8
	1 ($\hat{V}$=10, $\hat{\sigma}_V$=4)	>30	29.6	4.0	1733	2.09	6.4						
	1 ($\hat{V}$=10, $\hat{\sigma}_V$=2)	>30	29.6	3.8	1779	1.22	2.9						
	2	>30	12.4	16.6	7655	4.14	90.8	>30	1.9	20.6	12314	5.43	74.0
CROSSING TARGET COURSE	D step-size limiting	15	22.8	8.5	518	.30	3.8	15	19.4	9.8	518	.31	3.8
	D	15	25.6	7.5	520	.31	3.8	15	19.5	9.8	520	.31	3.8
	D (1 assumed)	15	21.4	10.1	555	.33	3.9	15	18.9	10.3	520	.31	3.8
	D (2 assumed)	15	17.9	11.5	531	.32	3.8	15	19.0	10.4	521	.31	3.8
	D (R=10 kyd)	12	26.0	6.8	400	.45	3.8	12	20.4	8.9	401	.45	3.8
	D (σ_B=.5)	>15	24.5	8.0	1253	.76	9.0	>15	19.5	10.2	1278	.80	9.3
	1	30	22.7	9.3	1586	.35	6.8	30	22.6	9.1	1559	.31	6.8
	1 ($\hat{V}$=10, $\hat{\sigma}_V$=4)	30	22.9	8.4	1595	.35	6.8						
	1 ($\hat{V}$=10, $\hat{\sigma}_V$=2)	30	21.8	9.0	1552	.34	6.8						
	2	>30	15.4	14.9	6180	1.51	21.4	>30	14.8	15.6	6324	1.22	22.6

*D=Direct Path, 1=First CZ, 2=Second CZ
**Convergence time is the time at which the velocity error bound (major axis) drops below 1.0 knot.
***Maximum number=30

016.304

information in the algorithm with step optimization decreases the whole run average computation cost of obtaining numerically-converged solutions for both closing and crossing-course geometries and for all propagation paths. The CZ cases for the crossing-course geometry, however, are only slightly affected. Solution convergence time appears to be unaffected by the use of *a priori* estimates. However, in the simulations used here, the defined convergence criterion often is not reached by the end of the problem time. Solution accuracy, as defined by RMS error averages across Monte Carlo repetitions, appears to be inconsistently improved by using the MAP algorithm. The crossing-course geometries show little difference in RMS range, speed and course errors at the convergence times between the MAP and MLE solutions. The direct and second CZ cases with closing-course geometry have slightly decreased range and speed RMS error from the use of correct *a priori* range information, and the first CZ case has decreased speed RMS error from *a priori* speed estimates. It should be noted that the error estimates compared are those at the solution convergence time only and that the results of Section 4.1.2 should be used for further comparisons. In addition, the error estimates based on the Monte Carlo repetition averages have limited usefulness since 30 repetitions are probably not sufficient for accurate estimation.

4.2 BEARINGS-ONLY MLE WITH THREE-STATE, RELATIVE-MOTION SOLUTION

The calculation of a three-state solution to the bearings-only TMA problem was incorporated into the MLE/MAP algorithms in order to optimally utilize the available data when the full solution is not theoretically observable. The results presented in this section are from simulations using the modified Gauss-Newton algorithm (with step optimization) with a range-normalized, relative-motion solution calculated during the first 5-minute TMA leg. This observable three-state solution, along with any range and/or speed *a priori* information, is used for initialization of the full, four-state solution after the first maneuver. The details of the three-state solution methodology and the optimum bootstrap procedure is presented in Section 2.2. This section presents an evaluation of the use of this procedure both in obtaining

useful TMA solutions during the first leg and for initializing the full, absolute solution. As in the previous section, the impact of the algorithm modification on the optimum use of *a priori* information is studied.

4.2.1 Numerical Convergence Properties of the Modified Gauss-Newton Algorithm Three-State Solution Initialization

Plotted in Figures 4-19 through 4-21 are the measurements representing convergence probability and average computation cost of Monte Carlo simulations of the MLE/MAP algorithms with a three-state, relative-motion solution calculated for the first 5 minutes of each run. The number of converged Monte Carlo runs at each time for the full solution are also plotted for comparison purposes. The average number of iterations for the four-state solution runs are not plotted since they are very nearly equal to the values for the merged solution runs already plotted. The simulated TMA runs presented are the direct-path cases for both closing and crossing-target courses and the second CZ path case with crossing-target course. All of the runs presented have bearing measurement error standard deviation of 0.2 degree, use correct assumed propagation paths for range initialization and *a priori* information, and use no velocity *a priori* estimates.

The results for the direct-path runs indicate that the use of the three-state solution as initialization to the observable full solution does not improve the number of Monte Carlo runs which converge nor decrease the number of Gauss-Newton iterations required for convergence. It does, however, provide observable three-state solutions during the first leg with high probability of numerical convergence and low computational cost. This provides a great advantage over the four-state solution which has very low convergence probability and high computation cost during the initial leg because of its lack of observability. The three-state solution, therefore, provides for better use of available data and *a priori* information when the full solution is unobservable. In Figure 4-21, the use of the three-state solution during the first leg of the second CZ, crossing-course case is again shown to provide

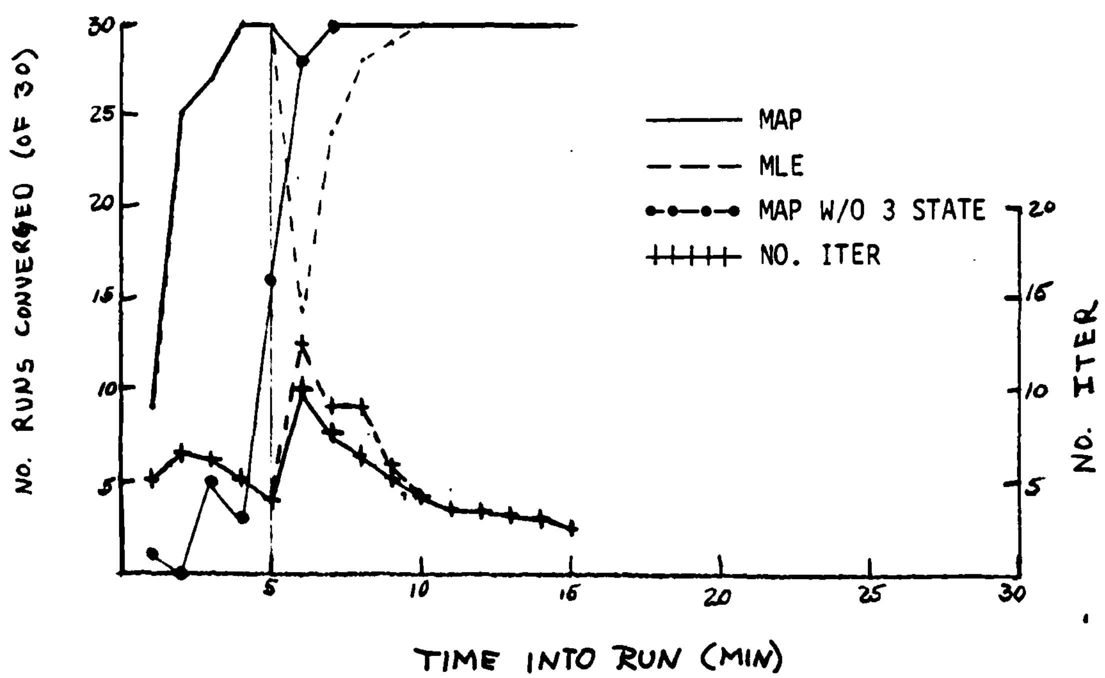

Figure 4-19. Convergence of Bearings-Only Algorithm With Three-State Solution (Direct Path, Closing-Target Course)

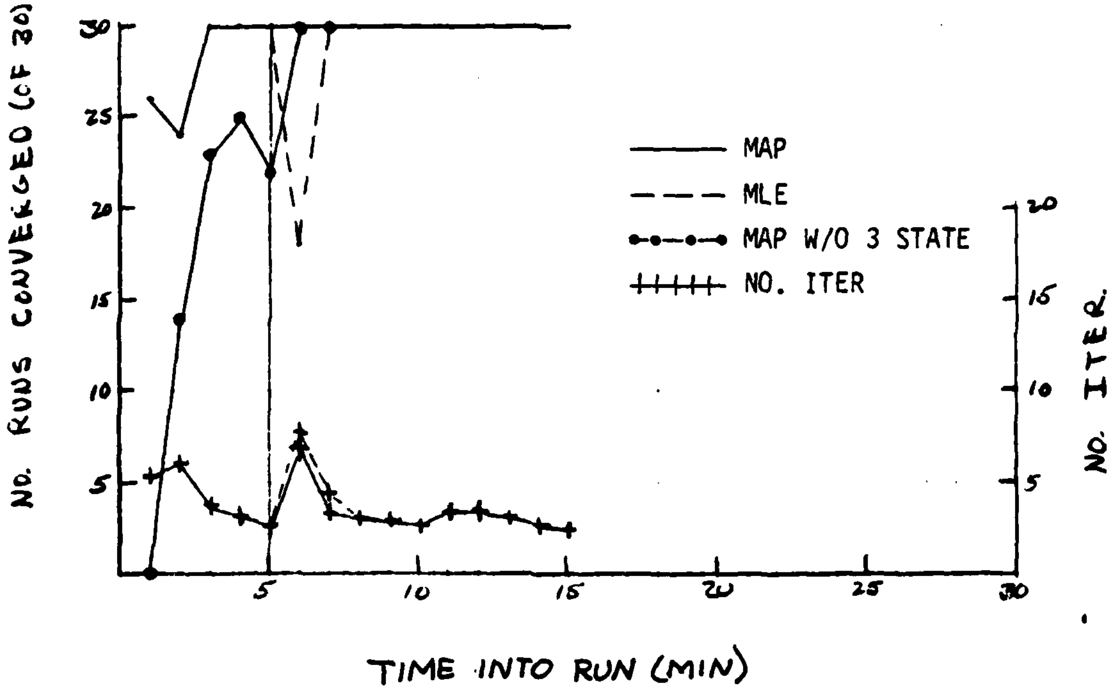

Figure 4-20. Convergence of Bearings-Only Algorithm With Three-State Solution (Direct Path, Crossing-Target Course)

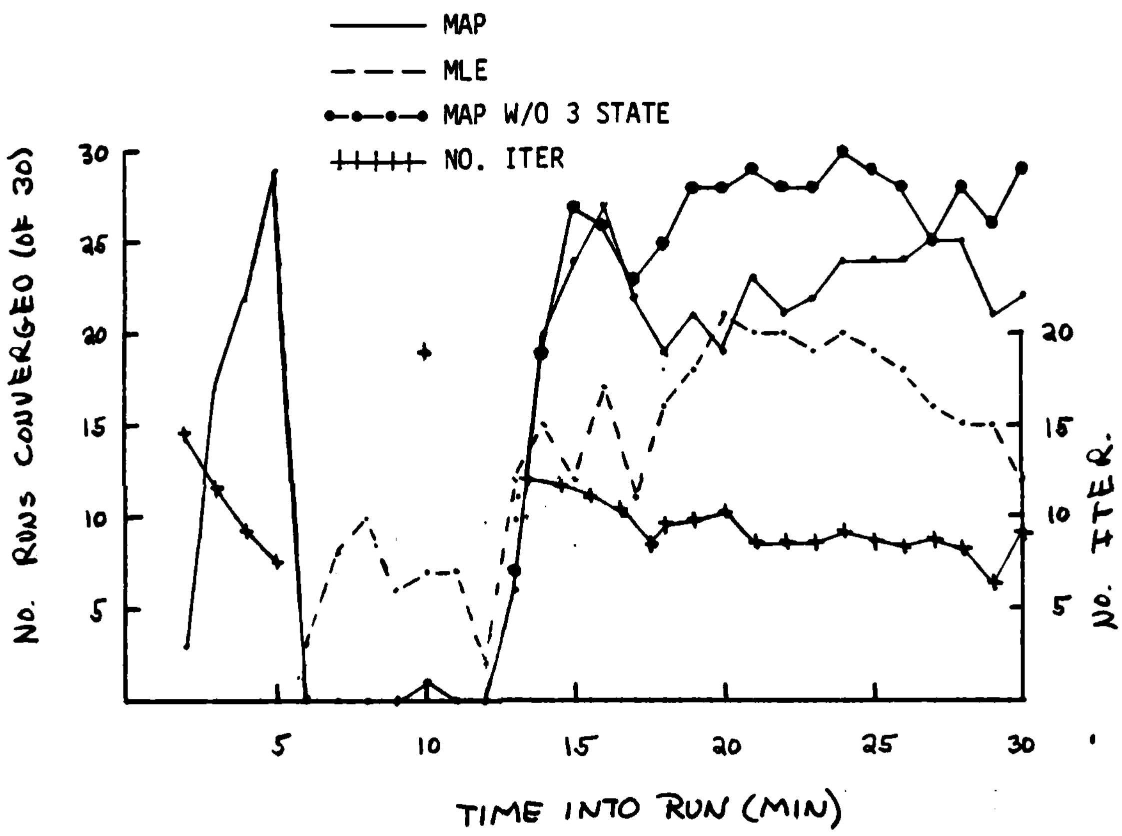

Figure 4-21. Convergence of Bearings-Only Algorithm With Three-State Solution (Second CZ Path, Crossing-Target Course)

improvement during the first leg but no improvement to the later, full-solution calculations. In fact, the probability of convergence is reduced when the three-state solution is used for initialization. In the CZ cases, the three-state solution should really be calculated beyond the first leg when the observability remains poor. Unfortunately the three-state solutions are distinct from one leg to the next and cannot be continued.

4.2.2 Error Behavior of the Calculated Solutions

The range, bearing, speed and course RMS errors over the Monte Carlo repetitions are plotted in Figures 4-22 and 4-23 for the direct-path (true and assumed) simulations using the MLE/MAP algorithms with three-state solution calculated during the first leg. The full-solution values from which the plotted errors are calculated are determined during the first leg from the relative-motion solutions combined with own-ship motion values and the *a priori* estimates or initializations. For the MAP algorithm, these calculations are made in an optimal manner with the *a priori* estimates weighted by their uncertainties. Also plotted are the RMS error values for the MAP Monte Carlo repetitions of the completely four-state algorithm. These values are also included in Section 4.1.2. These plots indicate no difference in solution quality for any of the parameters after the first leg. Therefore, the three-state solution initialization to the MAP algorithm does not appear to enhance solution accuracy. During the first leg, the MAP algorithm with the three-state solution has greater range RMS errors and basically no difference in bearing, speed and course errors as compared to the full solution. This occurs in spite of improved convergence properties during this leg before the full solution is theoretically observable. In addition, the measured usefulness of *a priori* information is the same between the two procedures.

4.2.3 Summary

Table 4-2 summarizes the Monte Carlo statistics for the TMA solutions of the MLE and MAP algorithms with and without the range-normalized, relative-motion solution calculation during the first leg. The convergence properties

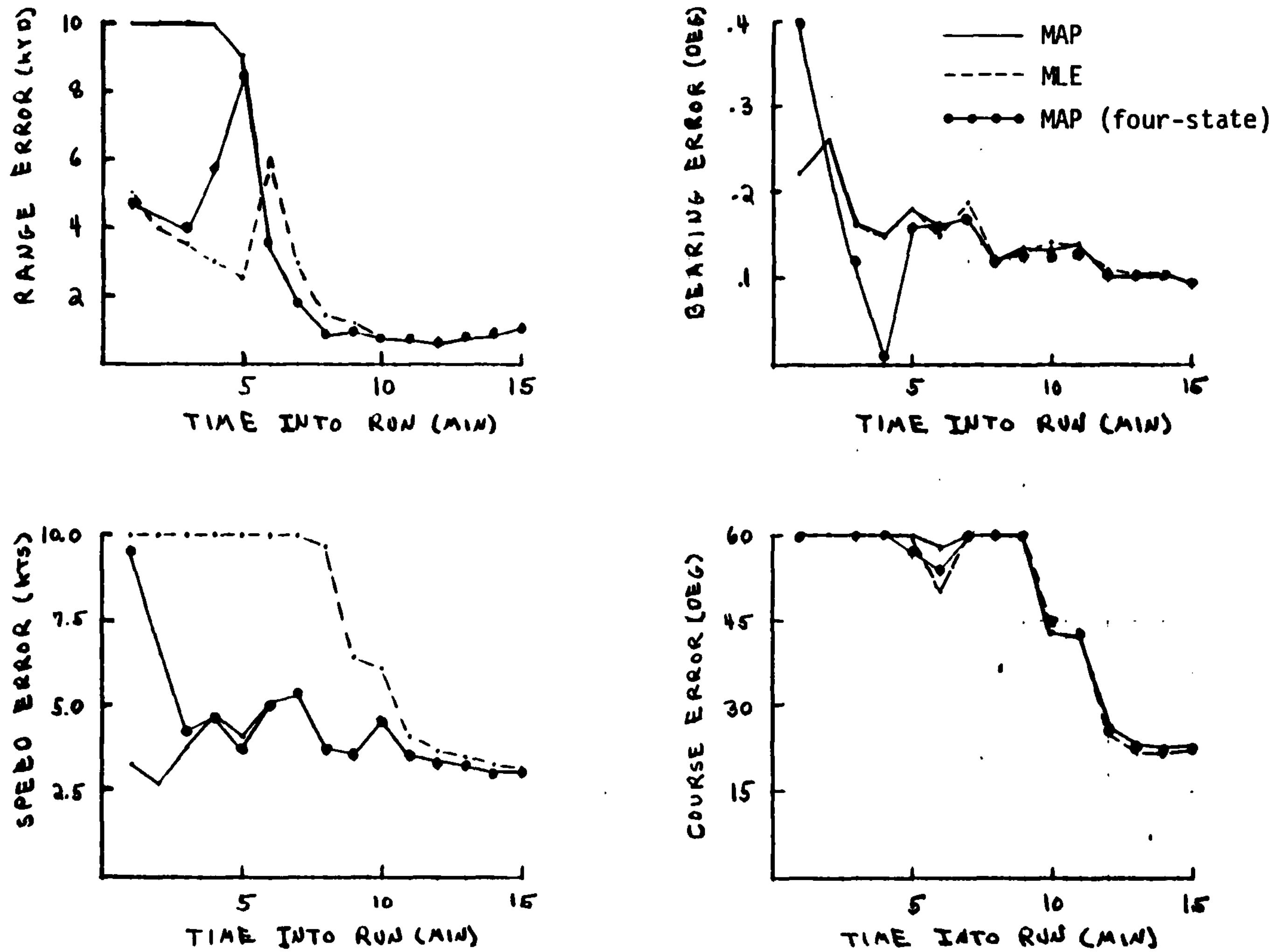

Figure 4-22. Accuracy (RMS Errors) of Bearings-Only Algorithm With Three-State Solution Over Monte Carlo Repetitions (Direct-Path, Closing-Target Course)

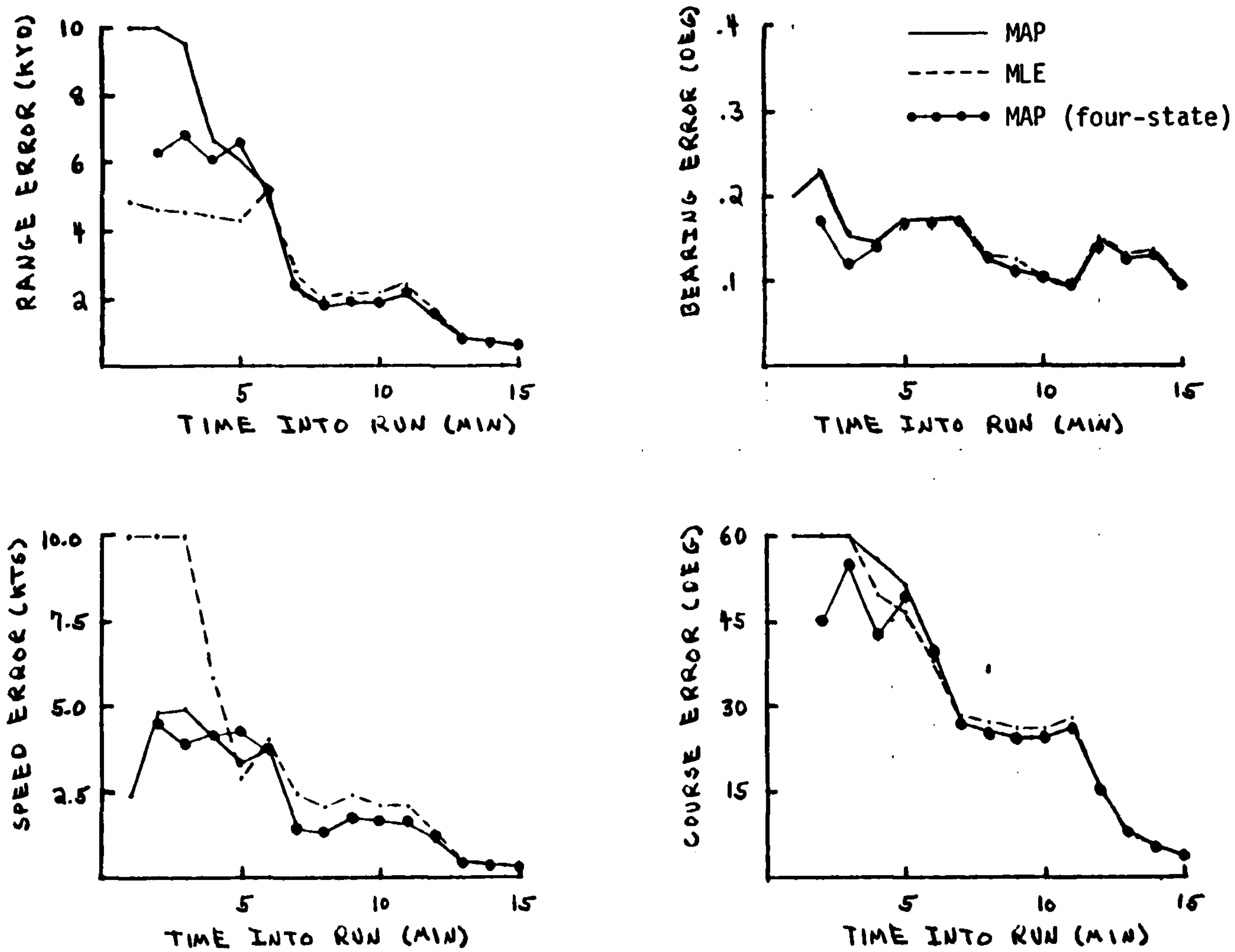

Figure 4-23. Accuracy of Bearings-Only Algorithm With Three-State Solution Over Monte Carlo Repetitions (Direct-Path, Crossing-Target Course)

Table 4-2. Solution Statistics for Direct-Path Cases With and Without Use of Three-State Solution During First Leg

GEOM	TIME	SOLUTION TYPE	NO. CONVERGED REPETITIONS	NO. ITERATIONS PER M. C. REP.	RMS ERROR*			
					RANGE (kyd)	BEARING (deg)	SPEED (knots)	COURSE (deg)
CLOSING COURSE	5 min	4/MLE	0	---	---	---	---	---
		4/MAP	16	13.2	8498	.17	3.75	57.2
		3/MLE	30	4.0	2565	.18	29.40	77.7
		3/MAP	30	4.0	9093	.18	4.12	75.3
	6 min**	4/MLE	17	10.8	5005	.21	12.70	72.9
		4/MAP	28	10.0	3591	.17	5.02	54.6
		3/MLE	14	12.5	6013	.15	11.80	50.6
		3/MAP	28	9.8	3538	.16	5.01	57.7
CROSSING COURSE	5 min	4/MLE	2	16.0	12,620	.16	22.70	51.7
		4/MAP	22	10.7	6697	.17	4.36	49.4
		3/MLE	30	2.7	4318	.17	2.91	46.5
		3/MAP	30	2.7	6165	.17	3.40	51.0
	6 min**	4/MLE	21	11.0	6214	.19	5.14	45.2
		4/MAP	30	7.0	5280	.17	3.77	40.2
		3/MLE	18	7.9	5177	.17	4.03	38.4
		3/MAP	30	7.0	5258	.17	3.75	40.0

*Three-state solution RMS errors calculated using initial range of 15 kiloyards (error of 5 kiloyards).

**If did not converge at 5 minutes, used the standard initializations (R=15 kiloyards, Speed=0 knots).

and the RMS errors are given for the solutions calculated at the end of the first leg (5 minutes) and at the beginning of the second leg (6 minutes). These solutions, therefore, represent the initialization to and the calculation of the first solution after a maneuver (i.e., after the problem becomes theoretically observable). The cost and value for the use of the three-state solution initialization, as well as that for the use of *a priori* information may be studied. This summary basically substantiates the findings of the previous two sections. The only real advantage of the three-state solution as implemented here is in obtaining numerically converged solutions with relatively low computation cost when the full solutions are not observable. A more important influence on the quality of the initial, observable, full-solution is the use of *a priori* estimates.

4.3 BEARING/FREQUENCY MULTISENSOR MLE WITH THE MODIFIED GAUSS-NEWTON ALGORITHM

Results are presented from simulations of bearing/frequency (Doppler) TMA without own-ship maneuvers using the MLE and MAP procedures modified to accept multisensor measurements. The numerical solution method used is the modified Gauss-Newton algorithm with step optimization. The mathematical development of the estimation procedure and details of the algorithm used are given in Chapter 2 and the Appendix. The TMA simulations presented are the direct-path cases (10-kiloyard range) with closing and crossing initial target course and the first CZ case with crossing target course. The bearing measurement error standard deviation is 0.2 degree for all cases, and the frequency error standard deviations used are 10^{-2} and 10^{-3} in relative units to the mean center frequency ($\overline{f}_0 = 1$). The *a priori* information utilized by the MAP estimation procedure and for initialization of both the MLE and MAP solutions consist of range (propagation path), velocity and center frequency estimates with their uncertainties. For all runs the range *a priori* estimate is the true propagation path, the velocity estimate is zero with magnitude limit defined by the standard deviation of 15 knots, and the center frequency estimate is the true value with standard deviation weights of 10^{-2} and 10^{-4}. The measurements describing the numerical convergence behavior and solution

quality of the procedure are plotted and discussed in the following sections. Again, the results are analyzed with regard to an evaluation of the benefits provided by *a priori* information use. Comparisons are made among the MLE algorithm, the MAP without accurate center frequency information ($\sigma_{f_0} = 10^{-2}$) and the MAP with accurate center frequency estimate ($\sigma_{f_0} = 10^{-4}$), denoted MAP_f, for each TMA geometry and the two frequency error standard deviations.

4.3.1 Numerical Convergence Properties of the Algorithm

The number of converged Monte Carlo repetitions and the average number of Gauss-Newton iterations per repetition are plotted in Figures 4-24 through 4-26 for each calculation time. These measurements represent the probability of, and the computational cost for obtaining convergence of the MLE and MAP algorithms. The results for all cases indicate a general enhancement (increased likelihood and decreased cost) of the numerical convergence derived from the *a priori* information as used by the MAP algorithm. The use of a center frequency *a priori* estimate with low uncertainty (the MAP_f runs), in particular, provide the greatest improvement. This solution provides nearly complete convergence with few required iterations throughout all runs simulated. The difference between the MAP and MAP_f runs is particularly large in the runs with the more accurate frequency measurements. It appears, therefore, that in order to optimally use the measurements along with the *a priori* information, an accurate center frequency estimate is important. Without this, the numerical convergence of the MAP algorithm is only slightly better than that of the MLE algorithm for runs with the more accurate frequency measurements ($\sigma_{f_m} = 10^{-3}$).

4.3.2 Accuracy of the Calculated Solutions

The accuracy of the MLE, MAP and MAP_f solutions are presented in Figures 4-27 through 4-32 for the direct and first CZ path cases, each with frequency error standard deviations of 10^{-2} and 10^{-3}. The RMS and mean errors over the Monte Carlo repetitions are plotted for the range, speed and course

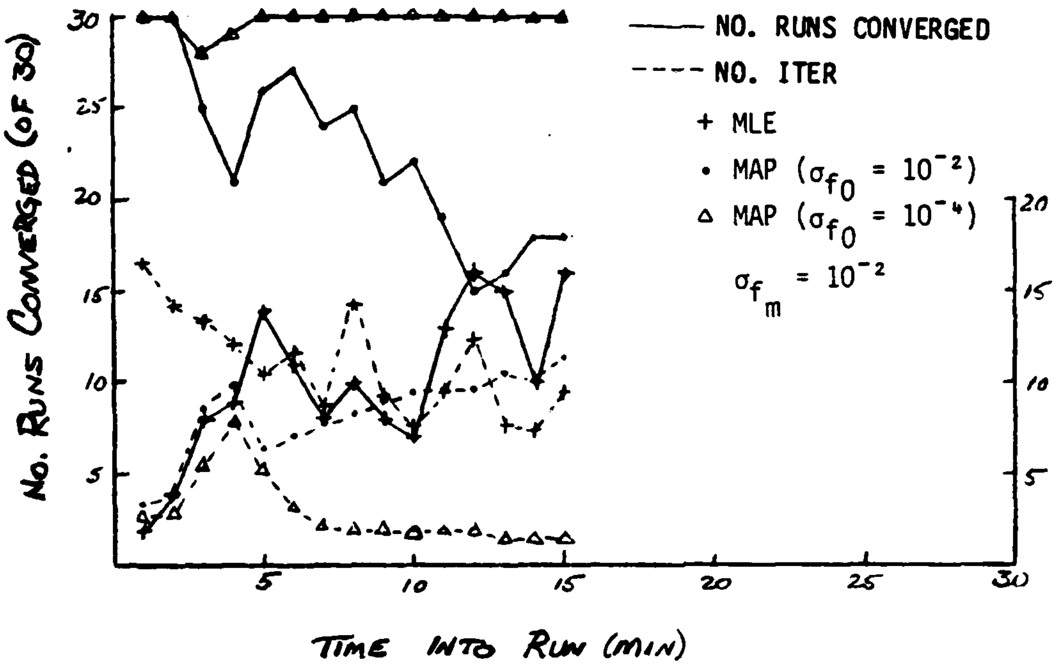

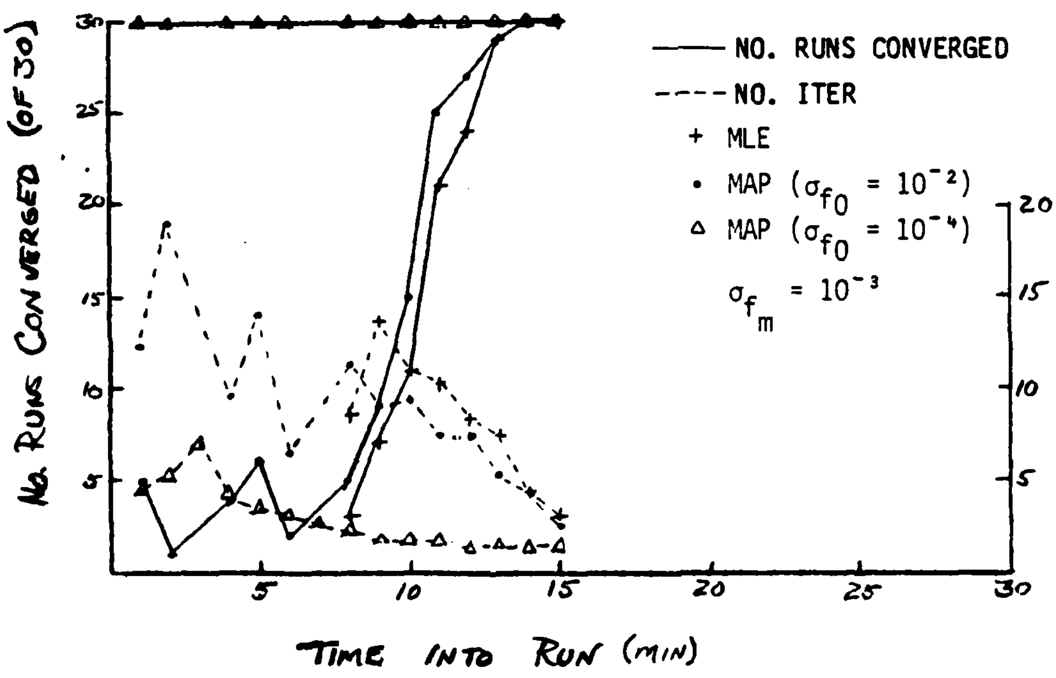

Figure 4-24. Numerical Convergence of Bearing/Frequency Multisensor TMA Algorithm (Direct-Path (10 kiloyards) Closing-Target Course)

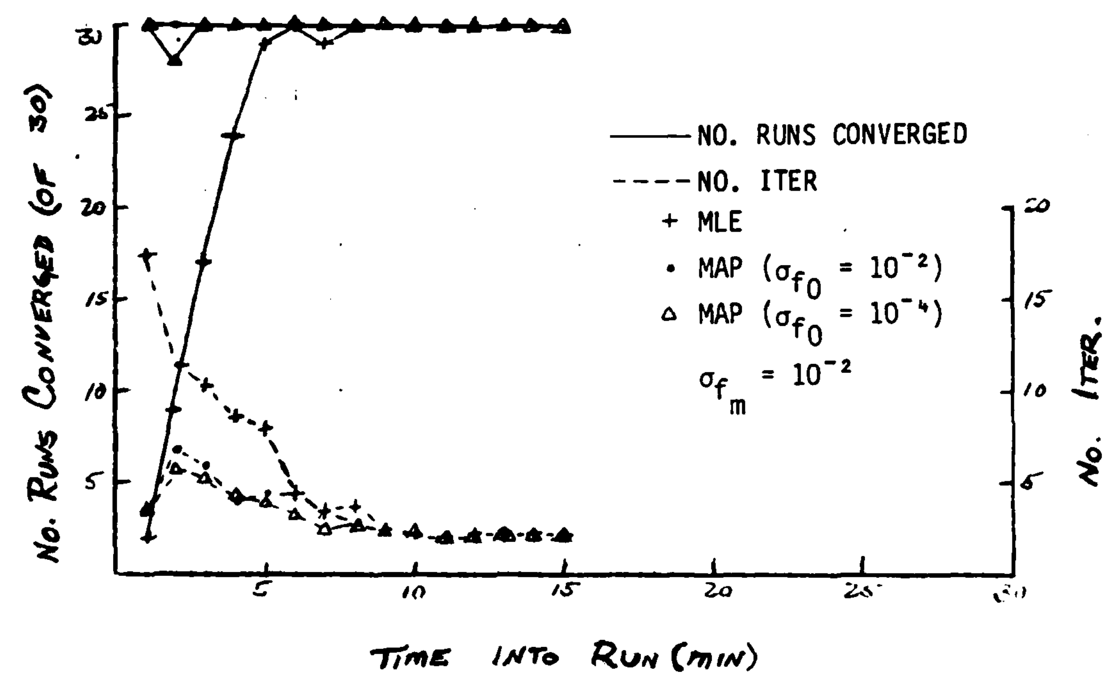

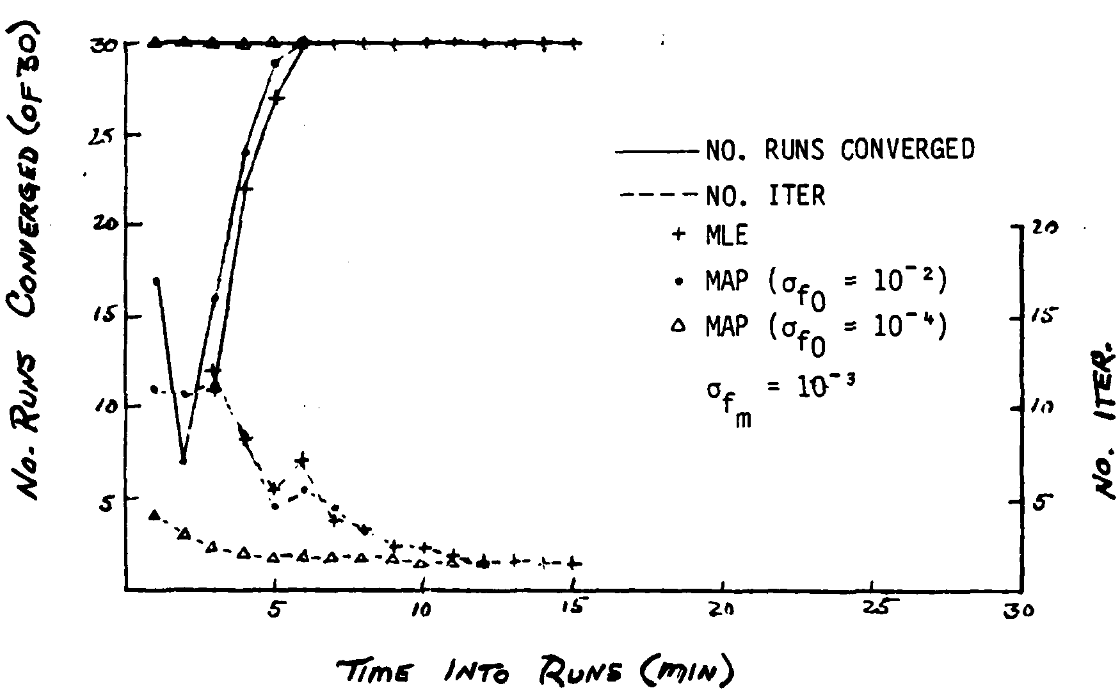

Figure 4-25. Numerical Convergence of Bearing/Frequency Multisensor TMA Algorithm (Direct-Path (10 kiloyards) Crossing-Target Course)

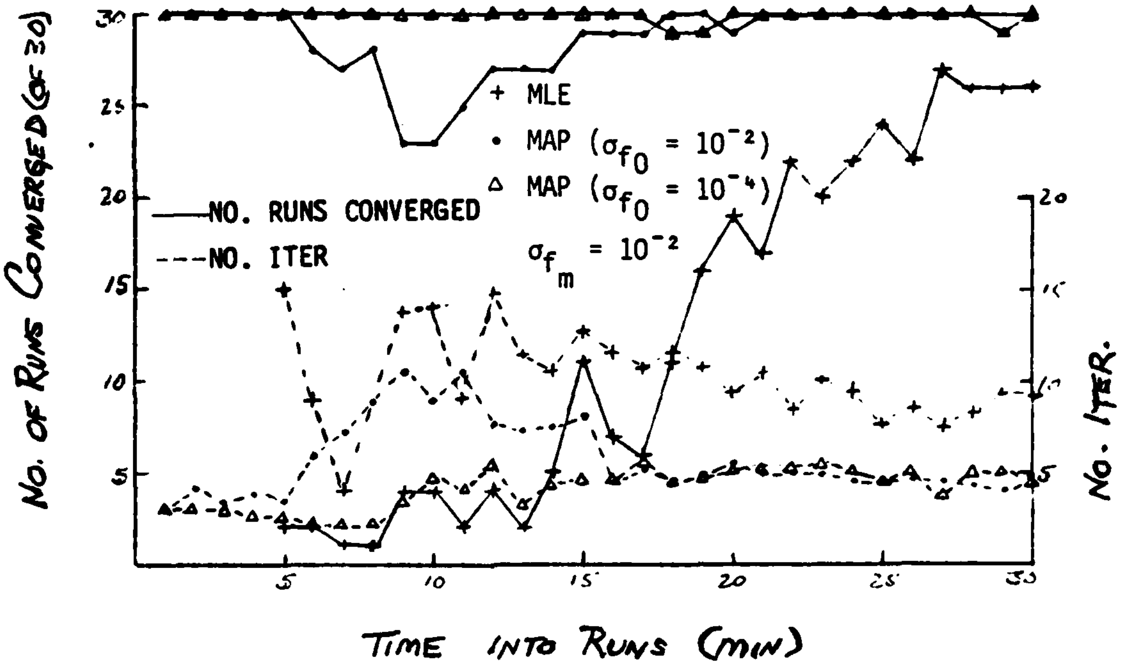

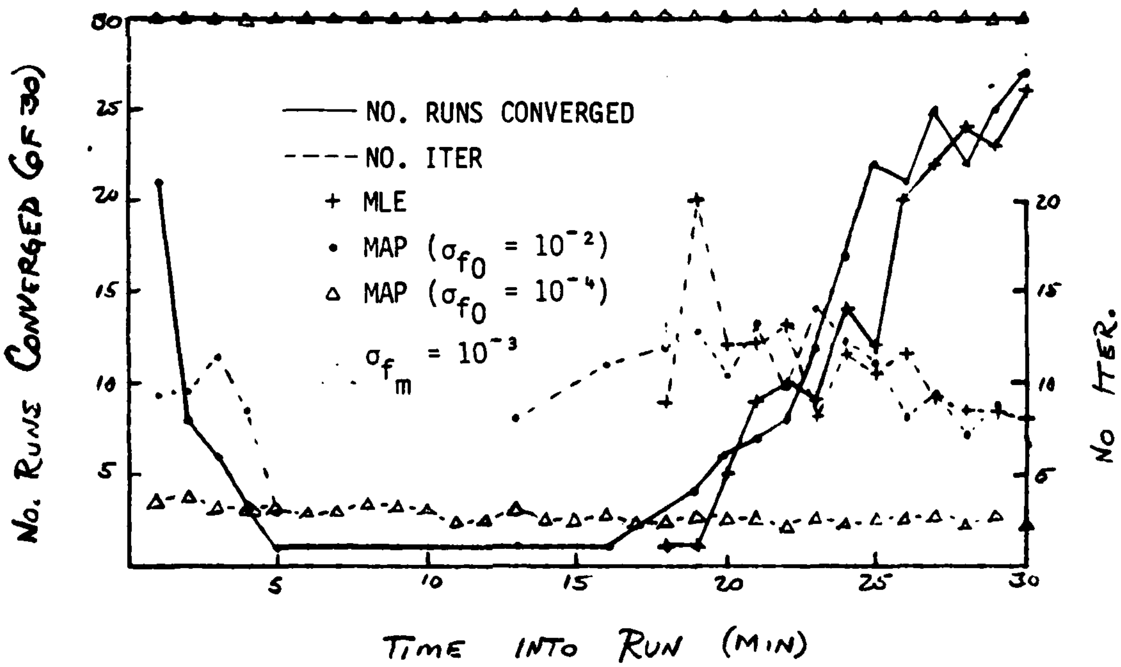

Figure 4-26. Numerical Convergence of Bearing/Frequency Multisensor TMA Algorithm (First CZ Path, Crossing-Target Course)

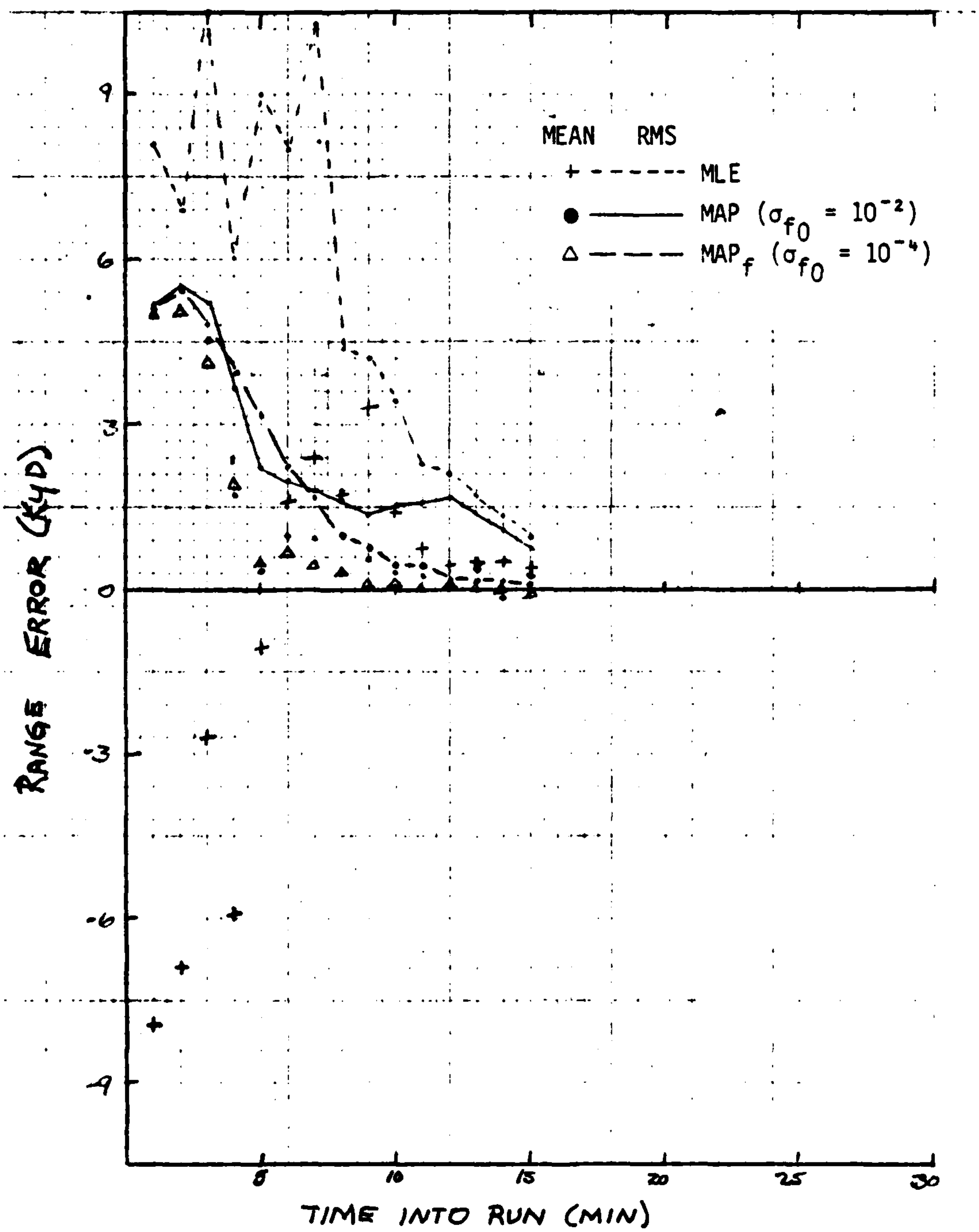

Figure 4-27a. Range Error for Bearing/Frequency Multisensor Solution (Direct-Path, Closing-Target Course, $\sigma_{f_m} = 10^{-2}$)

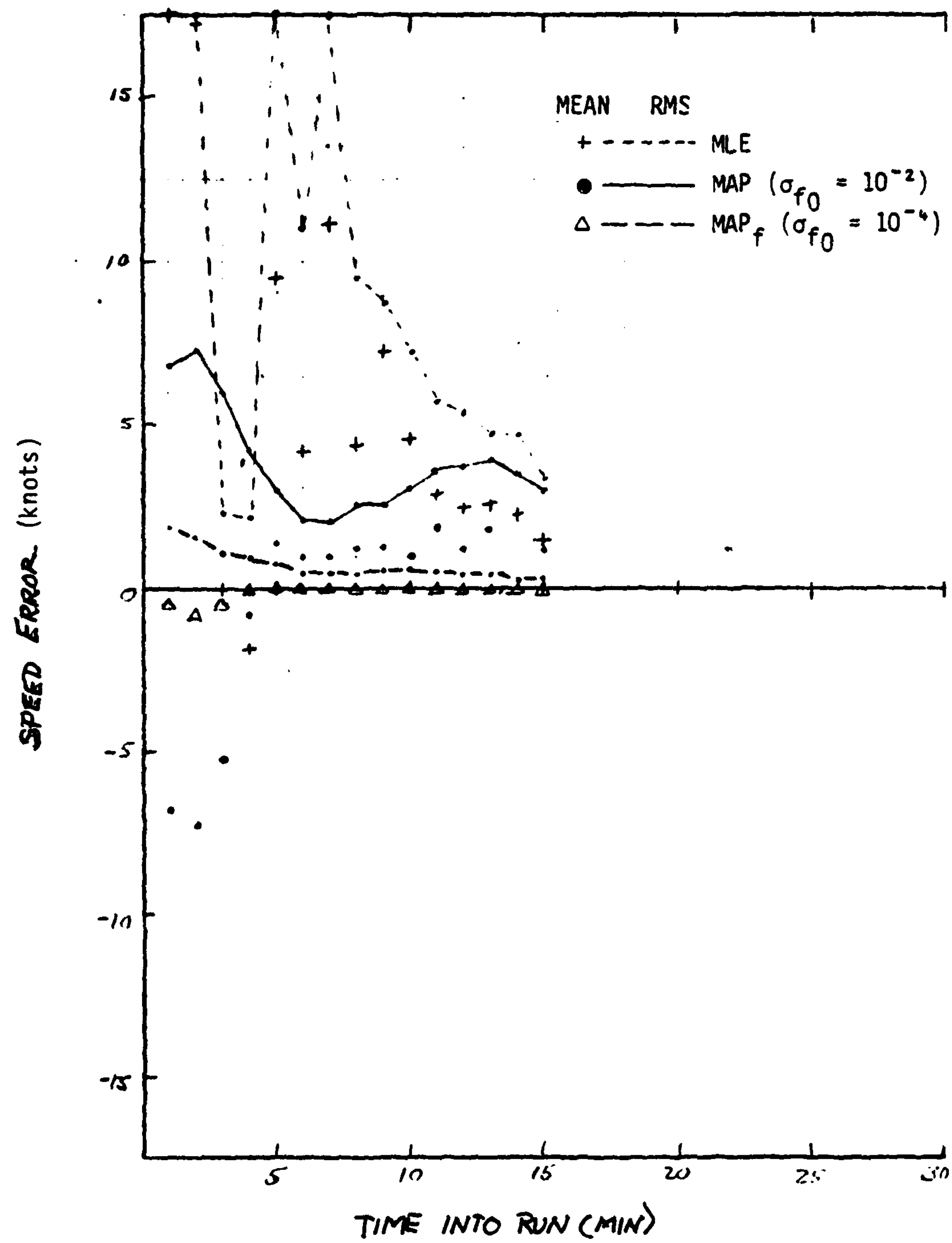

Figure 4-27b. Speed Error for Bearing/Frequency Multisensor Solution (Direct-Path, Closing-Target Course, σ_{f_m} = 10^{-2})

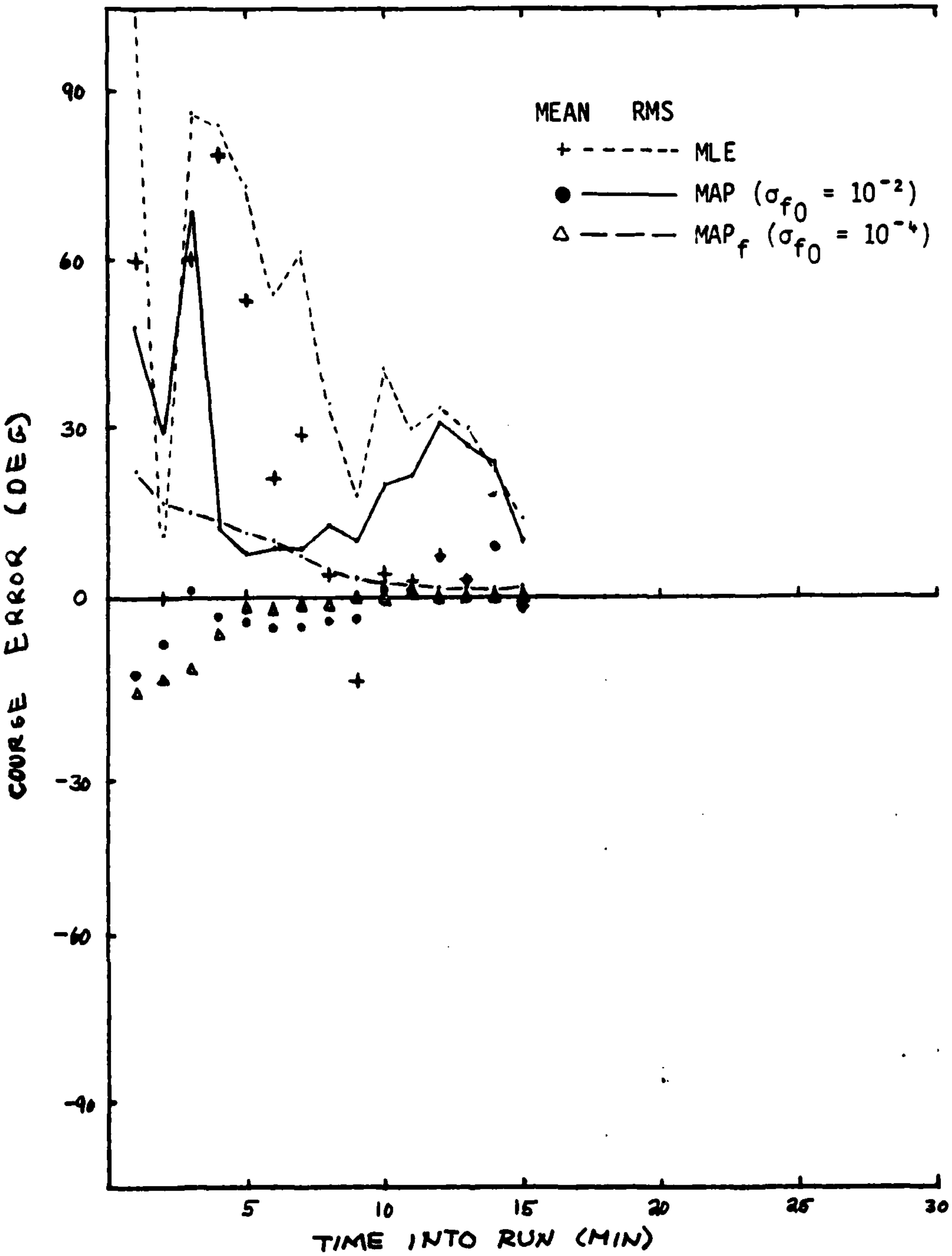

Figure 4-27c. Course Error for Bearing/Frequency Multisensor Solution (Direct-Path, Closing-Target Course, $\sigma_{f_m} = 10^{-2}$)

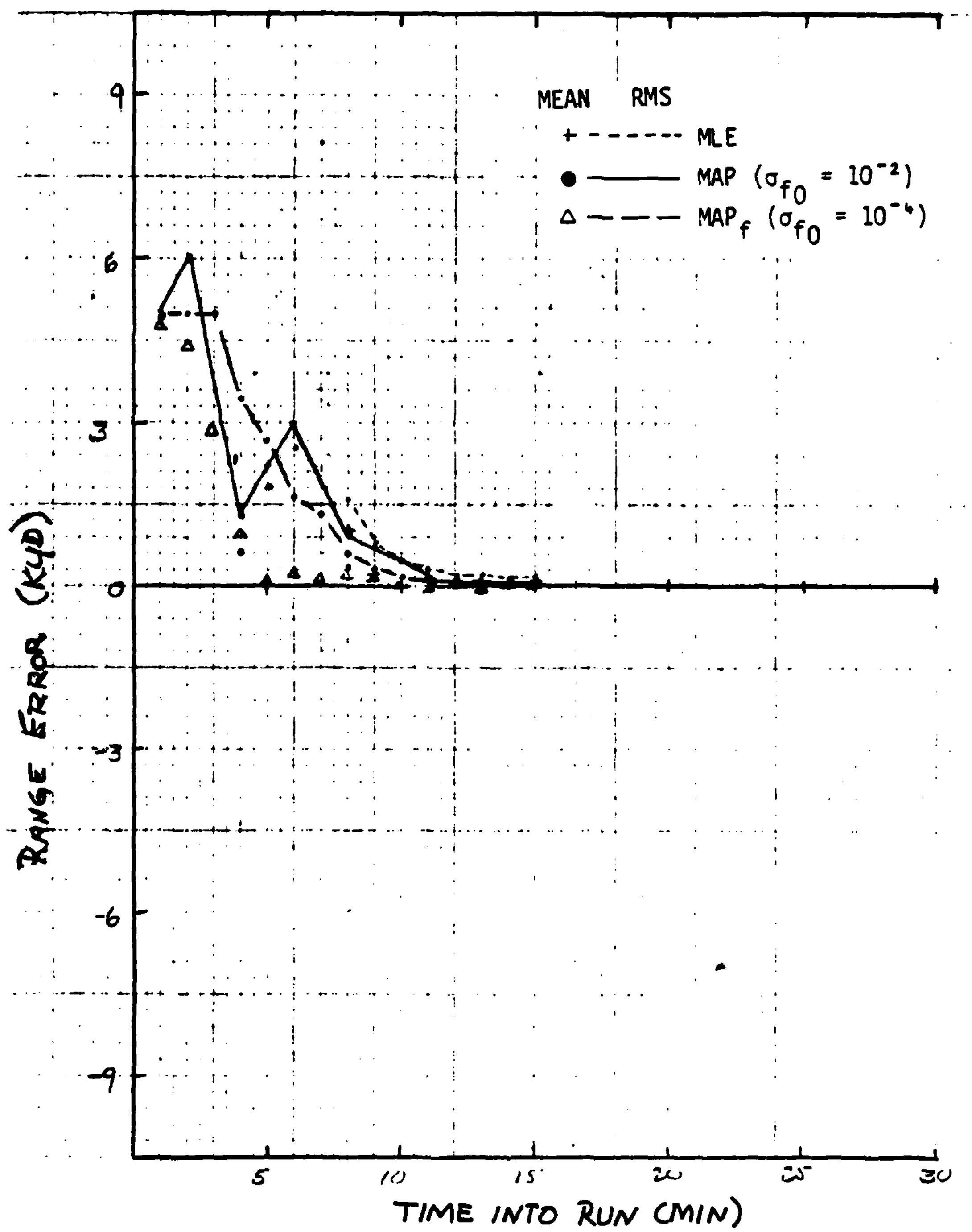

Figure 4-28a. Range Error for Bearing/Frequency Multisensor Solution (Direct-Path, Closing-Target Course, σ_{f_m} = 10^{-3})

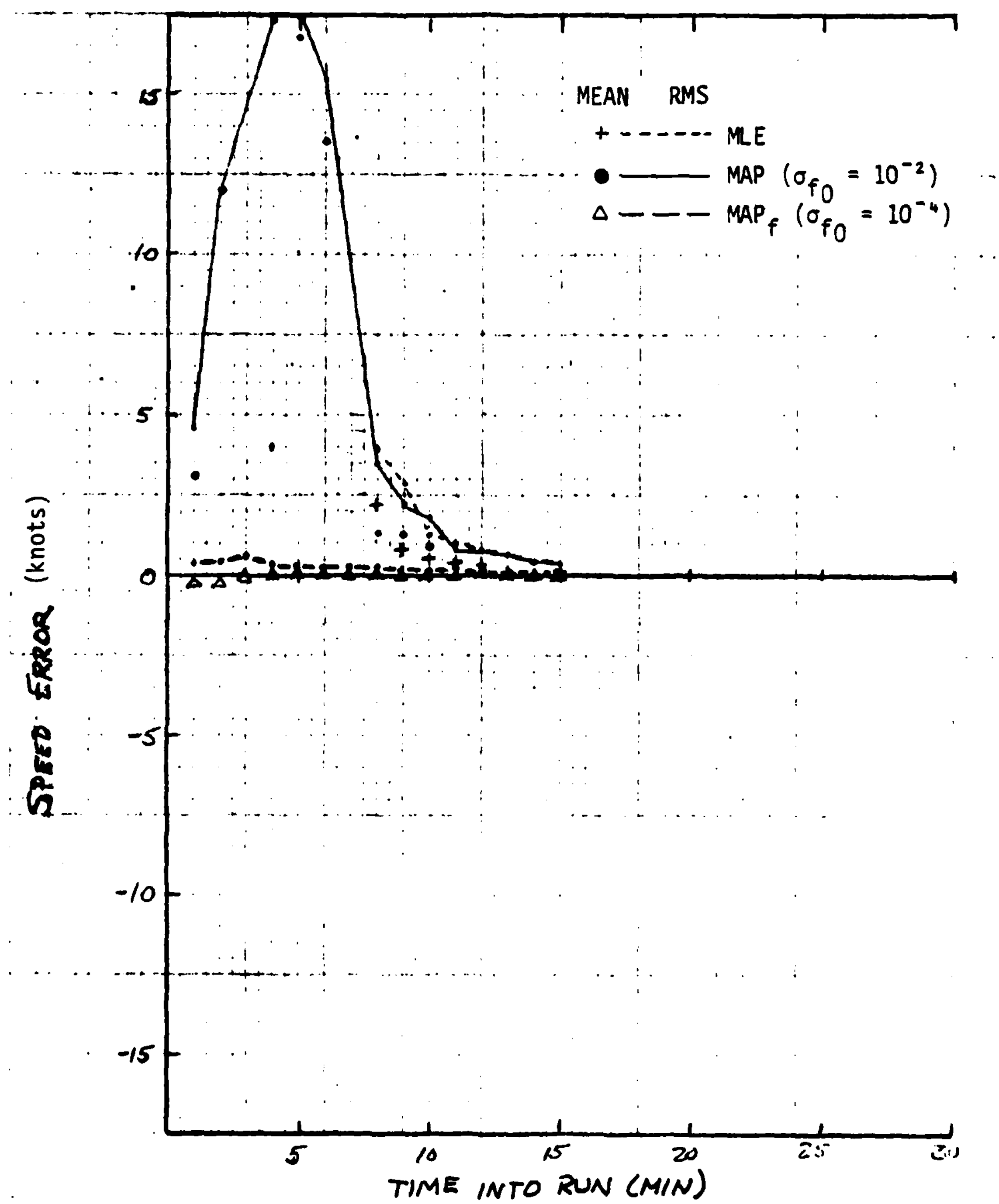

Figure 4-28b. Speed Error for Bearing/Frequency Multisensor Solution (Direct-Path, Closing-Target Course, $\sigma_{f_m} = 10^{-3}$)

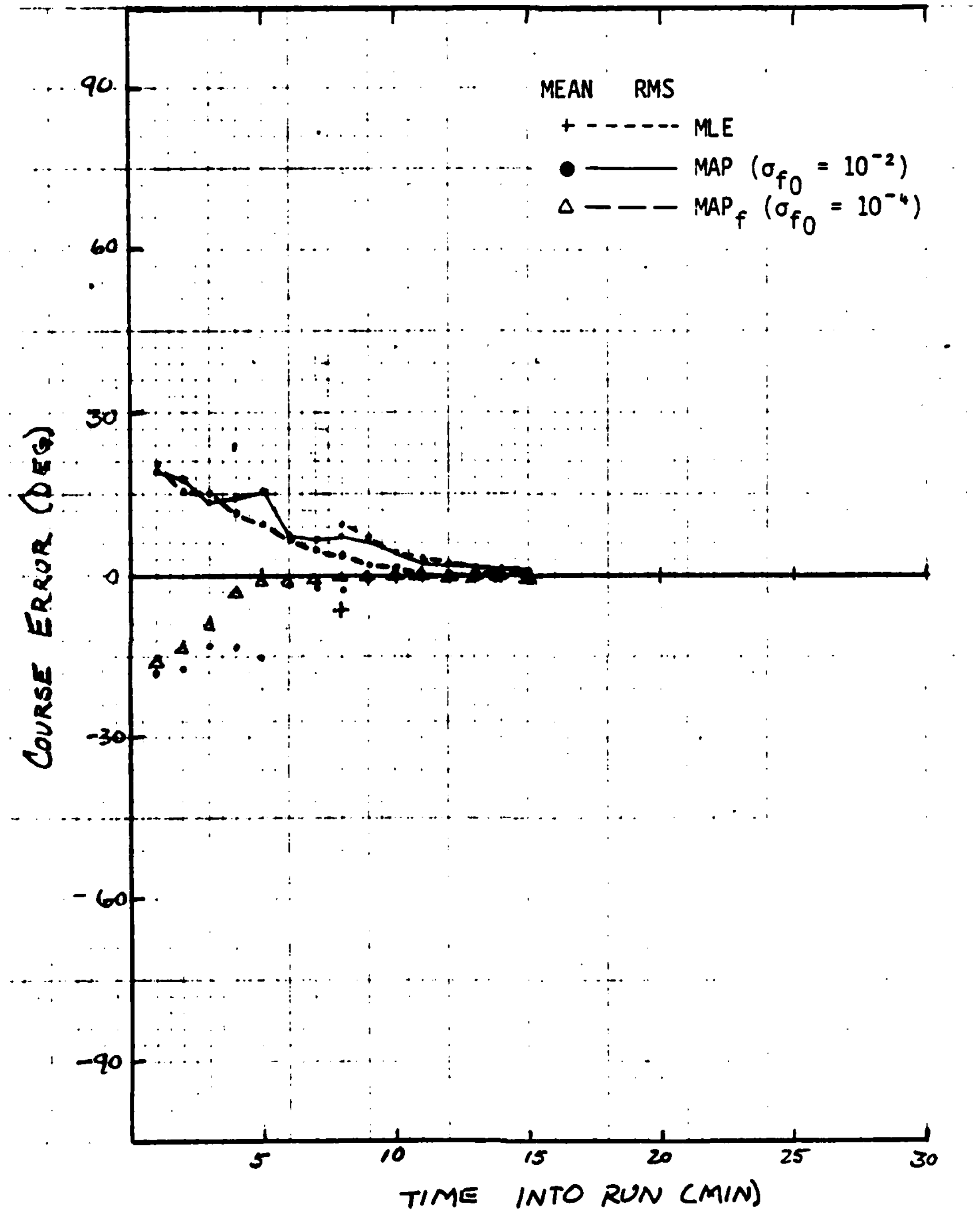

Figure 4-28c. Course Error for Bearing/Frequency Multisensor Solution (Direct-Path, Closing-Target Course, $\sigma_{f_m} = 10^{-3}$)

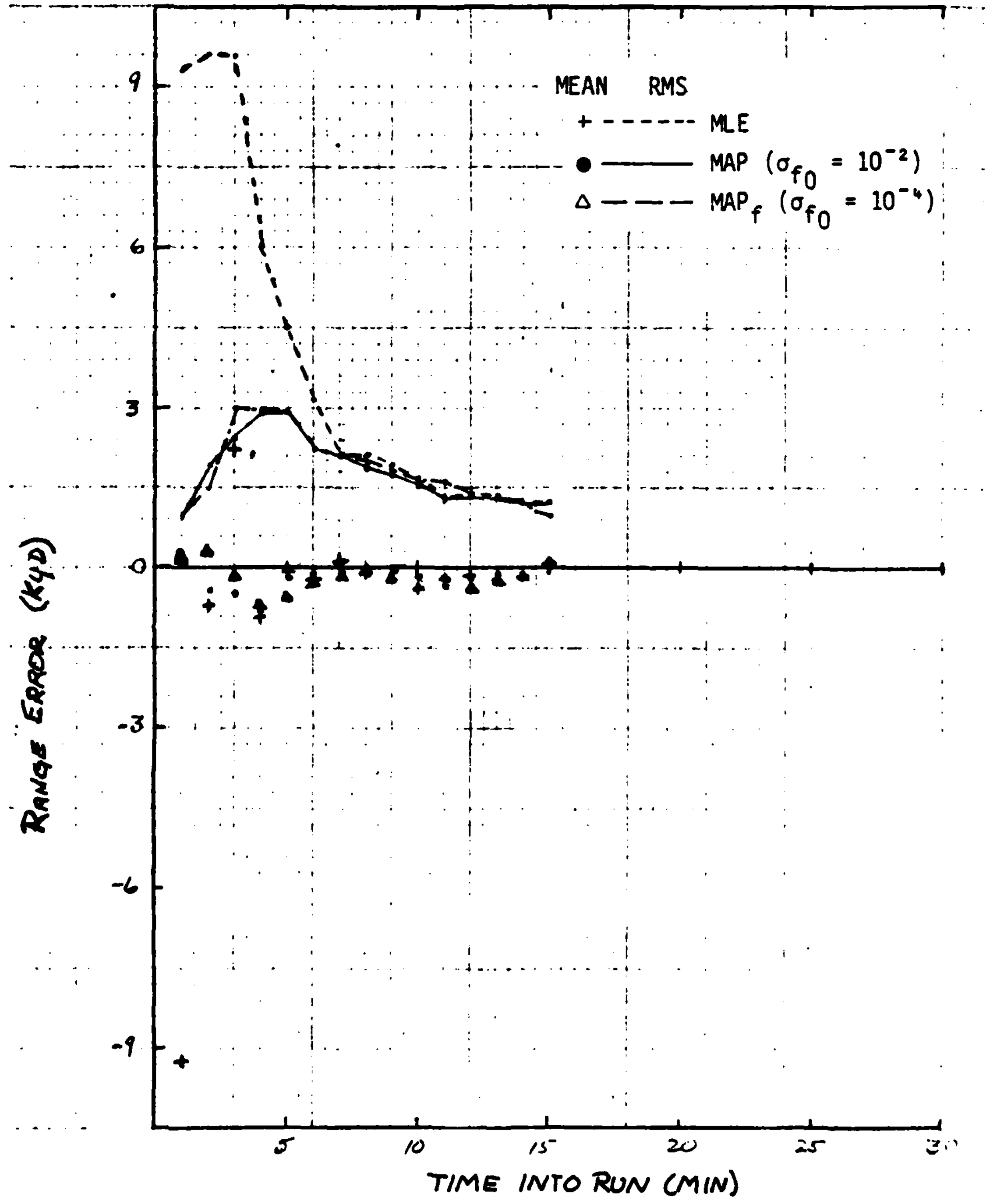

Figure 4-29a. Range Error for Bearing/Frequency Multisensor Solution (Direct-Path, Crossing-Target Course, $\sigma_{f_m} = 10^{-2}$)

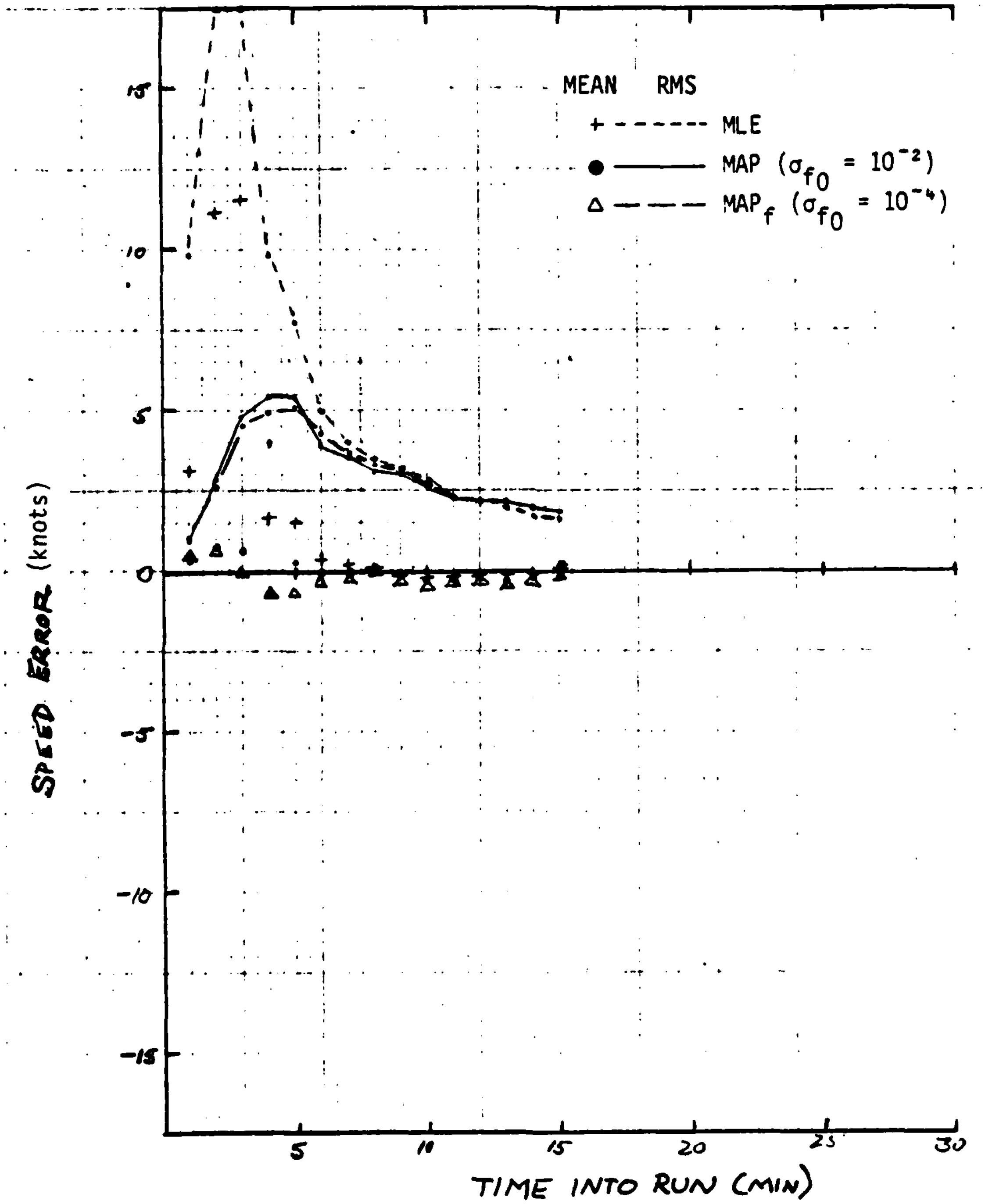

Figure 4-29b. Speed Error for Bearing/Frequency Multisensor Solution (Direct-Path, Crossing-Target Course, $\sigma_{f_m} = 10^{-2}$)

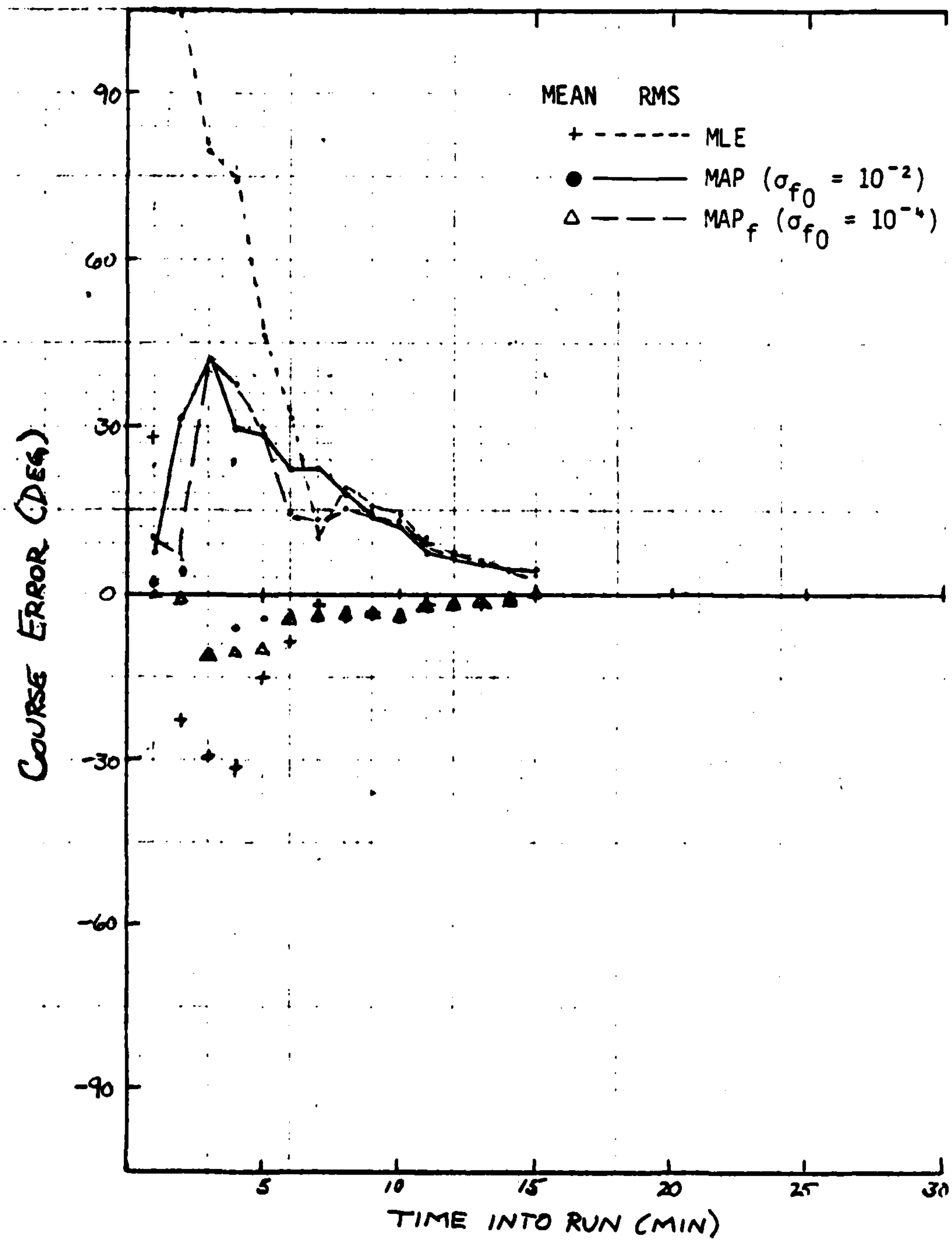

Figure 4-29c. Course Error for Bearing/Frequency Multisensor Solution (Direct-Path, Crossing-Target Course, $\sigma_{f_m} = 10^{-2}$)

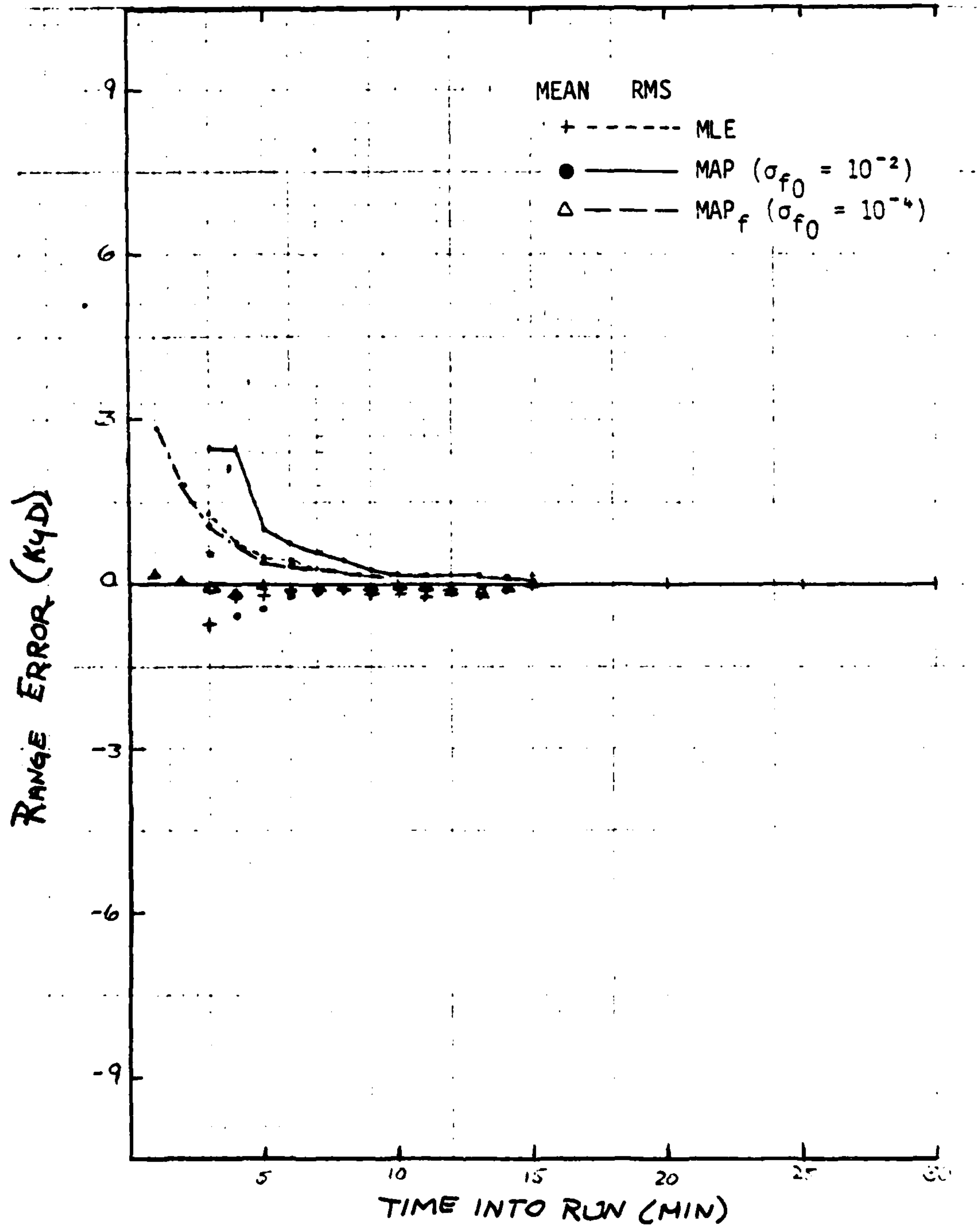

Figure 4-30a. Range Error for Bearing/Frequency Multisensor Solution (Direct-Path, Crossing-Target Course, $\sigma_{f_m} = 10^{-3}$)

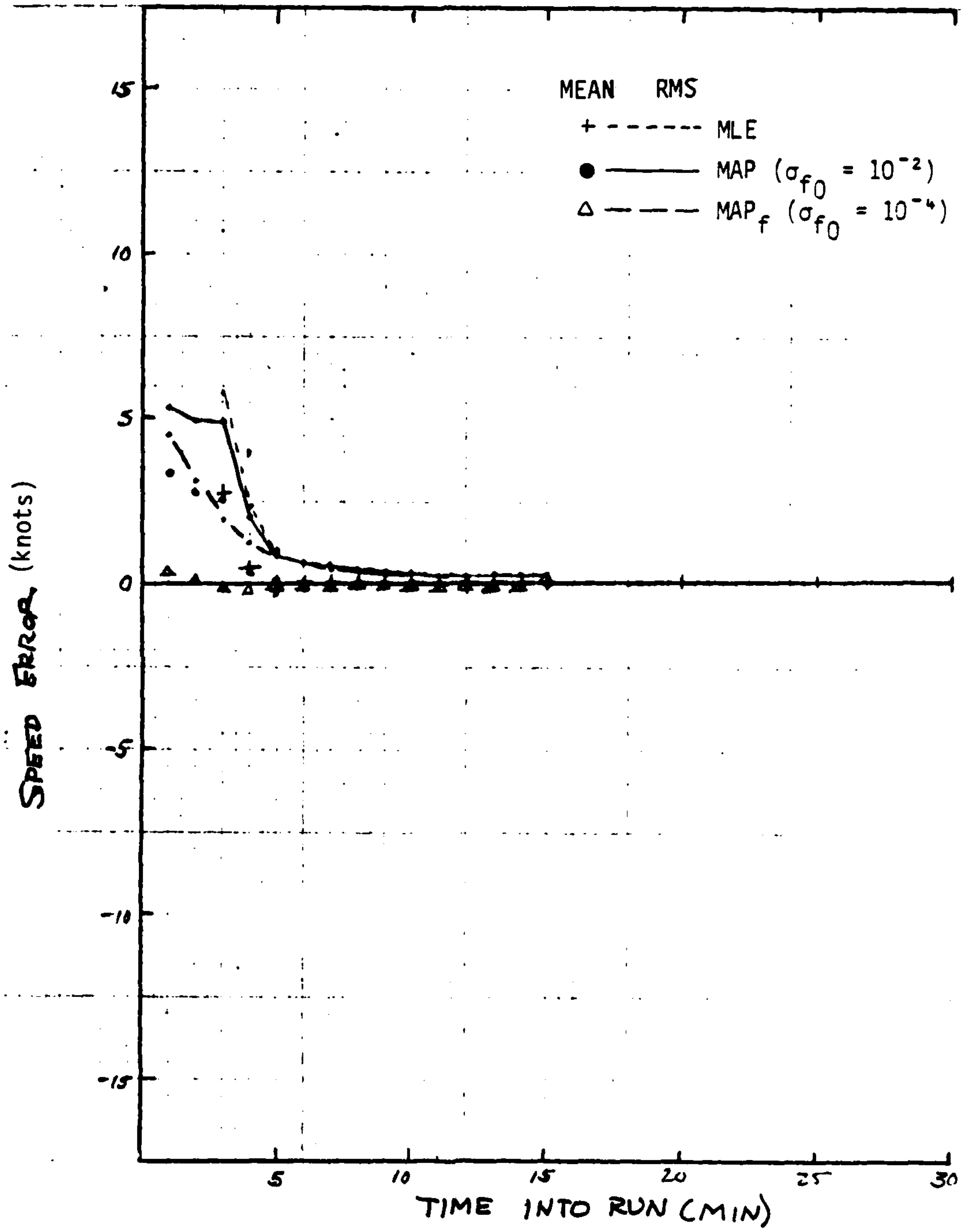

Figure 4-30b. Speed Error for Bearing/Frequency Multisensor Solution (Direct-Path, Crossing-Target Course, σ_{f_m} = 10^{-3})

AD-A109 627 ANALYSIS AND TECHNOLOGY INC NORTH STONINGTON CT F/G 12/1
TARGET MOTION ANALYSIS WITH A PRIORI INFORMATION.(U)
OCT 81 C B BILLING, H F JARVIS N00014-80-C-0379
UNCLASSIFIED P-515-2-81 NL

2 of 2

END
DATE
FILMED
82
DTIC

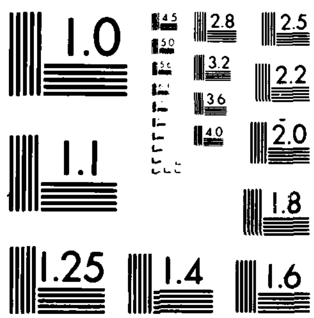

MICROCOPY RESOLUTION TEST CHART
NATIONAL BUREAU OF STANDARDS 1963 A

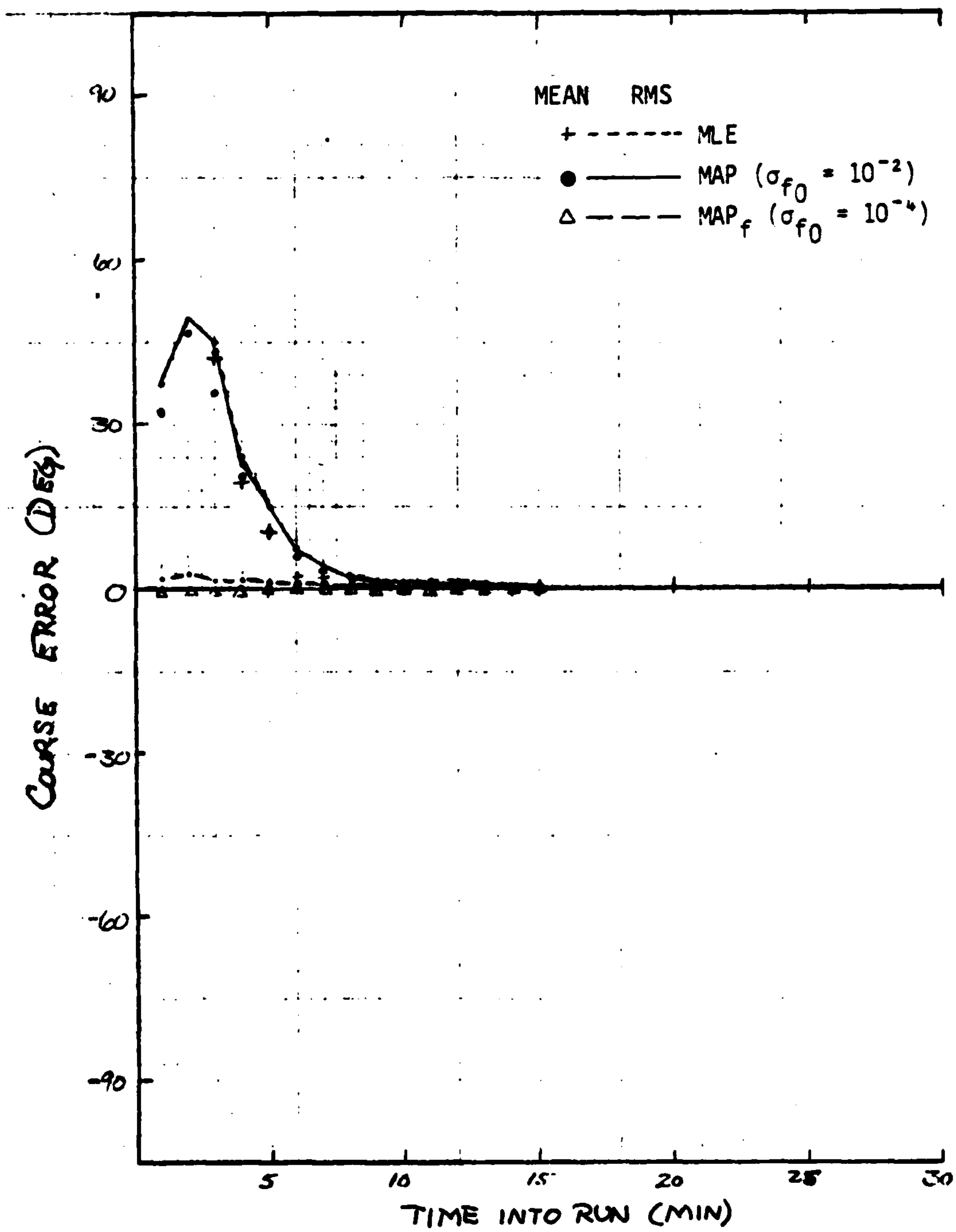

Figure 4-30c. Course Error for Bearing/Frequency Multisensor Solution (Direct-Path, Crossing-Target Course, $\sigma_{f_m} = 10^{-3}$)

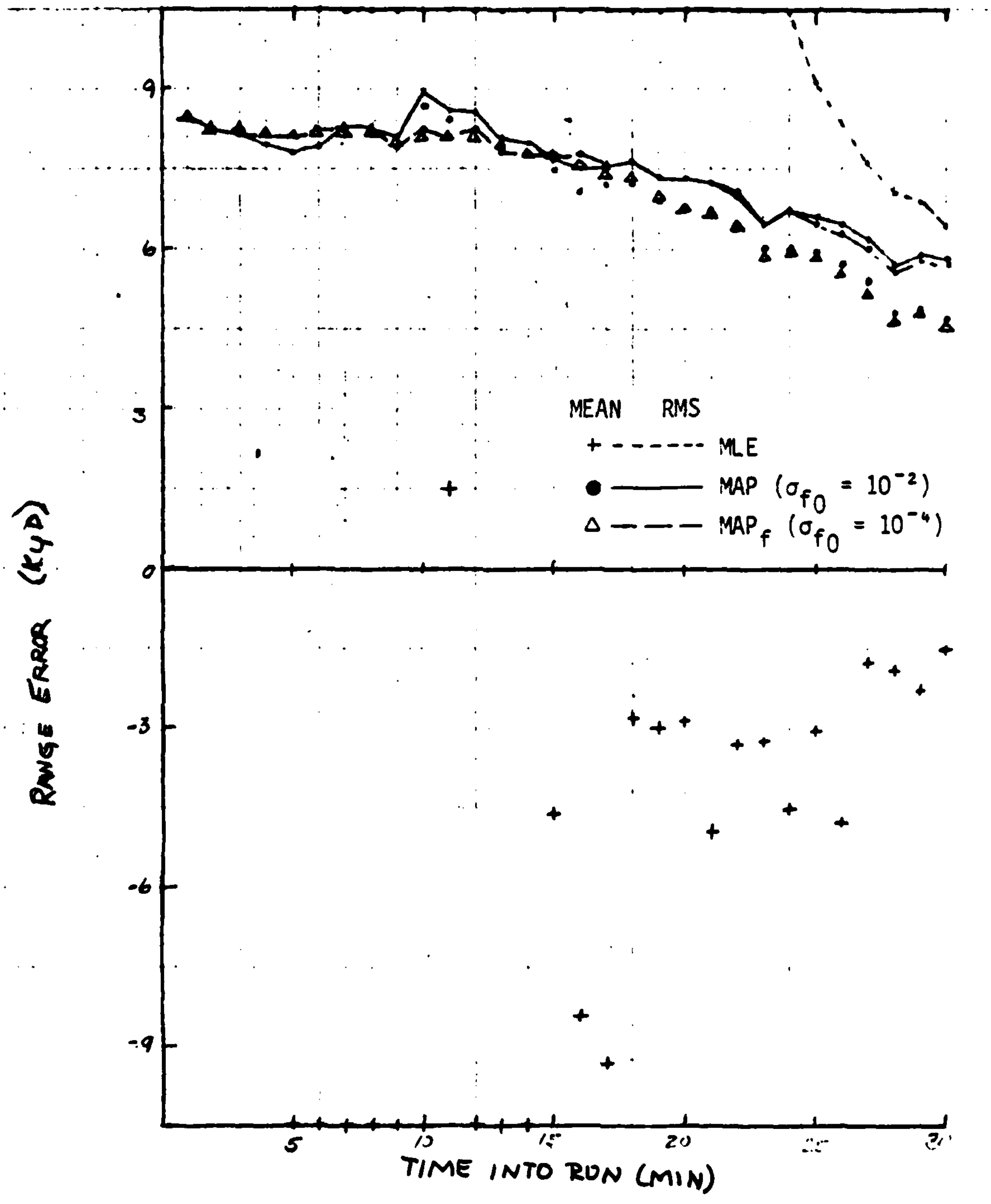

Figure 4-31a. Range Error for Bearing/Frequency Multisensor Solution (First CZ Path, Crossing-Target Course, $\sigma_{f_m} = 10^{-2}$)

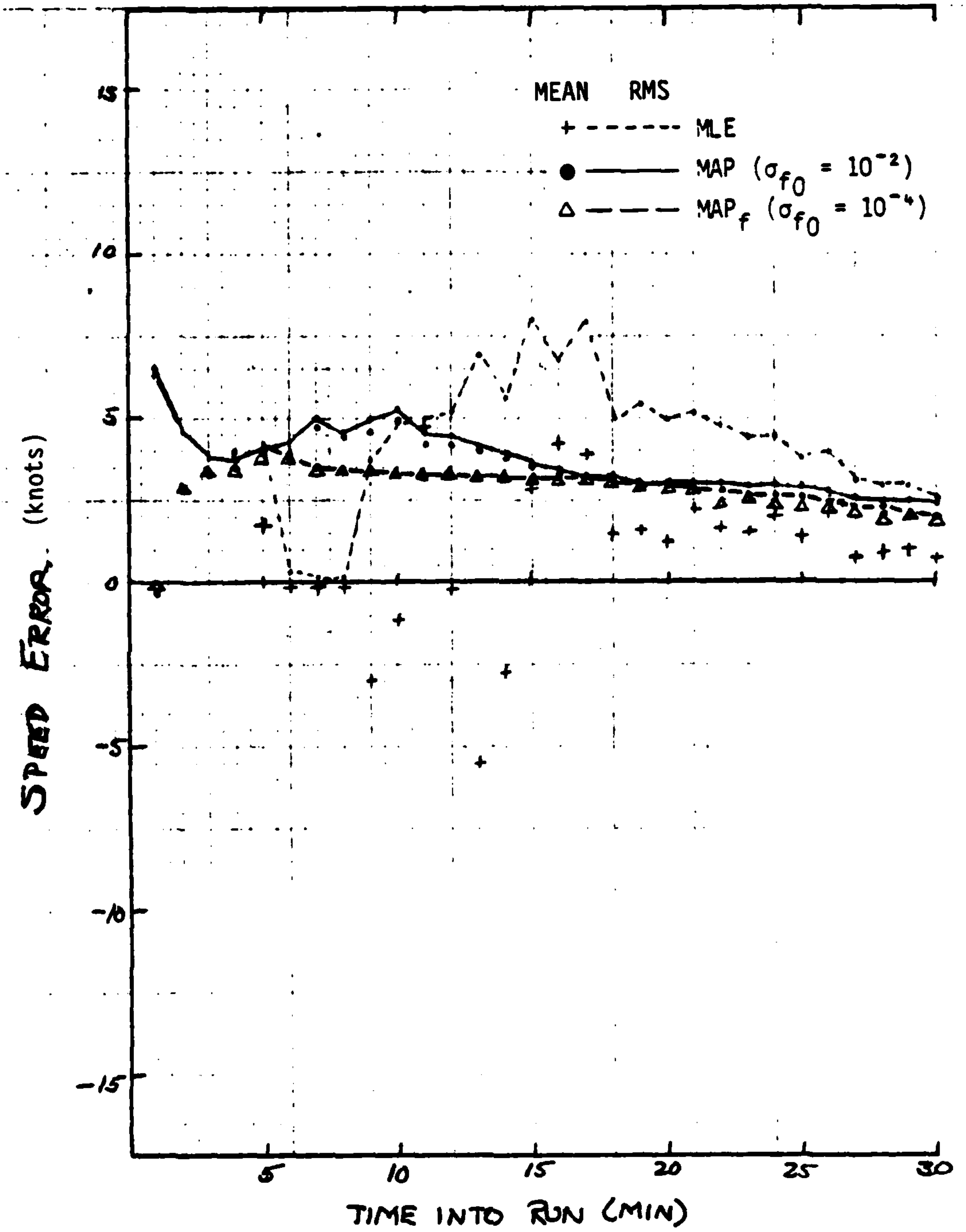

Figure 4-31b. Speed Error for Bearing/Frequency Multisensor Solution (First CZ Path, Crossing-Target Course, $\sigma_{f_m} = 10^{-2}$)

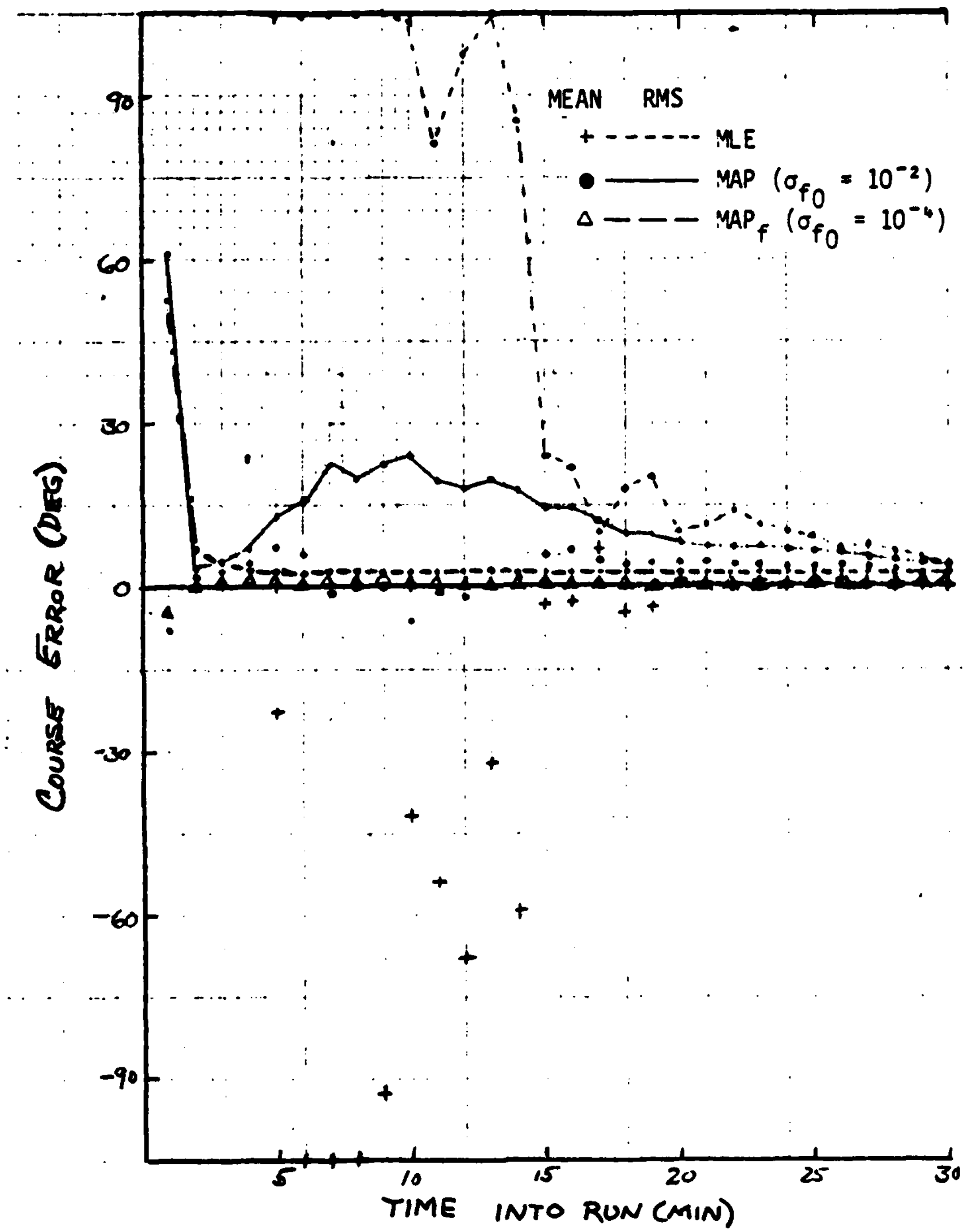

Figure 4-31c. Course Error for Bearing/Frequency Multisensor Solution (First CZ Path, Crossing-Target Course, $\sigma_{f_m} = 10^{-2}$)

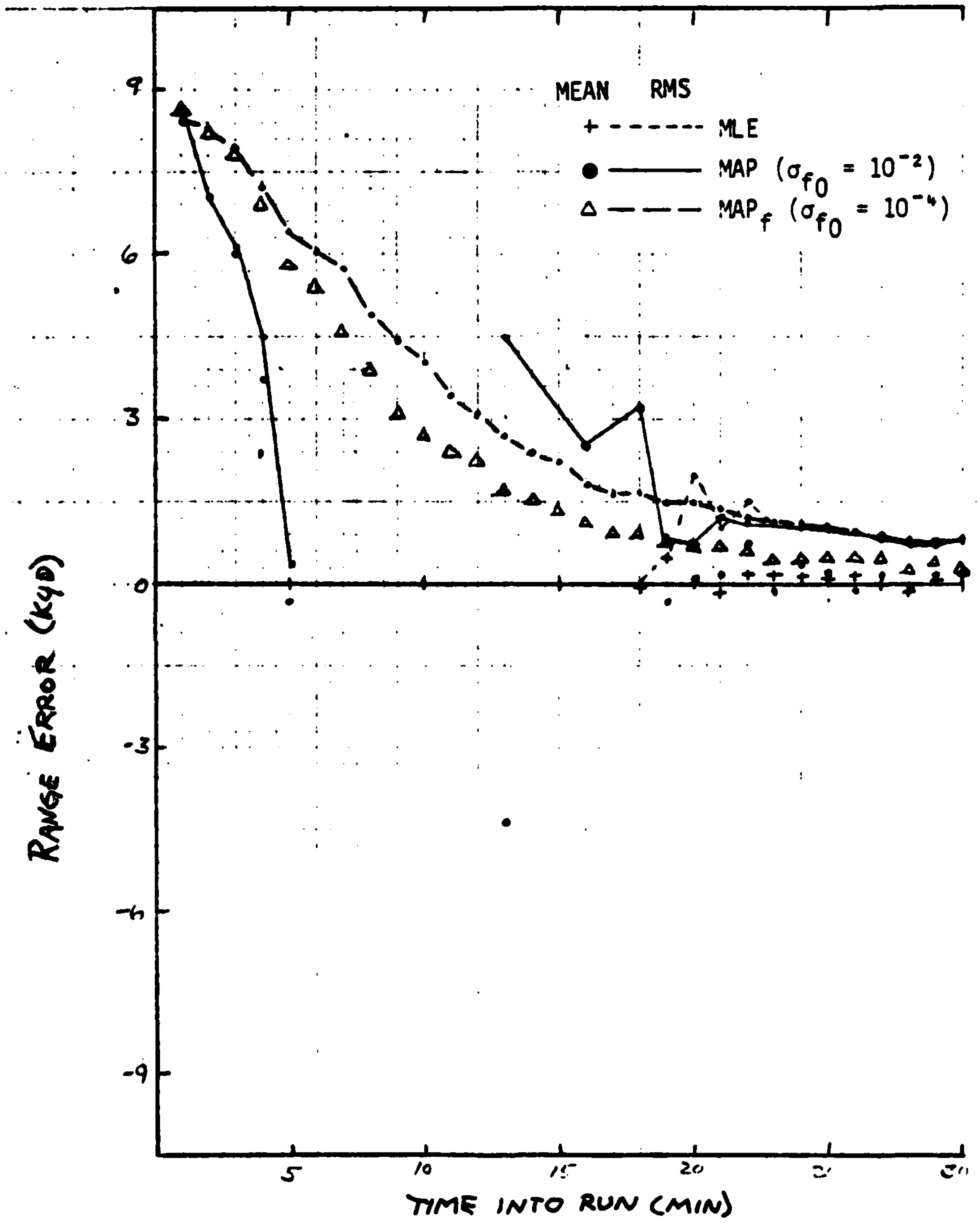

Figure 4-32a. Range Error for Bearing/Frequency Multisensor Solution (First CZ Path, Crossing-Target Course, $\sigma_{f_m} = 10^{-3}$)

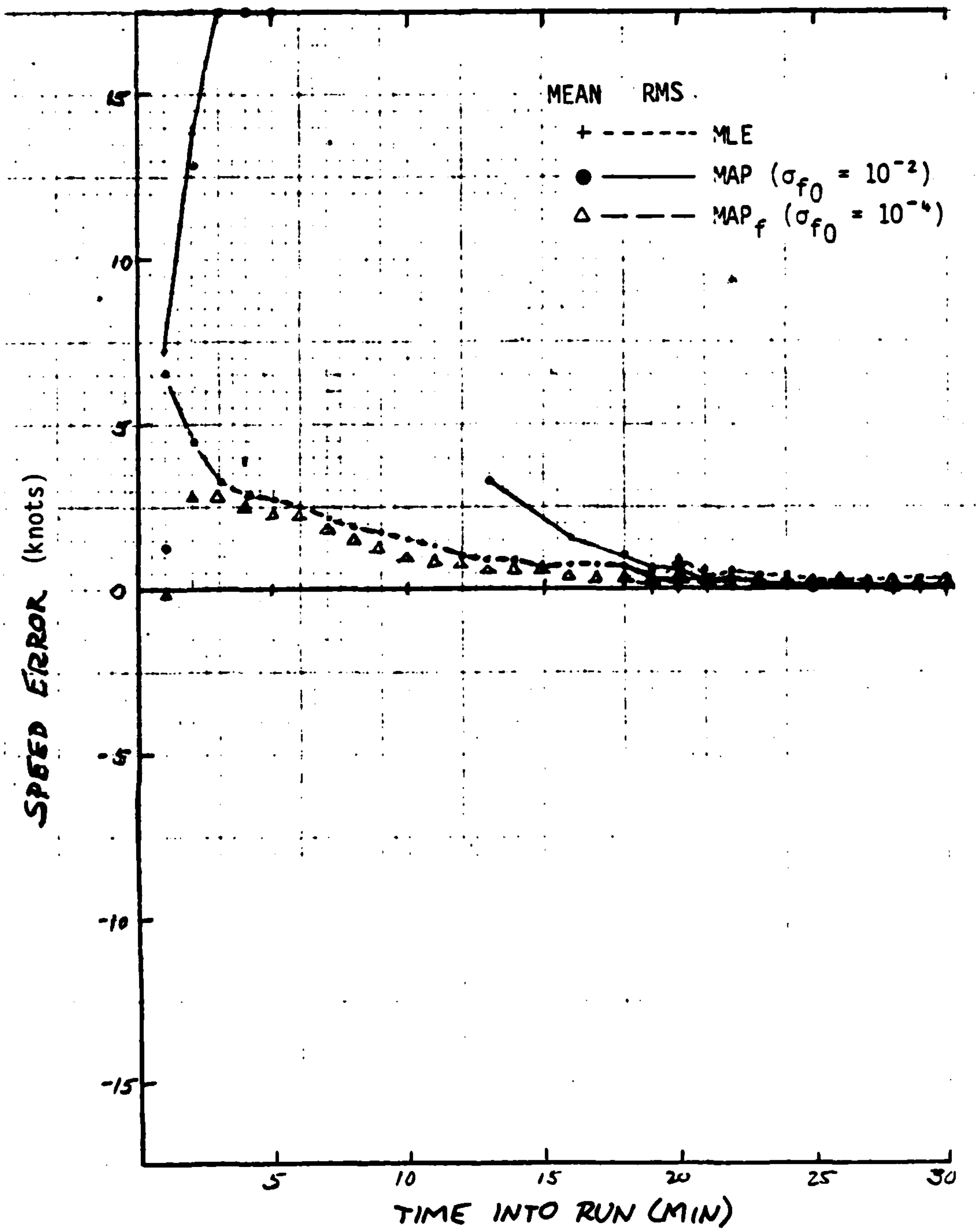

Figure 4-32b. Speed Error for Bearing/Frequency Multisensor Solution (First CZ Path, Crossing-Target Course, $\sigma_{f_m} = 10^{-3}$)

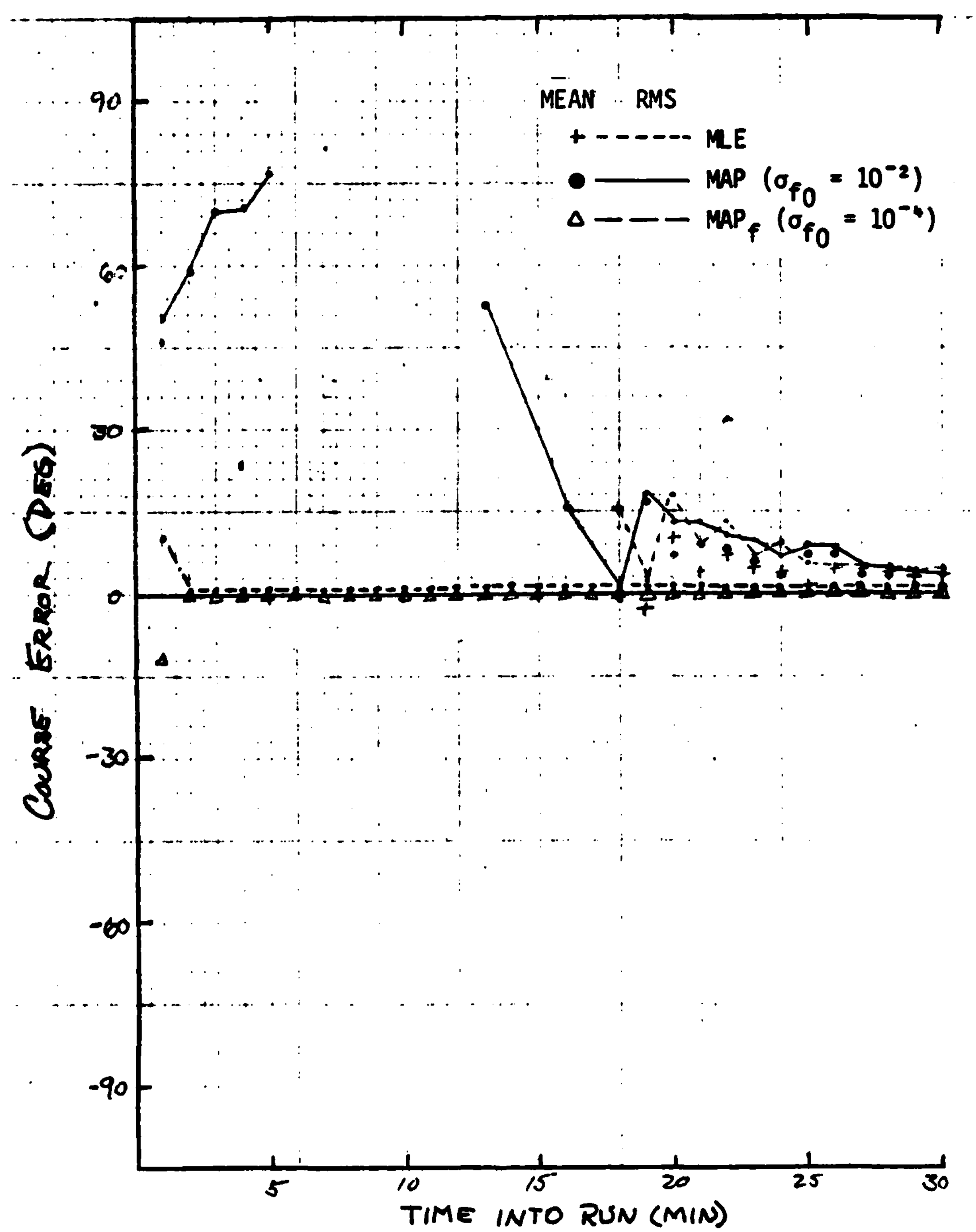

Figure 4-32c. Course Error for Bearing/Frequency Multisensor Solution (First CZ Path, Crossing-Target Course, $\sigma_{f_m} = 10^{-3}$)

values calculated from the algorithms' solutions. The realized solution accuracy, as demonstrated by the RMS errors plotted in the figures, is generally improved by the *a priori* information as used by the MAP algorithm. In addition, the inclusion of an accurate center frequency estimate in the *a priori* information (the MAP_f solution) further improves the solution quality.

The errors in the solutions for the direct-path, closing-course case (Figures 4-27 and 4-28) are reduced for the most part by both the MAP and MAP_f procedures. Most of the reduction of range error early in the problem comes from the use of the MAP algorithm; however, later in the run the most significant reduction comes from the additional use of an accurate center frequency estimate. Speed and course errors, however, tend to benefit from both throughout the run. The same case with more accurate frequency measurements ($\sigma_{f_m} = 10^{-3}$) does not benefit from *a priori* information as greatly. Range and speed errors show close to zero decrease from the use of MAP, and the course error improvement is significant only in the early problem stage. For the direct-path, crossing-course case (Figures 4-29 and 4-30) the MAP procedure provides improved solution accuracy, again early in the problem. However, little difference occurs after the first 6 or 7 minutes into the run. The improvement due to the *a priori* information again is less for the case with the more accurate frequency measurements. The first CZ, crossing-course case again shows improvement in solution accuracy using the MAP and MAP_f procedures. The exact relationships among the three procedures are, however, difficult to see due to the poor convergence of the MLE algorithm for most of the run.

In general, the *a priori* information improves solution accuracy to a greater degree for cases with the more difficult geometries and less accurate measurements. In other words, the more observable and accurate the solution is with measurements alone, the less impact any *a priori* information will have. It should be noted how well the MAP procedure with accurate center frequency does for all geometries and measurement errors throughout the entire run. The mean errors additionally show a high degree of average accuracy with generally very low bias.

4.3.3 Theoretical Range-Error Lower Bounds

Theoretical lower bounds for the range-error standard deviations are represented in Figures 4-33 through 4-35 for the simulations run. The plotted values are the major axes of the position eigenvalues for the inverse psi matrix computed during the Gauss-Newton solution procedure. These estimates for range-error lower bounds may represent the relative potential solution quality achieved from all available information from the different solution procedures. In addition, although the values are averaged over Monte Carlo repetition the lower bound estimates are independent of the number of converged repetitions and do not, in actuality, vary significantly between repetitions. An indication of the value of *a priori* information to solution quality and solution convergence may be observed. The range RMS errors are also plotted in order to compare the theoretical values to the solution quality actually achieved by the algorithms. The plotted results again indicate the value to range accuracy of using the MAP and MAP_f procedures over the MLE, particularly in the cases with the lowest solution quality. Figure 4-33 shows the reduction in range error bounds achieved from the use of the MAP algorithm and the accurate center frequency estimate for the direct-path, closing-course case. The effect is seen to be much lower for the case with greater frequency measurement accuracy. Relatively little difference is observed in Figure 4-34 among the different algorithms for the more observable direct-path, crossing-course geometry. The first CZ, crossing-course case plotted in Figure 4-35 shows improvement due to the MAP algorithm but very little from the use of accurate center frequency estimates.

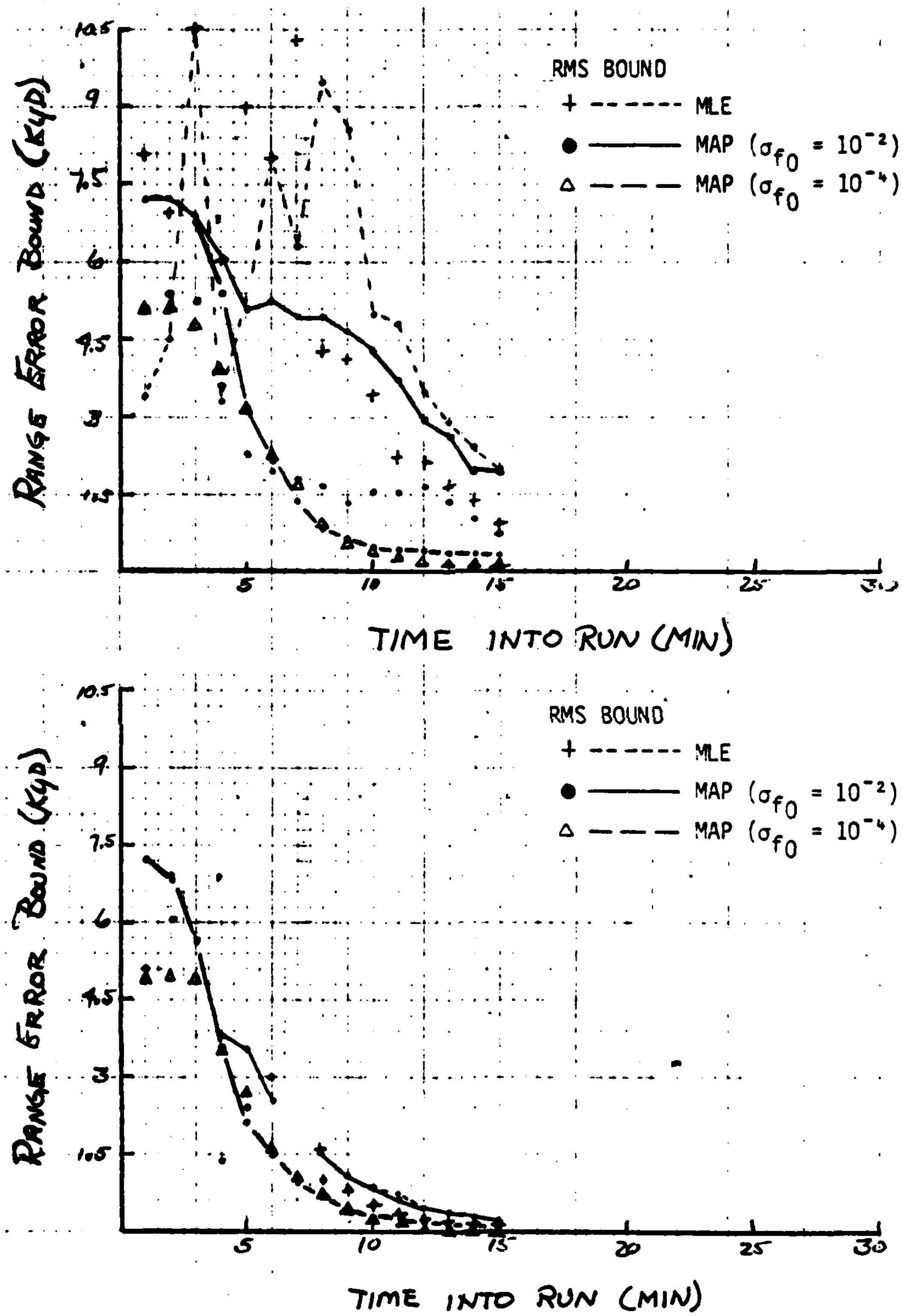

Figure 4-33. Theoretical Lower Bound on Range Error for Bearing/Frequency Multisensor Solution (Direct-Path, Closing-Target Course)

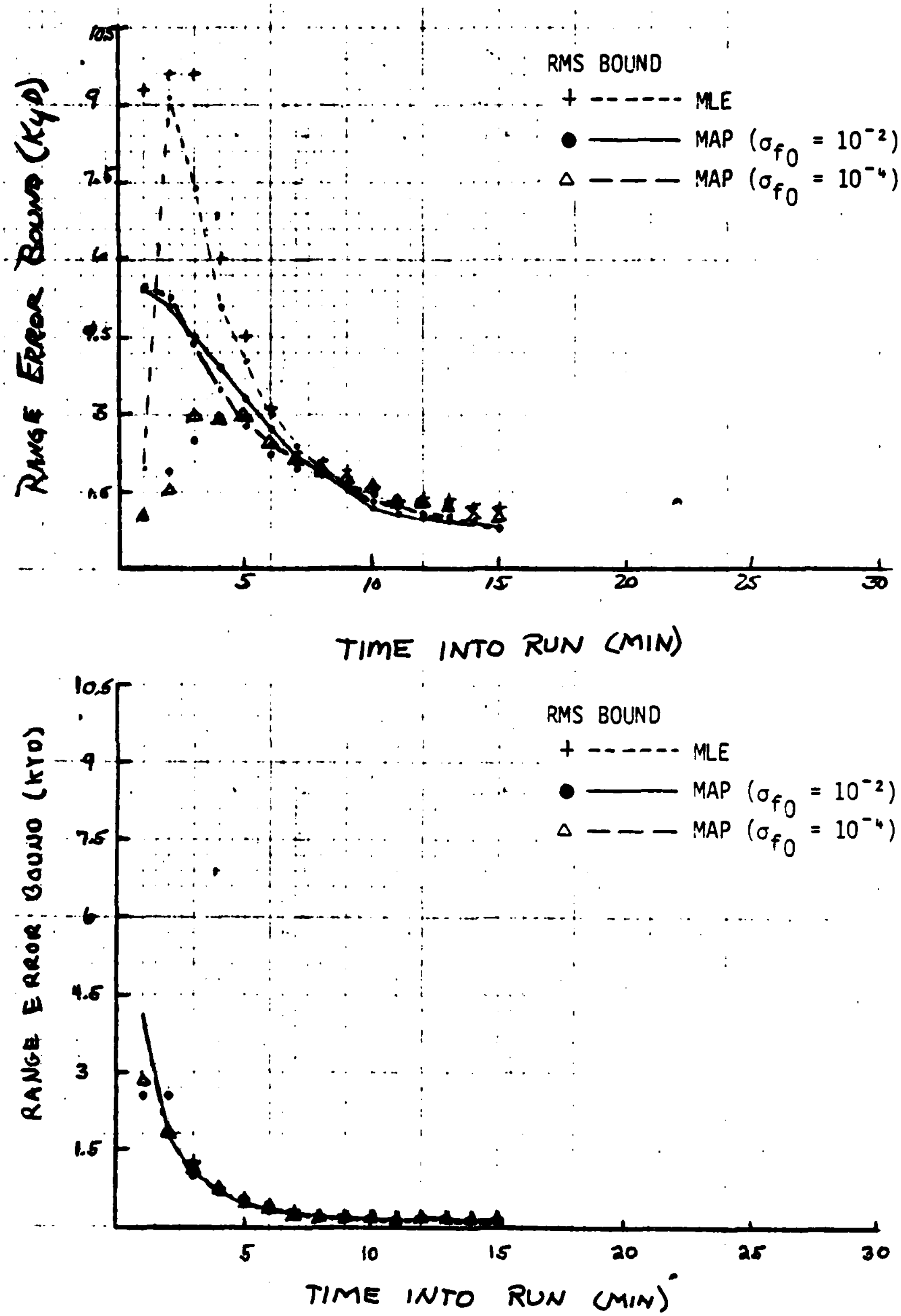

Figure 4-34. Theoretical Lower Bound on Range Error for Bearing/Frequency Multisensor Solution (Direct-Path, Crossing-Target Course)

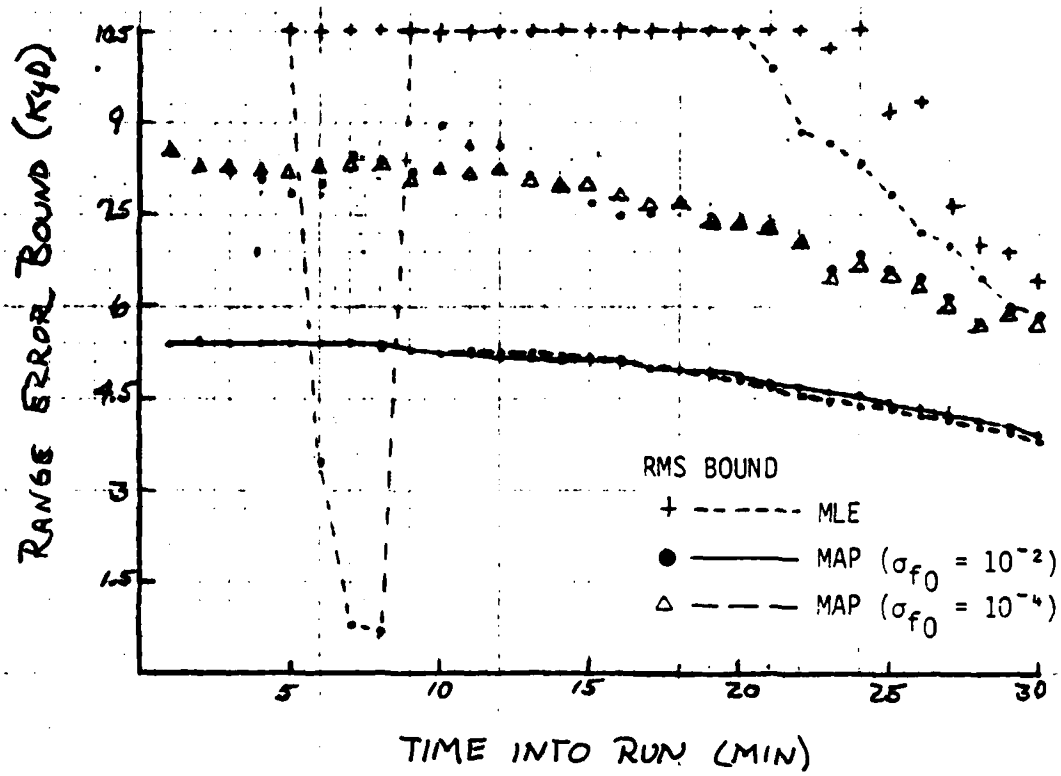

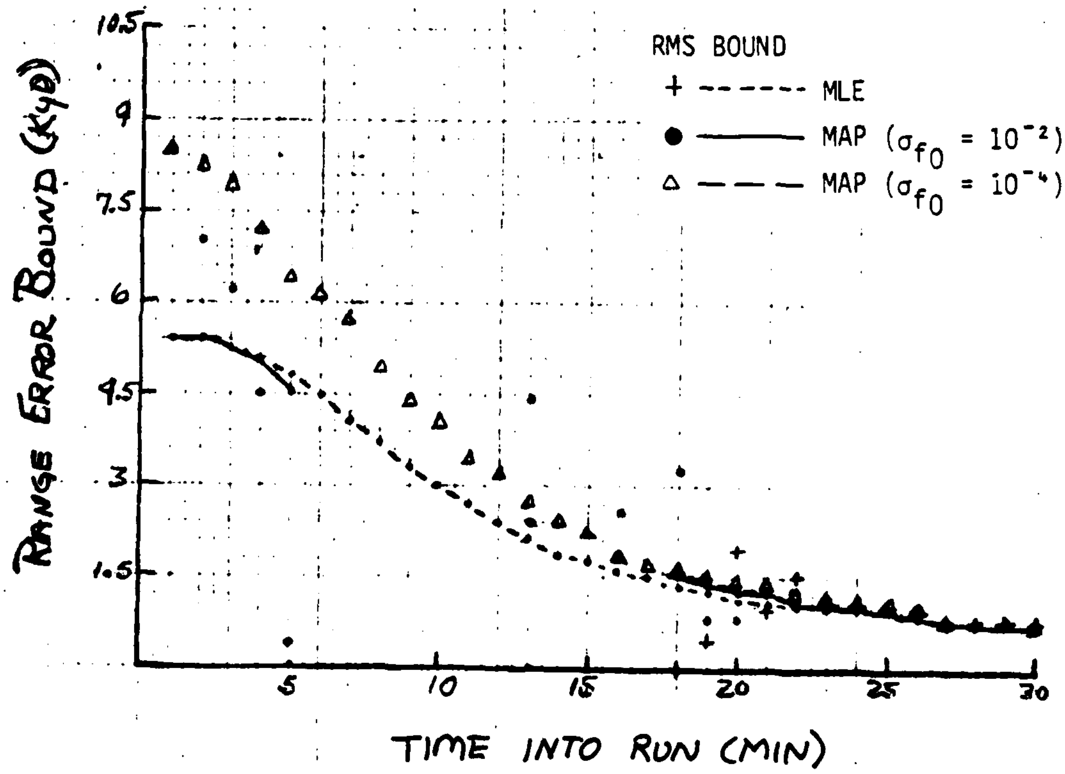

Figure 4-35. Theoretical Lower Bound on Range Error for Bearing/Frequency Multisensor Solution (First CZ Path, Crossing-Target Course)

CHAPTER V
SUMMARY AND CONCLUSIONS

The value of incorporating *a priori* information into a TMA solution was investigated as described in Reference 4. The conclusion of that study, based on Monte Carlo simulations of Maximum Likelihood and Maximum *a posteriori* estimates, was that *a priori* speed information was very beneficial in early solution performance; however, (crude) *a priori* range estimates primarily aided the initial numerical convergence of the solution iteration procedure. In effect, the *a priori* range variance produces a positive definite mean Hessian matrix which allows numerical convergence.

5.1 IMPROVED ITERATION PROCEDURES

This study examined two procedures for improving solution convergence during early parts of the problem to ascertain whether the original solution procedure was optimum. The previous solution procedure iterated towards a null of the gradient of the *a posteriori* density function (or likelihood ratio) using step-size constraints to bound the iteration excursions. In this study, the procedure was modified to minimize the logarithm of the *a posteriori* density function (or the log likelihood ratio) using a line search along the direction of the Gauss-Newton step. Several useful results were obtained from that study.

The line search does not always produce convergence to the minimum solution. At times when observability is poor, the line search occasionally produces a zero step which would retain the original solution and, therefore, not incorporate the added measurements. It was found that a heuristic procedure should be used in that case, which involves taking a limited step in the Gauss-Newton direction without regard for minimizing the cost function. This procedure eventually resulted in obtaining a minimum solution. In effect,

when this procedure is invoked the cost function is not approximately quadratic at the current solution iteration and one must step away from that solution before proceeding with the normal optimization process.

The modified Gauss-Newton procedure does improve numerical convergence for both MAP and MLE solutions, but the MAP solution still converges more often during periods of poor observability. The net cost of incorporating the line search is increased even though the number of iterations is reduced. The increased cost is not significant and is within the tolerance of program optimization.

The modified Gauss-Newton procedure does result in a significant improvement in course and speed solutions during periods of poor observability when *a priori* range estimates are included. When sufficient data is processed, the solutions converge to the same values regardless of numerical procedure and essentially without regard to use of *a priori* range information.

The other procedure tested was the estimation of an observable (three-state) relative motion solution on the first leg which is bootstrapped to a full solution on the second leg. The procedure can be applied with or without *a priori* information by using a line search on range during the second leg. It was found that the relative motion solution can be solved consistently with little cost because it is observable. It can be coupled with *a priori* range or speed information to generate single-leg solutions for tactical information. It was found, however, that numerical convergence on the second leg was not significantly improved by using the bootstrapped solution rather than a zero-speed initialization. However, the relative motion situation is still a useful feature because it can be computed along with the full solution and be used for tactical inputs when the full solution does not converge. One approach that was not studied was estimation of range by combining relative motion solutions from individual legs. There were insufficient resources available to pursue that study but it would be similar to the widely used Ekelund procedure. In any event, it is recommended that one incorporate *a priori* information on the first TMA leg by solving for the relative motion

solution and combining that with the *a priori* information in a least-squares sense. This conclusion is based on numerical convergence behavior of the three-state and four-state solutions. After the first own-ship maneuver, the four-state problem should be solved if it converges because the previous relative motion solution is invalid after a maneuver.

5.2 BEARING/FREQUENCY MULTISENSOR TMA

The using of both bearing and frequency (Doppler ranging) measurements can allow solution of the TMA problem without maneuvers. In the context of this study, that problem was examined to ascertain the value of *a priori* estimates of range, speed and/or base frequency. The multisensor MLE and MAP procedures generally performed quite well when bearing and frequency measurement were accurate. For all cases simulated, *a priori* information provided enhanced numerical convergence of the algorithm with the use of an accurate center frequency estimate providing the greatest improvement. The improvement in convergence was particularly large for the runs which had both the more accurate frequency measurements and an accurate center frequency *a priori* estimate. Without the latter, the value of the other *a priori* information was minimal. The solution accuracy, as measured by the RMS errors, was improved by both the use of *a priori* range information and an accurate frequency estimate. However, in this situation the runs with the less accurate frequency measurements were those which were most improved. This result was reflected as well by the theoretical range lower bounds on range error standard deviation. Solution accuracy was most enhanced by the *a priori* information for the cases with difficult geometries and less accurate measurements.

APPENDIX

DEVELOPMENT OF GRADIENT COMPUTATIONS FOR BEARING AND FREQUENCY MLE

Assuming that independent Gaussian bearing and frequency measurements (B_m, f_m) are made at discrete times, t_k, the log likelihood ratio for the multiple observations is

$$-\ln\Lambda = \frac{1}{2\sigma_B^2}\sum_{k=1}^{N}(B_m(k) - \hat{B}(k))^2$$

$$+ \frac{1}{2\sigma_f^2}\sum_{k=1}^{N}(f_m(k) - f_o\hat{\eta}(k))^2$$

$$+ \frac{N}{2}\log(2\pi\sigma_B^2\sigma_f^2) \tag{1}$$

where Λ is the conditional probability density function for the joint measurement sequences, given the solution $(\underline{x}(k))$ and the true base frequency (f_o). The target solution vector is contained in $\hat{B}$ and $\hat{\eta}$.

$$\hat{B}_{(k)} = \tan^{-1}\left[\frac{\hat{x}_1(t_o) + (t_k - t_o)\hat{x}_3(t_o) - x_{1os}(t_k)}{\hat{x}_2(t_o) + (t_k - t_o)\hat{x}_4(t_o) - x_{2os}(t_k)}\right] \tag{2}$$

$$\hat{\eta}(k) \equiv 1 - \frac{\hat{\dot{R}}(k)}{c} \tag{3}$$

$$\hat{\dot{R}}(k) = (\hat{x}_3(t_o) - \dot{x}_{3os}(t_k))\sin\hat{B}(k) + (\hat{x}_4(t_o) - \dot{x}_{4os}(t_k))\cos\hat{B}(k) \tag{4}$$

When *a priori* knowledge of base frequency has a Gaussian distribution, the *a priori* information can be incorporated and a likelihood ratio developed which is conditional only an $\hat{x}$. Note:

$$\Lambda \equiv P_{\{B_m\}/\underline{x}}\,P_{\{f_m\}/\underline{x},\,f_o} \tag{5}$$

Then, if $p_{f_o}(f_o)$ is the *a priori* probability density for f_o:

$$\Lambda' \equiv \int_{-\infty}^{\infty} \Lambda p_{f_o}(f_o)df_o$$

$$= p_{\{B_m\}/\underline{x}}\, p_{\{f_m\}/\underline{x}} \tag{6}$$

$$p_{\{f_m\}/\underline{x}} = \int_{-\infty}^{\infty} p_{\{f_m\}/\underline{x},\, f_o}\, p_{f_o}(f_o)df_o \tag{7}$$

for

$$p_{f_o}(f_o) = \frac{1}{\sqrt{2\pi}\sigma_{f_o}} e^{-\frac{(f_o - \overline{f}_o)^2}{2\sigma^2_{f_o}}} \tag{8}$$

and

$$p_{\{f_m\}/\underline{x}} = \frac{1}{(2\pi\sigma_f^2)^{N/2}} e^{-\frac{(f_m - f_o\hat{\eta})^2}{2\sigma_f^2}} \tag{9}$$

then

$$p_{\{f_m\}/\underline{x}} = \frac{1}{(2\pi\sigma_f^2)^{N/2}\sqrt{2\pi\sigma^2_{f_o}}} \int_{-\infty}^{\infty} e^{-\frac{I(f_o)}{2}} df_o \tag{10}$$

$$I(f_o) = \sum_{k=1}^{N} \frac{(f_m(k) - f_o\eta(k))^2}{\sigma_f^2} + \frac{(f_o - \overline{f}_o)^2}{\sigma^2_{f_o}} \tag{11}$$

$$I(f_o) = \sum_{k=1}^{N} \frac{f_m^2(k)}{\sigma_f^2} + \frac{\overline{f}_o^2}{\sigma^2_{f_o}} + f_o^2\left(\frac{1}{\sigma^2_{f_o}} + \frac{1}{\sigma_f^2}\sum_{k=1}^{N} \eta^2(k)\right)$$

$$- 2\left(\frac{\overline{f}_o}{\sigma^2_{f_o}} + \frac{1}{\sigma_f^2}\sum_{k=1}^{N} f_m(k)\eta(k)\right)f_o \tag{12}$$

$$I(f_o) = \frac{(f_o - \hat{f}_o)^2}{\sigma^2_{\hat{f}_o}} + \sum_{k=1}^{N} \frac{f_m^2(k)}{\sigma_f^2} + \frac{\bar{f}_o^2}{\sigma^2_{f_o}} - \frac{\hat{f}_o^2}{\sigma^2_{\hat{f}_o}} \tag{13}$$

where

$$\hat{f}_o \equiv \frac{\frac{\sigma_f^2}{\sigma_{f_o}^2}\bar{f}_o + \sum_{k=1}^{N} f_m(k)\eta(k)}{\frac{\sigma_f^2}{\sigma_{f_o}^2} + \sum_{k=1}^{N} \eta^2(k)} \tag{14}$$

is the *a posteriori* mean and therefore the least squares estimate of f_o. Its conditional variance (given $\underline{x}$) is

$$\sigma^2_{\hat{f}_o} = \frac{\sigma^2{}_f}{\frac{\sigma_f^2}{\sigma_{f_o}^2} + \sum_{k=1}^{N} \eta^2(k)} \tag{15}$$

Note:

$$\hat{f}_o = \bar{f}_o + \frac{\sigma^2_{\hat{f}_o}}{\sigma_f^2}\sum_{k=1}^{N} (f_m(k) - \bar{f}_o\eta(k))\eta(k) \tag{16}$$

Equation 13 can be manipulated to an alternate form:

$$I(f_o) = \frac{(f_o - \hat{f}_o)^2}{\sigma^2_{\hat{f}_o}} + \sum_{k=1}^{N} \frac{(f_m(k) - \hat{f}_o\eta(k))^2}{\sigma_f^2} + \frac{(\hat{f}_o - f_o)^2}{\sigma^2_{f_o}} \tag{17}$$

The integral in Equation (10) over f_o can be computed as

$$P\{f_m\}/_{\underline{x}} = \frac{1}{(2\pi\sigma_f)^{N/2}} \frac{\sigma_{\hat{f}_o}}{\sigma^2_{f_o}} \exp -\frac{1}{2}\left(\sum_{k=1}^{N} \frac{(f_m(k) - \hat{f}_o\eta(k))^2}{\sigma_f^2} + \frac{(\hat{f}_o - \bar{f}_o)^2}{\sigma^2_{f_o}}\right) \tag{18}$$

The log likelihood ratio for $\underline{x}$ is therefore

$$-\ell n\Lambda' = \frac{1}{2\sigma_B^2}\sum_{k=1}^{N}(B_m(k) - \hat{B}(k))^2$$

$$+ \frac{1}{2\sigma_f^2}\sum_{k=1}^{N}(f_m(k) - \hat{f}_o\hat{\eta}(k))^2$$

$$+ \frac{1}{2\sigma_{f_o}^2}(\hat{f}_o - \overline{f}_o)^2$$

$$+ \frac{1}{2}\ell n\left(\frac{\sigma_f^2}{\sigma_{f_0}^2} + \sum_{k=1}^{N}\hat{\eta}^2(k)\right) \tag{19}$$

with

$$\hat{f}_o = \overline{f}_o + \frac{\sum_{k=1}^{N}(f_m(k) - \overline{f}_o\hat{\eta}(k))\hat{\eta}(k)}{\frac{\sigma_f^2}{\sigma_{f_o}^2} + \sum_{k=1}^{N}\hat{\eta}^2(k)} \tag{20}$$

The last term is much less sensitive to $\underline{x}$ than any other term and can be considered to be constant. The gradient of $J_{LR} = -\ell n\Lambda'$, with respect to $\hat{\underline{x}}(t_o)$, is therefore

$$\nabla_{\underline{x}}J_{LR} = -\frac{1}{\sigma_B^2}\sum_{k=1}^{N}(B_m(k) - \hat{B}(k))\nabla_{\underline{x}}\hat{B}(k)$$

$$-\frac{\hat{f}_o}{\sigma_f^2}\left[\sum_{k=1}^{N}(f_m(k) - \hat{f}_o\hat{\eta}(k))\nabla_{\underline{x}}\eta(k)\right]$$

$$+\frac{1}{\sigma_f^2}\left[-\sum_{k=1}^{N}\eta(k)(f_m(k) - \hat{f}_o\hat{\eta}(k))\right.$$

$$+ \frac{\sigma_f^2}{\sigma_{\hat{f}_o}^2} (\hat{f}_o - \bar{f}_o) \Bigg] \nabla_{\underline{x}} \hat{f}_o \tag{21}$$

The last term can be shown to be identically zero. Thus:

$$\nabla_{\underline{x}} J_{LR} = -\sum_{k=1}^{N} \left[\frac{(B_m(k) - \hat{B}(k))}{\sigma_B^2} \nabla_{\underline{x}} \hat{B}(k) \right.$$

$$\left. + \frac{\hat{f}_o(f_m(k) - \hat{f}_o \hat{\eta}(k))}{\sigma_f^2} \nabla_{\underline{x}} \eta(k) \right] \tag{22}$$

The second gradient of J_{LR} is

$$\nabla_{\underline{x}} \nabla_{\underline{x}}^T J_{LR} = \sum_{k=1}^{N} \frac{\nabla_{\underline{x}} \hat{B}(k) \nabla_{\underline{x}}^T \hat{B}(k)}{\sigma_B^2} - \sum_{k=1}^{N} \frac{(B_m - \hat{B})}{\sigma_B^2} \nabla_x \nabla_{\underline{x}}^T \hat{B}$$

$$+ \frac{\hat{f}_o^2}{\sigma_f^2} \sum_{k=1}^{N} \nabla_{\underline{x}} \hat{\eta}(k) \nabla_{\underline{x}}^T \hat{\eta}(k)$$

$$- \frac{\nabla_{\underline{x}} \hat{f}_o}{\sigma_f^2} \sum_{k=1}^{N} (f_m - 2\hat{f}_o \eta(k)) \nabla_{\underline{x}}^T \eta(k)$$

$$- \frac{\hat{f}_o}{\sigma_f^2} \sum_{k=1}^{N} (f_m(k) - \hat{f}_o \hat{\eta}(k))(\nabla_{\underline{x}} \nabla_{\underline{x}}^T \eta(k)) \tag{23}$$

with

$$\nabla_{\underline{x}}\hat{f}_o = \sum_{k=1}^{N} \frac{(f_m(k) - 2\hat{f}_o \eta(k))\nabla_{\underline{x}}\eta(k)}{\frac{\sigma_f^2}{\sigma_{f_o}^2} + \sum_{k=1}^{N} \eta^2(k)} \tag{24}$$

The expected value of the second gradient is required for the Gauss-Newton procedure. Under the assumption that $\hat{x}$ is correct, then one can compute after tedious algebra:

$$\psi_{LR} \equiv E\{\nabla_{\underline{x}}\nabla_{\underline{x}}^T J_{LR}\}$$

$$= \frac{1}{\sigma_B^2} \sum_{k=1}^{N} \nabla_{\underline{x}}\hat{B}(k)\nabla_{\underline{x}}^T\hat{B}(k)$$

$$+ \frac{\overline{f}_o^2}{\sigma_f^2}\left(1 + \frac{\sigma_{f_o}^2}{\overline{f}_o^2}\right)\left[\sum_{k=1}^{N} \nabla_{\underline{x}}\hat{\eta}(k)\nabla_{\underline{x}}^T\hat{\eta}(k)\right.$$

$$\left. - \frac{\left(\sum_{k=1}^{N} \hat{\eta}(j)\nabla_{\underline{x}}\eta(j)\right)\left(\sum_{k=1}^{N} \hat{\eta}(k)\nabla_{\underline{x}}\hat{\eta}(k)\right)}{\sum_{k=1}^{N} \eta^2(k) + \frac{\sigma_f^2}{\sigma_{f_o}^2}}\right]$$

$$+ \frac{4\left(\sum_{j=1}^{N} \eta(j)\nabla_{\underline{x}}\eta(j)\right)\left(\sum_{k=1}^{N} \eta(k)\nabla_{\underline{x}}^T\eta(k)\right)}{\left(\sum_{j=1}^{N}\eta^2(j) + \frac{\sigma_f^2}{\sigma_{f_o}^2}\right)^2}$$

$$
- \frac{\sum_{k=1}^{N} \hat{n}(k)\nabla_{\underline{x}}\nabla_{\underline{x}}^{T}\hat{n}(k)}{\sum_{j=1}^{N} n^{2}(j) + \frac{\sigma_f^2}{\sigma_{f_o}^2}} \tag{25}
$$

The last two terms can be dropped because they are inconsequential when compared to the others when $\sigma_f/\overline{f}_o$ is small (e.g., of the order of $\dot{R}/c$). The equation can be simplified without hampering convergence to

$$
\psi_{LR} \approx \frac{1}{\sigma_B^2}\sum_{k=1}^{N} \nabla_{\underline{x}}\hat{B}(t_k)\nabla_{\underline{x}}^{T}\hat{B}(t_k)
$$

$$
+ \left(\frac{\hat{f}_o}{c\sigma_f}\right)^2 \left[\sum_{k=1}^{N} \nabla_{\underline{x}}\hat{\dot{R}}(k)\nabla_{\underline{x}}^{T}\hat{\dot{R}} - \frac{\left(\sum_{k=1}^{N} \hat{n}(k)\nabla_{\underline{x}}\dot{R}(k)\right)\left(\sum_{k=1}^{N} \hat{n}(k)\nabla_{\underline{x}}\dot{R}(k)\right)^{T}}{\sum_{k=1}^{N} \hat{n}^{2}(k) + \frac{\sigma_f^2}{\sigma_{f_o}^2}}\right] \tag{26}
$$

The term in brackets is positive semidefinite, since all quadratic forms reduce to

$$
\sum_{k=1}^{N} a_k^2 - \frac{\left(\sum_{k=1}^{N} \hat{n}(k)a_k\right)^2}{\sum_{k=1}^{N} \hat{n}^{2}(k) + \frac{\sigma_f^2}{\sigma_{f_o}^2}}
$$

where a_k is the projection of any vector on $\nabla_x \hat{\dot{R}}$. This quantity is zero only for a vector which is orthogonal to the gradient at all time steps. Otherwise this quantity is positive. The second term in brackets represents the information lost by not knowing the actual base frequency. If $\sigma_f >> \sigma_{f_o}$ or when N becomes sufficiently large, this information loss disappears.

The gradients of $\hat{B}$ and $\hat{\dot{R}}$ must be evaluated.

$$\hat{B}(t_k) = \tan^{-1}\left[\frac{x_1(t_o) + (t_k - t_o)x_3(t_o) - x_{1os}(t_k)}{x_2(t_o) + (t_k - t_o)x_4(t_o) - x_{2os}(t_k)}\right] \tag{27}$$

$$\hat{\dot{R}}(t_k) = (x_3(t_o) - x_{3os}(t_k))\sin \hat{B}(t_k) + (\hat{x}_4(t_o) - x_{4os}(t_k))\cos \hat{B}(t_k) \tag{28}$$

$$\nabla_{\underline{x}(t_o)}\hat{B}(t_k) = \frac{1}{R(t_k)}\begin{bmatrix} \cos \hat{B}(t_k) \\ -\sin \hat{B}(t_k) \\ (t_k - t_o)\cos \hat{B}(t_k) \\ -(t_k - t_o)\sin \hat{B}(t_k) \end{bmatrix} \tag{29}$$

$$\nabla_{\underline{x}(t_o)}\hat{\dot{R}}(t_k) = \begin{bmatrix} 0 \\ 0 \\ \sin \hat{B}(t_k) \\ \cos \hat{B}(t_k) \end{bmatrix} + v_{cr}\nabla_{\underline{x}(t_o)}\hat{B}(t_k) \tag{30}$$

$$v_{cr} \equiv (x_3(t_o) - x_{3os}(t_k))\cos \hat{B}(t_k) - (x_4(t_o) - x_{3os}(t_k))\sin \hat{B}(t_k) \tag{31}$$

The modified Gauss-Newton solution for the step in $\underline{x}$ is

$$\underline{\Delta x} = -a\psi^{-1}\nabla_{\underline{x}}J \equiv a\underline{\Delta x}_o \tag{32}$$

The projection of this step along the gradient is

$$\underline{\Delta x}^T \nabla_{\underline{x}} J = -a \nabla_{\underline{x}}^T J \psi^{-1} \nabla_{\underline{x}} J = -a \underline{\Delta x}_0^T \psi \underline{\Delta x}_0$$

$$= a \left[\sum_{k=1}^{N} \frac{\Delta B_k^2}{\sigma_B^2} + \sum_{k=1}^{N} \frac{\Delta \dot{R}_k^2}{\sigma_{\dot{R}}^2} - \frac{\left(\sum_{k=1}^{N} \eta_k \frac{\Delta \dot{R}}{\sigma_{\dot{R}}} \right)^2}{\sum_{k=1}^{N} \hat{\eta}^2(k) + \frac{\sigma_f^2}{\sigma_{f_0}^2}} \right] \tag{33}$$

with

$$\Delta B_k \equiv \nabla_{\underline{x}}^T \hat{B}_k \underline{\Delta x}_0 \tag{34}$$

and

$$\Delta \dot{R}_k \equiv \nabla_{\underline{x}}^T \hat{\dot{R}}_k \underline{\Delta x}_0 = \Delta \dot{R}_v + v_{cr} \Delta B \tag{35}$$

$$\Delta \dot{R}_v = \Delta x_3 \sin \hat{B} + \Delta x_4 \cos \hat{B} \tag{36}$$

$$\sigma_{\dot{R}} = (\sigma_f c)/\hat{f}_0 \tag{37}$$

Unless both ΔB_k and $\Delta \dot{R}_k$ are zero at every time step, the projection is always positive.

The accuracy of the base frequency estimate ($\hat{f}_0$) depends on both error in the measurement and error in the solution ($\hat{\underline{x}}$). Let f_0 be the true center frequency and w_k be the frequency measurement error. Then

$$\hat{f}_0 - f_0 = \overline{f}_0 - f_0 + \frac{\sum_{k=1}^{N} (f_m(k) - \overline{f}_0 \hat{\eta}(k)) \hat{\eta}(k)}{\frac{\sigma_f^2}{\sigma_{f_0}^2} + \sum_{k=1}^{N} \hat{\eta}^2(k)} \tag{38}$$

$$\hat{f}_o - f_o = \frac{\bar{f}_o - f_o + \sum_{k=1}^{N} (w_k + f_o \eta(k) - \bar{f}_o \hat{\eta}(k))\hat{\eta}(k)}{\frac{\sigma_f^2}{\sigma_{f_o}^2} + \sum_{k=1}^{N} \hat{\eta}^2} \tag{39}$$

$$\hat{f}_o - f_o \approx \frac{(\bar{f}_o - f_o) \frac{\sigma_f^2}{\sigma_{f_o}^2} + \sum_{k=1}^{N} (w_k - \bar{f}_o(\hat{\eta}(k) - \eta(k)))\hat{\eta}(k)}{\frac{\sigma_f^2}{\sigma_{f_o}^2} + \sum_{k=1}^{N} \hat{\eta}^2} \tag{40}$$

and

$$\sigma_{\hat{f}_o}^2 = \frac{\sigma_f^2}{\sum_{k=1}^{N} \hat{\eta}^2(k) + \frac{\sigma_f^2}{\sigma_{f_o}^2}} \left\{ 1 + \left(\frac{\bar{f}_o}{e\sigma_f}\right)^2 \underline{q}^T \psi^{-1} \underline{q} \right\} \tag{41}$$

where

$$\underline{q} \equiv \frac{\sum_{k=1}^{N} \hat{\eta}(k) \nabla_{\underline{x}} \hat{\dot{R}}(k)}{\sqrt{\sum_{k=1}^{N} \hat{\eta}^2(k) + \frac{\sigma_f^2}{\sigma_{f_o}^2}}} \tag{42}$$

REFERENCES

1. Chou, S. I., Exploitation of Environmental Data Knowledge in Surface Ship ASW Target Motion Analysis, PM-4 Study Proposal, March 1978.

2. Chou, S. I., Anti-Submarine Warfare (ASW) Passive Target Tracking, Naval Ocean Systems Center, January 1980.

3. Hartley, H. O., "The Modified Gauss-Newton Method for the Fitting of Non-Linear Regression Functions by Least Squares," Technometrics, Vol 3, No. 2, May 1961.

4. Jarvis, H. F., and N. B. Nill, Target Tracking with Multiple Data Sources, Analysis and Technology, Inc., 15 August 1979.

Distribution List for

Target Motion Analysis with *A Priori* Information

	No. of Copies
Defense Technical Information Center Bldg. 3, Cameron Station Alexandria, VA 22314	12
Office of Naval Research Department of the Navy Arlington, VA 22217 (Attn: Mr. J. G. Smith, Code 411SP)	2
Director Naval Research Laboratory Washington, D.C. 20375 (Attn: Code 2627)	1
Naval Ocean Systems Center 271 Catalina Boulevard San Diego, CA 92152 (Attn: Dr. P. Reeves, Code 632) (Attn: Dr. J. Zeidler, Code 6212)	 1 1
Naval Underwater Systems Center New London Laboratory New London, CT 06320 (Attn: Dr. C. G. Carter, Code 3331)	1
Naval Sea Systems Command Navy Department Washington, D.C. 20360 (Attn: Mr. D. Porter, Code 63R11) (Attn: Mr. C. Marin, Code 63R16)	 1 1
Naval Electronic Systems Command National Center Building No. 1 Washington, D.C. 20360 (Attn: Mr. J. Schuster, Code 612)	1
Naval Surface Weapons Center White Oak Laboratory Silver Spring, MD 20910 Code U-20	1
Defense Advanced Research Projects Agency 1400 Wilson Boulevard Arlington, VA 22209	1

Distribution List (cont'd)

	No. of Copies
Massachusetts Institute of Technology Laboratory for Information and Decision Systems Cambridge, MA 02139	1
Commander, Submarine Development Squadron 12 Box 70 Naval Submarine Base, New London Groton, CT 06340	1
Office of Naval Research Branch Office Building 114, Section D 666 Summer Street Boston, MA 02210	1
Dr. Harold A. Titus Naval Postgraduate School Department of Electrical Engineering Code 62TS Monterey, CA 93940	1
Naval Underwater Systems Center Newport, R.I. 02840	
Code 352	1
Code 351	1
Naval Intelligence Support Center Suitland, MD 20390 Code 20C	1